Tomasz Wierzbicki
Myung Sung Suh

Denting Analysis of Tubes Under Combined Loadings

MIT Sea Grant
College Program

Massachusetts
Institute of Technology
Cambridge, MA 02139

MITSG 86-5

DENTING ANALYSIS OF TUBES UNDER COMBINED LOADING

Tomasz Wierzbicki and Myung Sung Suh

MIT Sea Grant
College Program

Massachusetts Institute
of Technology
77 Massachusetts Ave.
Cambridge, MA 02139

MITSG 86-5
March, 1986

NA84AA-D-0046
R/O-19

AUTHORS

Tomasz Wierzbicki — Professor of Applied Mechanics, Department of Ocean Engineering, MIT

Myung Sung Suh — Graduate student, Department of Ocean Engineering, MIT

ORDERING INFORMATION

This publication is the final report for a joint industry/MIT Sea Grant project, "Residual Strength of Dented Tubes."

Copies are available through:

Sea Grant Information Center
MIT E38-302
Massachusetts Institute of Technology
77 Massachusetts Ave.
Cambridge, MA 02139

617/253-7041

ABSTRACT

A theoretical analysis is presented of large plastic deformations of tubes subjected to combined loading in the form of lateral indentation, bending moments and axial force. A considerable effort was made to develop and justify an accurate and yet mathematically tractable model of the shell. The model is capable of describing with some realism local damage of tubes involving large strains, rotations and shape distortion. The force-deflection characteristics of tubes were shown to depend strongly on the magnitude of the bending moment and axial force (tensile or compressive), applied to the tube ends. The calculations revealed that the resistance of the tube to lateral indentation and thereby the energy that the tube can absorb sharply diminishes with changing the direction of axial force from pre-tension to pre-compression. With increasing compression the tube were found to loose stability and fail by local plastic sectional collapse at the load equal 0.75 of the plastic squash load. The residual strength of dented tubes was also determined in the case of rotationally restraint boundary conditions. The present results were shown to give good correlation with few well documented experiments reported in the literature.

TABLE OF CONTENTS

Notation

g	gravitational acceleration
ℓ	length element of generator
r_1	R_1/R
$\dot{r}_2$	R_2/R
$\dot{r}_1$	$dr_1/d\phi$
r_2	$dr_2/d\phi$
s	coordinate in circumferential direction
s_1, s_2, s_3	length of each arc
t	thickness of circular tube
u	axial displacement
$\dot{u}_o$	u at $x=\xi$
$\dot{u}$	tangential velocity of a generic point
w	lateral deflection of shell element
w_c	indentation depth at midspan
$\overline{w}_c$	w_c/R
$\dot{w}$	vertical velocity of a generic point
x	coordinate in axial direction
z	vertical distance between material point and centroidal axis for a ring
D	diameter of undeformed tube
$\dot{E}_{crush}$	rate of total crushing energy
$\dot{E}_{crush}$	rate of crushing energy per unit width
$\dot{E}_{ext}$	rate of external work
$\dot{E}_{gen}$	rate of total extensional energy
$\dot{E}_{gen}$	rate of extensional energy per unit width

$\dot{E}_{int}$	rate of internal energy dissipation
$\dot{E}_{shear}$	rate of shear energy
L	total span of tube
$\mathscr{L}$	total ring circumference
M	external bending moment
$M_{\alpha\beta}$	stress couple tensor
M_o	fully plastic bending moment
M_p	plastic moment capacity of undeformed cross section
$M_{x\theta}$	twisting moment
N	external axial force
$N_{\alpha\beta}$	stress resultant tensor
N_o	fully plastic axial force
N_p	plastic force capacity of cross section
$N_{x\theta}$	shear force
P	lateral concentrated load
$P_c(\bar{w}_c)$	instantaneous crushing force
R	radius of undeformed tube
R_1	larger radius of deformed tube
R_2	smaller radius of deformed tube
s	surface area of continuously deforming region
v	velocity of moving plastic hinge
v_1, v_2	tangential velocity of each moving plastic hinge
α	central angle
β	rotation angle of generator

β	angle in Fig.3
γ	shear strain
Γ	length of hinge line
δ	indentation depth
$\dot{\delta}$	rate of indentation depth
ε_{av}	average strain
ε_b	average through-thickness bending strain
$\dot{\varepsilon}_{x\theta}$	rate of shear strain
$\dot{\varepsilon}_{\theta\theta}$	rate of circumferencial strain
$\dot{\varepsilon}_{xx}$	axial strain rate
$\dot{\varepsilon}_1$	strain rate due to local denting
$\dot{\varepsilon}_2$	strain rate due to uniform compression or extension
$\dot{\varepsilon}_3$	strain rate due to overall bending and rotation of cross section
$\dot{\theta}$	rate of rotation
$\dot{K}$	rate of curvature
K_o	initial curvature of undeformed tube
ΔK	change in curvature
$\dot{K}_{xx}$	rate of longitudinal curvature
$\dot{K}_{x\theta}$	rate of twist
$\dot{K}_{\theta\theta}$	rate of circumferential curvature
$(\dot{K}_{\theta\theta})_1$, $(\dot{K}_{\theta\theta})_2$	rate of circumferential curvature in each arc s_1 and s_2
ξ	half-length of dented region
ρ	mass density of tube material
σ_o	flow stress

σ_y	yield stress
ϕ	current position of lower plastic hinge
$\dot{\phi}$	rate of angle change
ϕ_o	initial position of lower plastic hinge
$\dot{\psi}_1, \psi_2$	angular velocity of each moving plastic hinge
ψ	angle in Fig.3
[ ]	jump in the enclosed quantity across stationary or moving hinges
$(\cdot)$	$\partial/\partial\phi(\ )$, differentiation with respect to ϕ

LIST OF FIGURES

Fig. 34 Plot of residual strength of dented tube versus the dent depth. Exact solution denoted by full line and approximate solution by dotted line.

1. INTRODUCTION

Moderately thick fabricated or cold drawn metal tubes encountered in various industrial applications are often subjected to accidental loading in addition to normal service loading. The service loads consist of axial tension or compression, bending moment, shear loading and sometimes twisting moment. The accidental loading may be of various origin and is typically applied in the transverse direction to the longitudinal axis of a tube. Examples of such loading are minor collisions of supply boats with multi-story offshore oil platforms, impact caused by dropped objects, mishandling during launching or installation of marine structures, ice scouring of Arctic pipelines, collisions of offshore installations with moving ice features and hydrodynamic wave impact. The combination of service and accidental loads may lead to a severe local shape distortion of tubes, loss of axial and bending strength and stiffness and catastrophic collapse of a given member.

From the point of view of economy of design and safety of operation it is important to be able to predict the response of tubes under all possible combination of external load. With the exception of Ref. [12], in all previous analyses of similar problems only one component of external loading was applied to the tube at a time. For example tubes were subjected to either indentation or axial compression. The problem of a combined loading, which often occurs in many practical situations, has not been studied theoretically or experimentally in the literature. Also the effect of different boundary conditions on a local crushing strength of tubulars appears not to be fully understood.

The general objective of the present paper is to get an insight into the mechanisms of plastic deformation of tubes undergoing large shape

distortion and sectional collapse. A thorough understanding of those local processes is a prerequisite for solving the whole class of boundary value problems of interest to various industrial applications. A typical shape of a locally damaged zone in tubulars is shown in Fig. 1. Our particular objective is to derive the load-deflection characteristics of cylinders subjected to lateral concentrated loading under variety of boundary conditions. Additionally, we want to predict the depth and shape of the locally damaged zone as well as the magnitude of overall shortening and rotation of the given member.

A distinctive feature of the present analysis is that all predictions are made on a purely theoretical basis and that no recourse is made in the analysis to the experimental data. Taby and Moan [28] introduced an empirical factor in their formula for the axial stresses in the dented zone. Smith in a series of excellent publications [20-24] calculated the residual strength of dented tubes using the concept of a reduced strength and stiffness of shell elements in the damage-affected zone. The reduction coefficient was then determined from the least fit of experimental data. In the computational model adopted by the above mentioned authors the radius of the tube was considered as constant with increasing dent depth. This is a reasonable assumption for relatively shallow dents [32], but limits the applicability and accuracy of the respective solutions for deeper dents. Ueda and Rashed [30] reported a good agreement of the theoretically calculated ultimate bending moments of zone-dented tubes with the independently performed tests. In all cases the maximum bending moment occurred early in the loading process when the sectional collapse was still very small.

a)

b)

Fig. 1 A photograph of a local plastic damage of a tube caused by unsymmetric indentation (a) (after Smith [24]) and Symmetric pinching (b) (after Montgomery [38]).

Our experience with the problem of propagating buckles in pipelines indicates that much of the strength of a tube comes from the ring mode of deformations [36]. Plastic collapse of rings were studied among others by Reid and Reddy [17]. Also experiments performed on short cylinders at the University of Manchester Institute of Science and Technology (UMIST) proved that such tubes resisted transverse loads by predominantly circumferential bending [29, 33, 34]. In addition to the already mentioned experimental studies on model and full scale tubes with dents, performed in Norway [25, 27], England [20-24] and Japan [30], tests on large diameter fabricated tubes were carried out in Canada [1, 18] and the United States [15, 19]. Birkemoe and Sato [1, 18] tested large diameter tubes in compression ($D/t>70$) and observed a "diamond" local failure mode on the compression size of the tube. Sherman reported on a very thorough experimental study in which tubes with D/t ranging from 30-70 were subjected to pure bending. In all cases the shape of the locally damaged zone was similar and resembled much that obtained in the indentation tests by a rigid punch. Ostapenko in a series of papers [14, 15] determined experimentally design curves for tubes subjected to compression. He found that tubes with $D/t<50$ developed their full compressive strength N_p. The effect of residual strength of dented tubes was not studied by Ostapenko.

Our intention in this introductory section is to discuss those references which are directly related to the development of the present computational model of the tube rather than to survey the vast literature concerned with the behavior of damaged tubes. For a comprehensive review of the state-of-the-art in this field the reader is referred to the paper by Ellinas and Valsgard [5]. A great deal of good work has been published on the plastic response of thinner shells [13, 32]. As thin tubes are outside the scope of the present study, the relevant publications are not commented upon.

In the early studies on local tube indentation, Morris and Calladine [11] and Soreide and Amdahl [25] emphasized the importance of bending and extensional deformation of the affected shell elements. Based on those observation a simple computational model was introduced by one of the co-author in Ref. [12]. The model consisted of a system of mutually interacting rings and generators. The work reported in Ref. [12] was considered proprietary for more than three years and it is only recently that its confidentiality has been released. The DnV Report has much of the flavor of the present findings. It points out on the importance of boundary conditions on the resistance of tubes to denting and predicts the existence of plastic instability of compressed tubes with an unsymmetric collapse mode. In Ref. [12] a circular section was modeled by a square section. We thought this assumption was too crude an approximation of the energy absorbed by the generators of the shell. Our present "exact" solution fully confirms all previous assumptions leading to the computational model while introducing important numerical corrections to the early results.

The paper is organized in the following way. First all assumptions are carefully spelled out in Sections 2 and 3 so that the finite strains and rotations of a cylindrical shell can be described by an accurate and yet mathematically tractable model. Then each of the basic mechanisms of the tube resistance, i.e., crushing of rings (Section 4) and extension of generators (Section 5) are analyzed in great details. Further the solutions of the large indentation problems are worked out in Section 6 for three typical boundary conditions and compared with the existing experimental data (Section 7). To bring the solution even closer to the experimental points, the influence of shear deformations is discussed in an approximate way in Section 8.

In Section 9 we move to an even more ambitious task of predicting the crush resistance of tubes subjected to an arbitrary tensile or compressive load combined with lateral load. The analysis has led to the discovery of a new phenomenon not previously reported in the literature. We have found that the resistance of tubes to lateral compression is reduced dramatically with the increasing amount of axial compression up to the point of instability. The instability may occur well before the full squash load is obtained. The solution for plastic instability contains as a special case the prediction of a residual strength of dented tubes which are restraint from rotational motion. This problem is discussed in Section 10. The extension of the present analysis to tubes in which both bending moment and axial force are prescribed at tube ends will be reported in a future publication.

Just as our report was ready for print an important contribution to the subject was made available to us in the summary form [38]. This work reports on a comprehensive experimental study on pinch loaded tubes in which the influence of the boundary condition on the crushing strength was studied in great details. A corresponding analytical solution was also derived based partially on Ref. [12] and partially on a new diamond model of the tube. A thorough discussion of this new development will be made when the corresponding results will be published in full.

2. FORMULATION OF THE PROBLEM

In this paper we shall be concerned with a class of problems for thick and medium thick tubes in which large sectional collapse takes place under the action of a rigid indentor, bending moment, axial compression or combination of the external loading, Fig. 2. The magnitude of the local dent is not restricted and theoretically can be as large as the diameter of the tube. For shells with the diameter to thickness ratio $D/t \leq 50$, which are of interest in offshore applications, the maximum lateral displacement can thus be fifty times larger than the wall thickness of the tube. Clearly, neither the infinitesimal nor the so-called "moderately large deflection" theories of cylindrical shells are applicable in this case.

The deformation process of the shell will be described here using the updated Lagrangian formulation by keeping track of the current geometry of the shell. In contrast to the advanced numerical codes with capabilities of handling large strain and displacement, the variable shell geometry will be updated analytically, using continuously varying functions with a few free parameters. Such an approach not only leads to a highly desirable closed-form solution to the problem of tube indentation but also provides an insight into the mechanism of shell deformations with severe unsymmetric shape distortion.

Constitutive Behavior - We shall adopt here a rigid-perfectly plastic material idealization. A concept of a rigid-plastic solid seems to be a much better representation of the real physical behavior of the material in the range of large strains than for example in the range of infinitesimal strains.

Indeed, the strains in the dented regions of the tube can reach considerable values. Experiments show that in the course of the loading process the shell

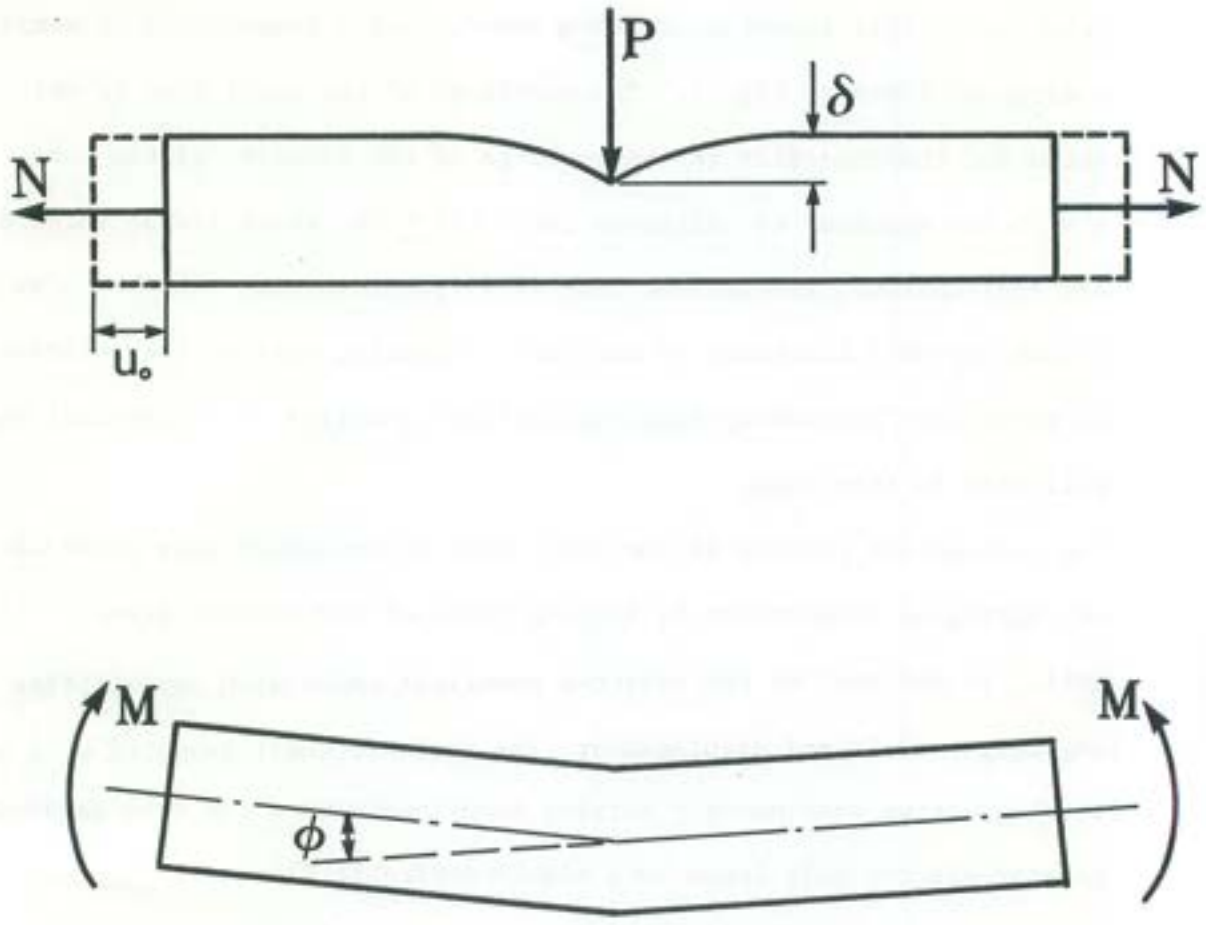

Fig. 2 Three components of generalized loading of the tube and corresponding displacement rates.

curvature in the circumferential direction changes from the initial uniform $K_o = 1/R$ to the highly localized which can be equal to $K = 6/R$ or more. The change in curvature $\Delta K = K-K_o$ is then of the order of $\Delta K \tilde{\div} 5/R$ or $\Delta K \tilde{=} 1/10t$ for a tube with $D/t = 50$. Recalling that the average through-thickness bending strain is $\varepsilon_b = t/2\ \Delta K$, we see that ε_b can easily attain 5%.

Similarly high strains may be developed in the axial direction of the affected shell element. This strain can be estimated from the approximate nonlinear formula $\varepsilon_x = 1/2(dw/dx)^2$ where w is the lateral deflection of the shell element and x is axial coordinate. Taking in the first approximation the shape of the dent to be triangular, the formula for the axial strain becomes $\varepsilon_x = 1/2(w/\xi)^2$ where ξ is the half-length of the dented zone. For severely distorted shells the central deflection may be set equal to the shell radius $w = R$. Experiments show that at this stage of the deformations, the extent of damage equals $\xi = (3 \div 5)R$; so that $\varepsilon_x \tilde{\approx} 3\%$. We can conclude that strains in the dented region can be one to two orders of magnitude higher than the maximum elastic strains that the metal tube can tolerate. This observation justifies the neglect of elastic strains and the use of the rigid-plastic material idealization in the present problem.

Equilibrium - The statement of equilibrium is expressed via the principle of virtual work or virtual velocity

$$\dot{E}_{ext} = \dot{E}_{int} \tag{1}$$

The left hand side of the above equation represents the rate of work of external forces on the corresponding velocities. In the absence of a twisting moment, the expression for the rate of change of external energy is given by, Fig. 2

$$\dot{E}_{ext} = M\dot{\theta} + N\dot{u}_o + P\dot{\delta} \tag{2}$$

The first term is due to the overall bending of the member. The second term results from the product of an axial force and the corresponding velocity of a neutral axis of the shell. The third term is due to the lateral crushing. In the case of plastic shells the rate of internal work $\dot{E}_{int}$ is given by the sum of contributions due to continuous deformations and discontinuous velocity fields in the stationary or moving plastic hinge lines

$$\dot{E}_{int} = \int_S (M_{\alpha\beta}\dot{K}_{\alpha\beta} + N_{\alpha\beta}\dot{\varepsilon}_{\alpha\beta})\, dS + \sum_{(i)} \int_{\Gamma(i)} M_o^{(i)}\dot{\psi}^{(i)}\, d\Gamma \qquad (3)$$

where dS and $d\Gamma$ denote respectively the current deformed surface element and hinge line element. The surface integration should be extended over the plastically deforming part of the shell. The symmetric components of the stress couple tensor (bending moments) and stress resultant tensor (membrane forces) are denoted respectively by $M_{\alpha\beta}$ and $N_{\alpha\beta}$. The corresponding components of the generalized strain rate tensors are curvature rates $\dot{K}_{\alpha\beta}$ and extension rates $\dot{\varepsilon}_{\alpha\beta}$. The rate of work at the "i-th" hinge line of the length $\Gamma^{(i)}$ is equal to the fully plastic bending moment $M_o^{(i)} = \sigma_o t^2/4$ times the relative rotation rate $\dot{\psi}^{(i)}$ on both sides of the hinge.

The advantage of working with the global rather than local formulation of equilibrium is that it offers a possibility of getting approximate solutions. This is accomplished by introducing into Eq. (1) a suitably chosen sub-class of the velocity and strain rate fields with only few degrees of freedom.

Geometrical Relations - With reference to the current deformed configuration, the relations between velocities and strain and curvature rates are linear and formally have the same form as those of the classical linear shell theory. In the present description the difficulty in dealing with geometrical nonlinearities has been shifted to the procedure of continuously updating the current shape

of the shell in the dented regions and the necessity of calculating first and second quadratic forms at each point of the shell. This procedure cannot be carried out in a rigorous and yet simple way. Therefore, for the sake of obtaining closed-form solutions, the formulas for the relevant components of the strain rate tensor will be derived using a simplified model of the shell to be developed in the next section. This model effectively decouples the problem of two-dimensional shell geometry into a set of one-dimensional problems, each much simpler to deal with analytically.

3. SIMPLIFIED SHELL MODEL

Our present computational model is based on the following premises:

(i) A careful inspection of actually damaged tubes reveals that the plastically deforming zone undergoing severe shape distortion is restricted to few diameters of the shell on both sides of the dent center. We assume here that the extent of the locally damaged zone is finite and is denoted by 2ξ, Fig. 3. The length ξ is unknown and is considered variable during the loading process. This assumption is fully compatible with the present rigid-plastic material idealization.

(ii) The cross-section at which the deformed part of the shell joins the undeformed part is taken to be plane and circular. Therefore no ovalization and warping of the tube exist beyond the dent-affected zone. Thomas et al. [29] reported severe ovalization and warping in short dented tubes. The observed mode clearly reduces the amount of shear and extensions in the shell walls. For longer tubes the process of ovalization and warping is suppressed by the presence of the continuing tube but this tendency can never be eliminated. Our model tube will be slightly stiffer than the actual tube because certain deformation modes have been eliminated.

(iii) Inside the plastically deforming zone the ovalization and its extreme form --the unsymmetric shape distortion are permitted. However, at the actual plane of symmetry the axial displacements are identically zero. Since there are no warping at both ends of a relatively short tube section $0 \leq x \leq \xi$, it is reasonable to assume that in addition to crushing all cross-sections undergo rigid-body translations and rotations. The above observations lead us to the present computational model of the shell. The model consist of a series of unconnected rings or slices and a bundle of unconnected generators, Fig. 4.

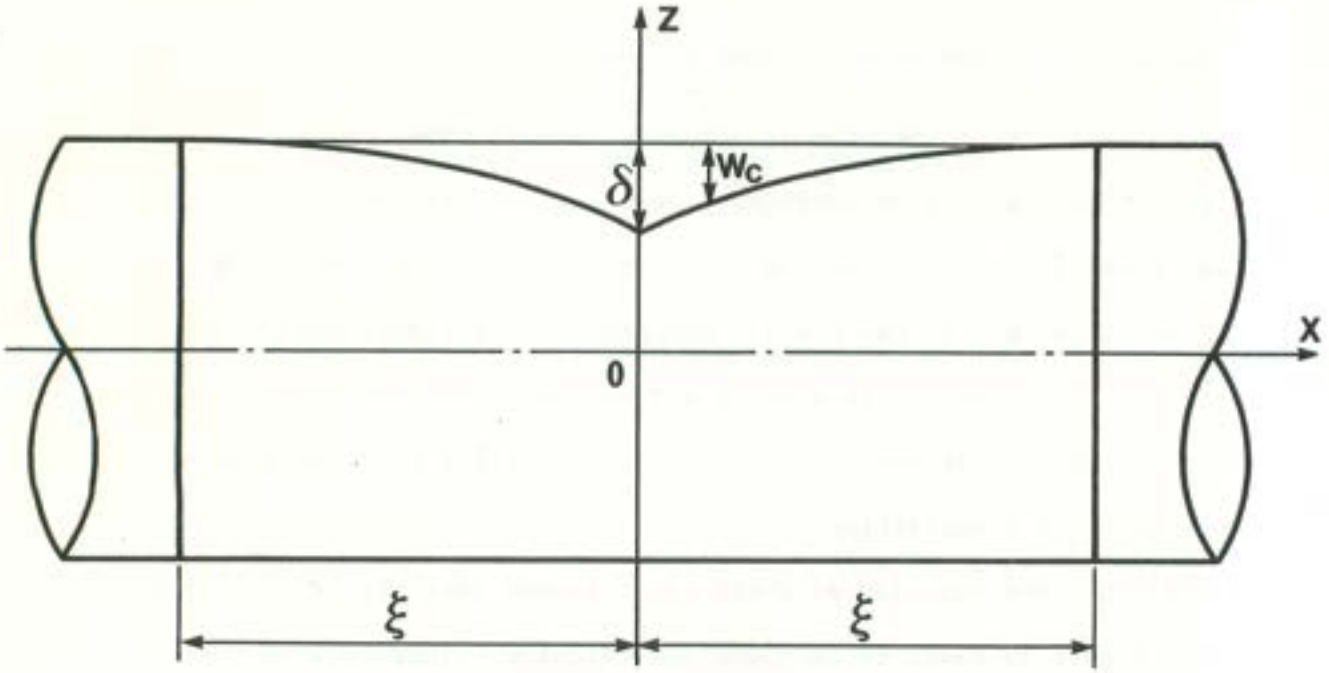

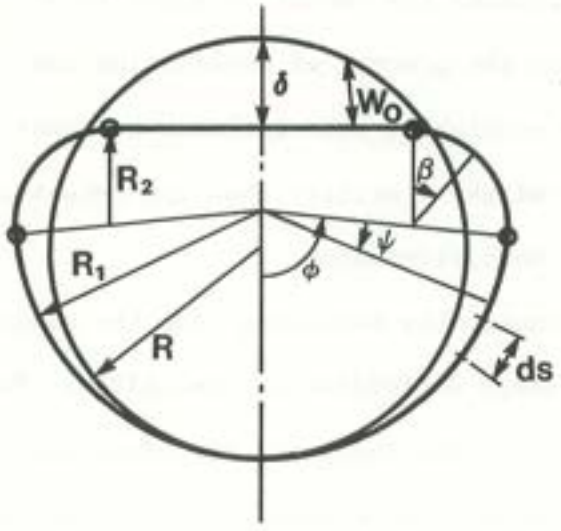

$W(x,\alpha)$

$W(x,0) = W_c(\alpha)$

$W(0,\alpha) = W_o(\alpha)$

$W(0,0) = \delta$

Fig. 3 Geometry of the plastically deforming zone.

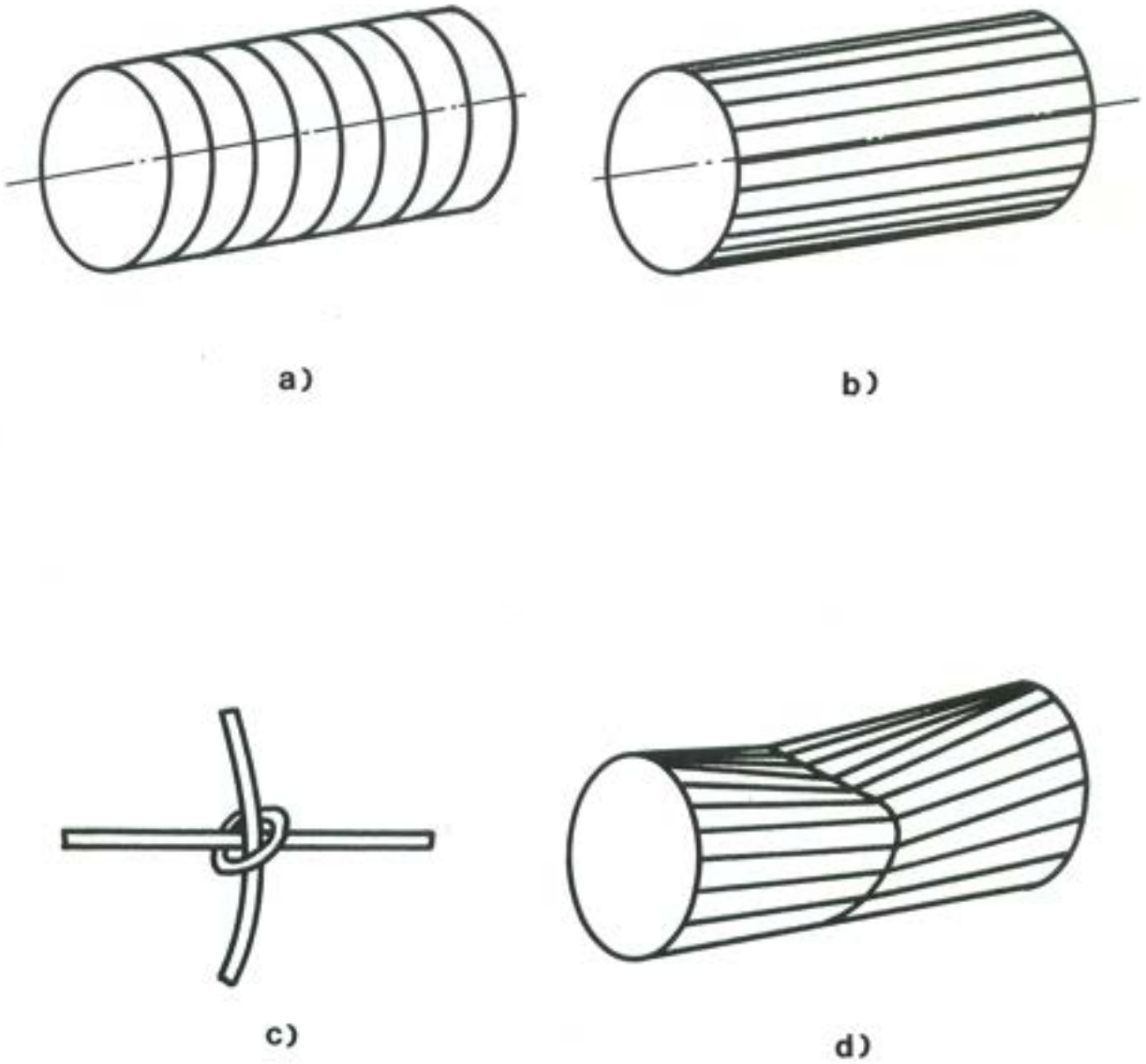

Fig. 4 Present computational model of the shell consisting of a system of rings and generators.

The rings are inextensible $\dot{\varepsilon}_{\theta\theta}=0$ and the energy is absorbed predominantly by circumferential bending in the continuous deformation field and in the stationary or moving plastic hinges. Thus, the so-called crushing energy per unit width of the ring consists of the terms

$$\bar{\dot{E}}_{crush} = \int_L M_o \dot{K}_{\theta\theta} ds + \sum_{(i)} M_o^{(i)} \cdot \dot{\psi}^{(i)} \tag{4}$$

where s is a parameter along the circumference of the ring, $L = 2\pi R$ is the total ring circumference and the summation is extended over the number of active plastic hinges. The total crushing energy in the dented zone is obtained by integrating $\dot{E}_{crush}$ over the length of the dented zone

$$\dot{E}_{crush} = 2 \int_0^{\xi} \bar{\dot{E}}_{crush} \, dx \tag{5}$$

Two points need emphasizing here. The problem of unsymmetric crushing of a plastic ring is a one-dimensional problem and can be solved without a need of calculated quadratic forms of a shell element in the deformed configuration. Secondly, the bending resistance of the ring described by M_o is taken for simplicity to be independent on axial resistance of generators N_o.

The generators are treated in our model as rigid-plastic beams which can bend and stretch or compress as the depth of the dent increases. However, the change in the longitudinal curvature of generators $\dot{K}_{xx}$ is much smaller than the change in the circumferential curvature of rings $\dot{K}_{\theta\theta}$.

In our calculations the term $M_{xx}\dot{K}_{xx}$ will be neglected. The contributions of generators in the overall energy dissipation reduce then to

$$\bar{\dot{E}}_{gen} = 2 \int_0^{\xi} \left| N_o \, \dot{\varepsilon}_{xx} \right| dx \tag{6}$$

where $N_o = \sigma_o t$ is the fully plastic membrane force in the generator of unit width. Since the axial strain $\dot{\varepsilon}_{xx}$ can be tensile in a part of the circumference and compressive in the remaining part, the absolute sign is introduced to ensure the non-negativeness of $\dot{\bar{E}}_{gen}$. As in the case of rings, the strain rate in the generators will be determined from one-dimensional consideration without making recourse to the deformed geometry of the shell. By assembling the dissipation of all generators we obtain an expression for the total rate of work of the deformed part of the shell in the longitudinal direction.

$$\dot{E}_{gen} = \int_0^{2\pi R} \dot{\bar{E}}_{gen} \, ds \tag{7}$$

The compatibility of deformation of ring and generators is ensured by requiring that the lateral displacement of the two types of one-dimensional structures be the same, Fig. 4.

The only components of the general expression for the internal energy dissipation not accounted for by the present model are twisting and shear energy $M_{x\theta}\dot{K}_{x\theta}$ and $N_{x\theta}\dot{\varepsilon}_{x\theta}$.

The calculations of those components require consideration of full shell geometry. In the present calculations the energy due to the twisting deformation $M_{x\theta}\dot{K}_{x\theta}$ is neglected. The twist rate $\dot{K}_{x\theta}$ is believed to be small compared to $\dot{K}_{\theta\theta}$. The resulting deficiencies in the energy balance equation is made up by overestimating the contribution of other components using a circumscribed yield condition.

On the other hand, the shear strain rate $\dot{\varepsilon}_{x\theta}$ does always exist in a cylindrical shell undergoing large unsymmetric deformations. The dissipation due to shear is given by

$$\dot{E}_{shear} = \int_S N_{x\theta} \, \dot{\varepsilon}_{x\theta} \, dS \tag{8}$$

In view of difficulties in evaluating the shear strain rate even in the present simple model, the shear energy will be calculated using a still more crude model of the tube with stationary plastic hinges and flat sides. The model will be described in Section 8.

4. CRUSHING OF RINGS

Our experience with locally dented tubes and also observation of other authors indicates that the cross-sectional shape of the tube in the damaged zone has a flat upper part, as shown in Fig. 1. Within the present rigid-plastic material idealization, such a flat segment can only be produced by moving plastic hinges. Suppose a plastic hinge sweeps with the tangential velocity through the material points of the ring. From the continuity of displacements it follows that the rate of rotation at the hinge $\dot{\psi}$ is linearly related to the change in curvature on both sides of the hinge $[K] = K_1 - K_2$ (see for example Hopkins [9])

$$\dot{\psi} = V[K] \tag{9}$$

The moving hinge can thus impose, remove or change the curvature of the ring as it passes through the material points. The concept of moving plastic hinges has been proved useful in the past in the dynamic analysis of rigid-plastic straight beams [16], [26]. More recently it has led to the improved solutions for axi-symmetric of quasi-static crushing of cylinders [35] and propagating buckles in pipelines [36].

The computational model of the ring is shown in Fig. 3. The ring is initially of radius R and thickness t. During the deformation process the ring flattens out and the amount of central displacement is denoted by w_c. At any stage of the crushing process, the ring consists of the top flat part and three arcs. The larger radius R_1 increases from the initial value R as the deformation process progresses while the radii of two remaining arcs shrink. The flats and arcs are separated by four symmetric moving plastic hinges. Initially, the

length of the flat segment is zero and the top central hinge splits into two hinges A and B traveling in the opposite direction. Two other hinges are also symmetric with respect to the vertical axis. They must be formed to ensure that sufficient degree of freedom exist in the ring.

The position of the lower hinge at any stage of the deformation process is denoted by ϕ, the initial value of it being ϕ_o. We define now the tangential velocity in the current, deformed configuration of the ring by

$$V_1 = \frac{ds_1}{dt} \; ; \quad V_2 = \frac{d(s_1+s_2)}{dt} \tag{10}$$

where the lengthsof arc segments s_1 and s_2 with the radii R_1 and R_2 respectively are

$$s_1 = R_1\phi \quad ; \quad s_2 = R_2(\pi-\phi) \tag{11}$$

At the same time the length of the flat segment is $s_3 = (R_1-R_2)\sin\phi$

According to the previous assumption, the ring is taken to be inextensible so that the sum of the length of the flat segment and two arcs should be constant and equal to the one half of the original circumference of the ring

$$s_1 + s_2 + s_3 = \pi R \tag{12}$$

Now, we are in the position to calculate from Eq. (9) the rate of rotation in both type of hinges

$$\dot{\psi}_1 = V_1[\frac{1}{R_2} - \frac{1}{R_1}], \quad \dot{\psi}_2 = V_2 \frac{1}{R_2} \tag{13}$$

As the hinges travel down the ring, the curvature of the two arcs changes continuously with reference to the deformed configuration, the rate of curvature

$\dot{K}_{\theta\theta}$ was found to be

$$(\dot{K}_{\theta\theta})_1 = -\frac{\dot{R}_1}{R_1^2} \quad ; \quad (\dot{K}_{\theta\theta})_2 = -\frac{\dot{R}_2}{R_2^2} \tag{14}$$

in the arcs of the lengths s_1 and s_2 respectively.

Substituting Eqs. (11), (13) and (14) into the Eq. (4) for the rate of energy in the crushing mode, we obtain

$$\bar{\dot{E}}_{crush} = 2M_o\left[\frac{V_2}{R_2} + V_1\left(\frac{1}{R_2} - \frac{1}{R_1}\right) + R_1\phi\left(-\frac{R_1}{R_1^2}\right) + R_2(\pi-\phi)\left(-\frac{\dot{R}_2}{R_2^2}\right)\right] \tag{15}$$

In the present derivation we choose the position of the hinge ϕ as a monotonically changing time like parameter. This parameter is related to the variable radii R_1, R_2 and central deflection w_c by

$$w_c = 2R - [R_1(1-\cos\phi) + R_2(1 + \cos\phi)] \tag{16}$$

By the chain rule of differentiation the derivative with respect to time is replaced by the derivative with respect to ϕ, $d/dt = d\phi/dt\ d/d\phi$.

In the present calculations we shall use the following four non-dimensional parameters

$$r_1 = \frac{R_1}{R}, r_2 = \frac{R_2}{R}, \quad \bar{w}_c = \frac{w_c}{R}, \quad \phi \tag{17}$$

Using the condition of inextensibility of Eq. (12) and the relation of Eq. (16) two out of four parameters can be eliminated. The same applies to the time rates of those parameters. In order to describe the crushing problem in terms of a single variable ($\bar{w}_c$ or ϕ) it remains to establish one more relation between the parameters involved. Noting that the radius r_2 decreases during the crushing process from the initial value $r_2=1$ at $\phi = \phi_o$, we suggest the power dependence

between r_2 and ϕ

$$r_2 = \left(\frac{\phi}{\phi_o}\right)^n \tag{18}$$

The rate form of the above equation is

$$\dot{r}_2 = n\left(\frac{\phi}{\phi_o}\right)^{n-1} \frac{\dot{\phi}}{\phi_o} \tag{19}$$

The coordinate of the initiation point of the hinge ϕ_o and the exponent n are considered as constant during the crushing process.

The parametric study was performed to find the dependence of the rate of energy due to crushing $\dot{E}_c$ on the magnitude of ϕ_o and n. This energy is a linear homogeneous function of the displacement rate $\dot{\bar{w}}_c$ and thus can be represented in the form

$$\dot{\bar{E}}_c = P_c(\bar{w}_c)\, \dot{\bar{w}}_c \tag{20}$$

where the function $P_c(\bar{w}_c)$ is independent of the velocity $\dot{\bar{w}}_c$ but does depend on the displacement.

The function $P_c(\bar{w}_c)$ represents an instantaneous crushing force necessary to deform the ring further from a given deformed shape. A short computer program was written to perform the necessary calculations and a full set of dimensionless equation used for the purpose is given in Appendix A.

The non-dimensional function $P/\left(\frac{4M_o}{R}\right)$ was plotted in Figs. 5-8 as a function of δ/R for the following combination of the parameters ϕ_o and n.

ϕ_o \ n	1/4	1/2	1	2	4
π		x	x	x	
$\pi/2$	x	x	x	x	x
0		x	x	x	

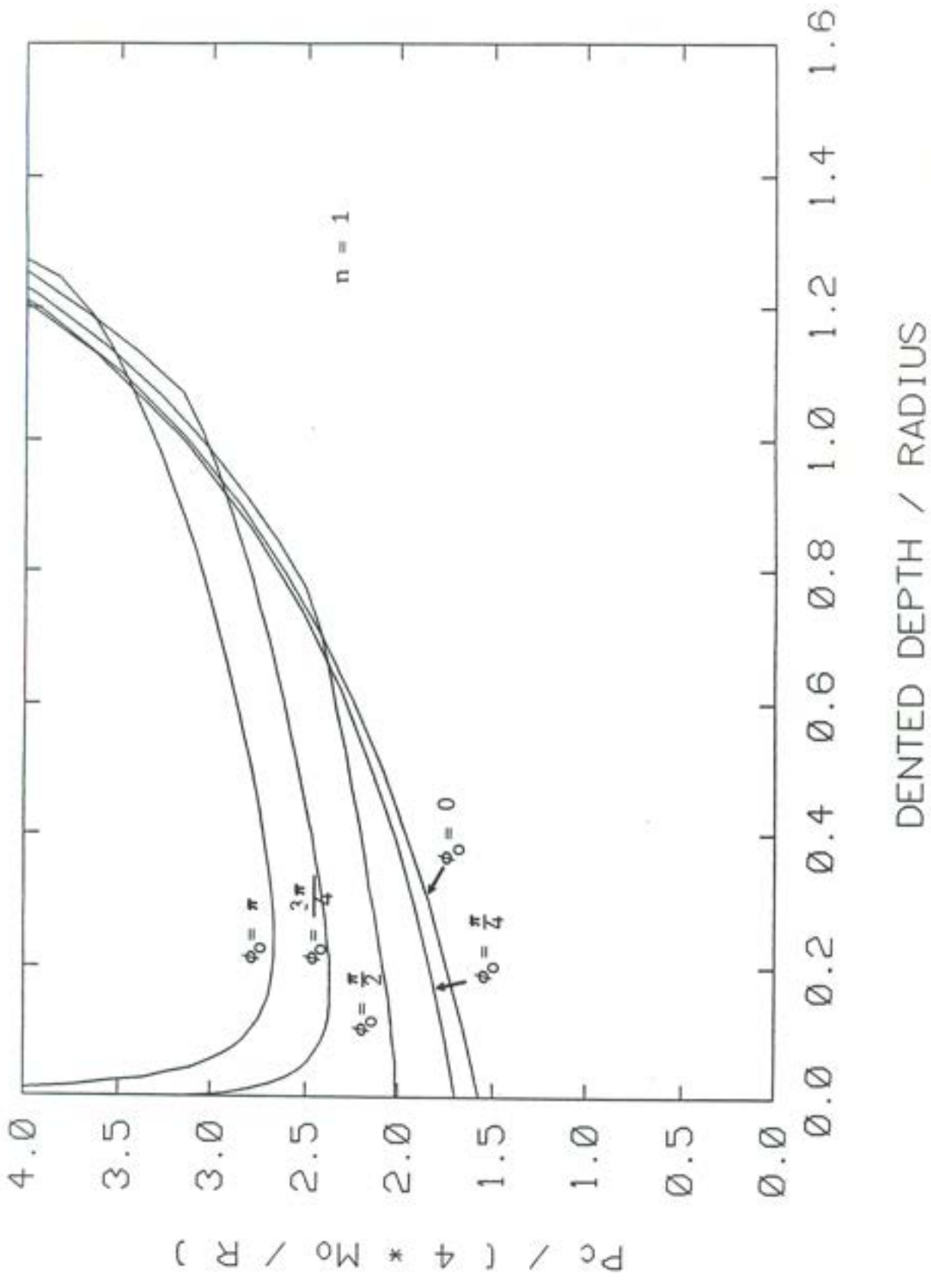

Fig. 5 Non-dimensional crushing strength of a ring versus dent depth δ/R. Constant n=1, variable ϕ_o.

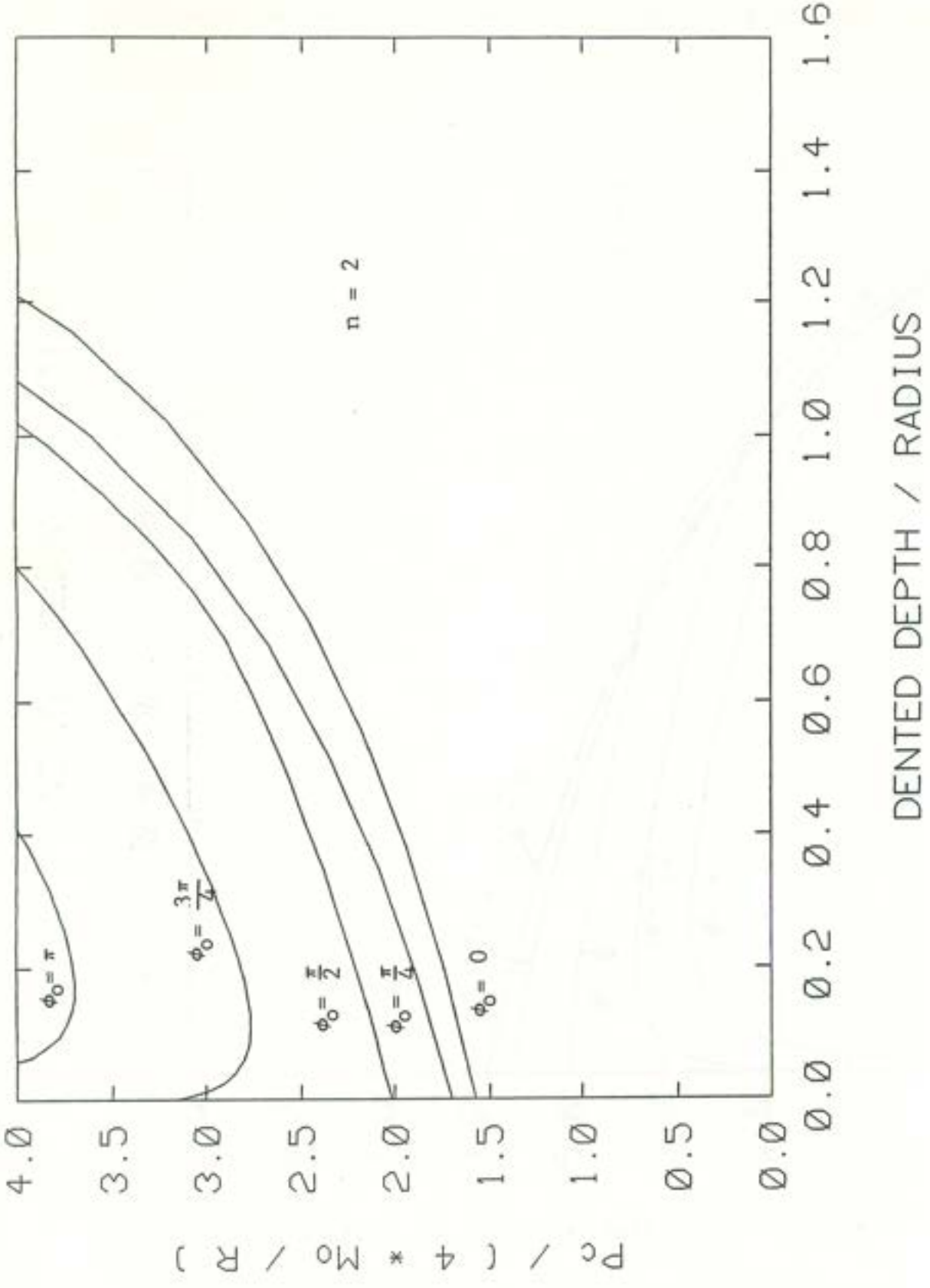

Fig. 6 Non-dimensional crushing strength of a ring versus dent depth δ/R. Constant n=2, variable ϕ_o.

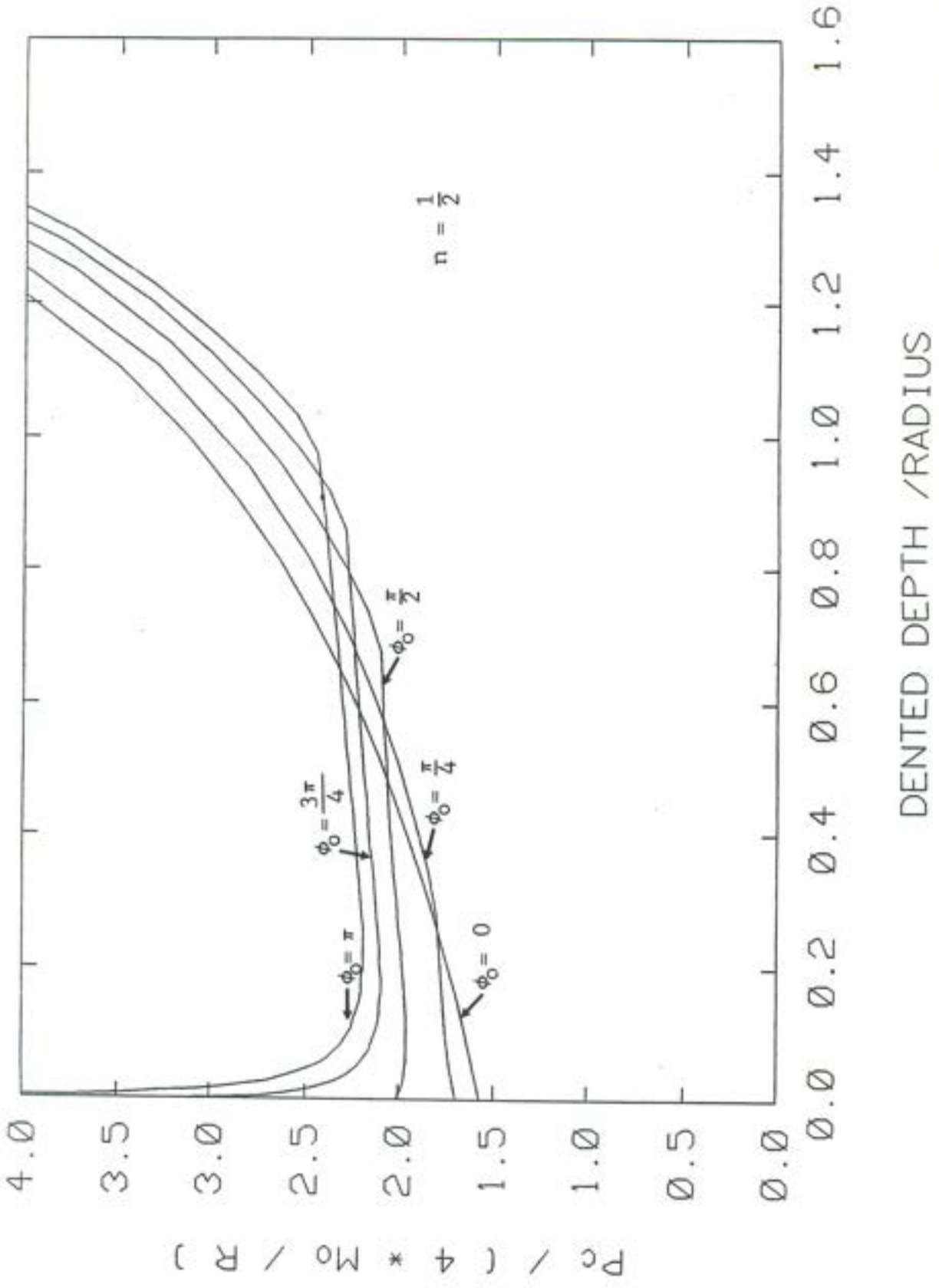

Fig. 7 Non-dimensional crushing strength of a ring versus dent depth δ/R. Constant n=1/2, variable ϕ_o.

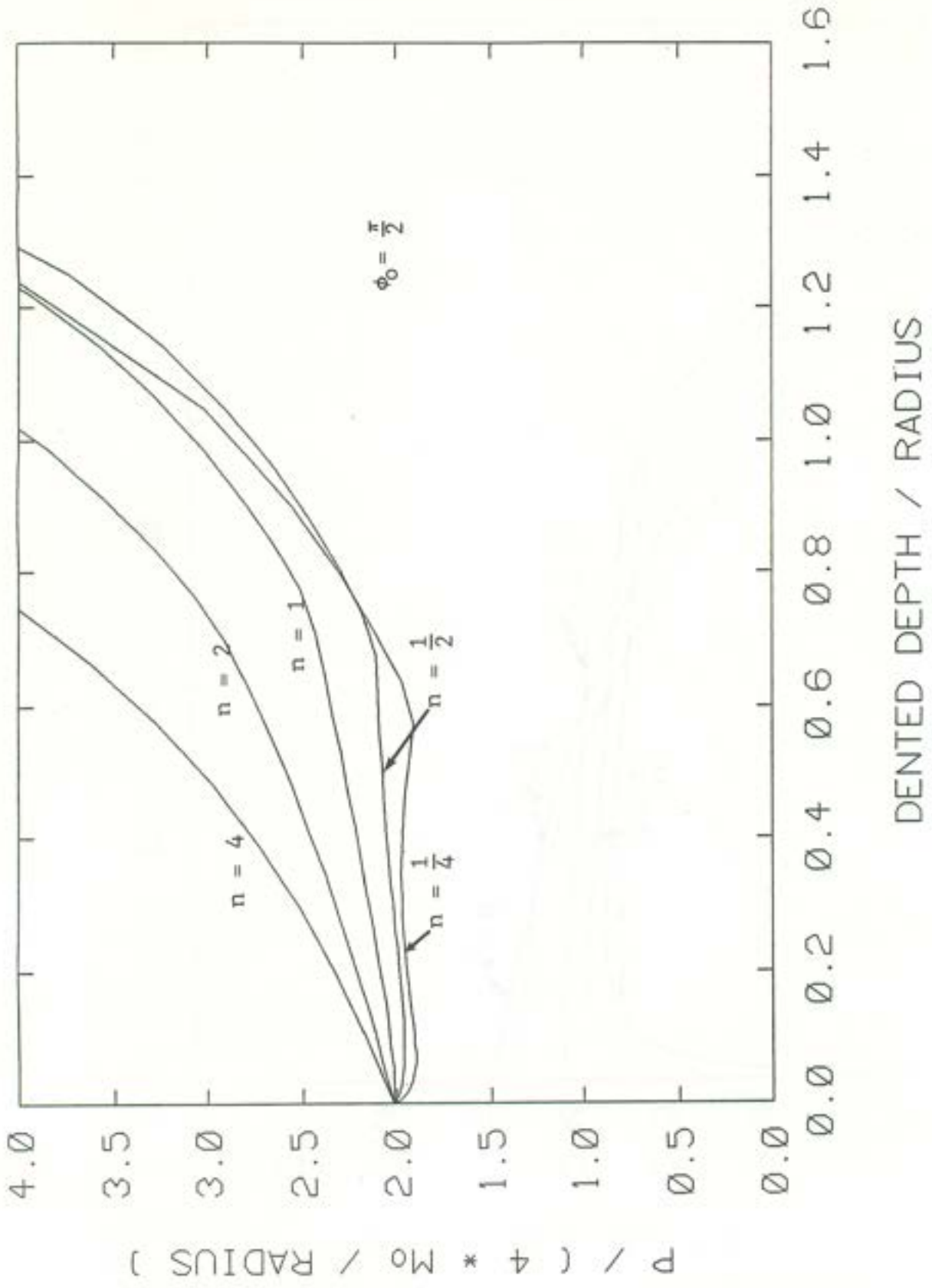

Fig. 8 Non-dimensional crushing strength of a ring versus depth depth δ/R.

Constant $\phi_o = \pi/2$, Variable n,

The corresponding shapes of the deforming rings are shown in Figs. 9-12 . It is seen that the deformation mode in which all hinges are initiated at one point $\phi_o = \pi$ gives initially an infinite crushing force and thus should not be considered as a valid mode. The lowest value of the crushing force corresponds initially to $\phi_o=0$ but the corresponding deformation mode is symmetric and thus unrealistic for our purposes. It appears that the most realistic description of the unsymmetric deformation mode of the ring is obtained for the set of parameters $\phi_o = \pi/2$, n=1. It is desirable for the present analysis to have a closed-form solution for the crushing strength of the ring. A lower bound constant force solution is given by the formula

$$P_c = \frac{8M_o}{R} \tag{21}$$

For larger deflections, a better approximation of the exact solution is the parabolic relation

$$P_c = \frac{8M_o}{R} [1 + \frac{1}{2} \bar{w}_c^2] \tag{22}$$

The above formulas will be used throughout the remainder of this paper. We would like to stress that the parameters ϕ_o and n cannot be uniquely determined from the analysis of rigid-plastic rings alone. It is possible though that certain deformation modes of tubes which dissipate less energy in crushing may actually dissipate more energy in extension of generators or in shear. There may then be a unique mode which yield an optimum solution. Such an optimization procedure will not be explored in the present paper. It should be noted that the crushing force corresponding to the simplest symmetric collapse mode consisting of four stationary plastic hinges [2] is given by

$$P_c = \frac{4M_o}{R} (1 - \frac{\bar{w}_c}{2})^{-1/2}$$

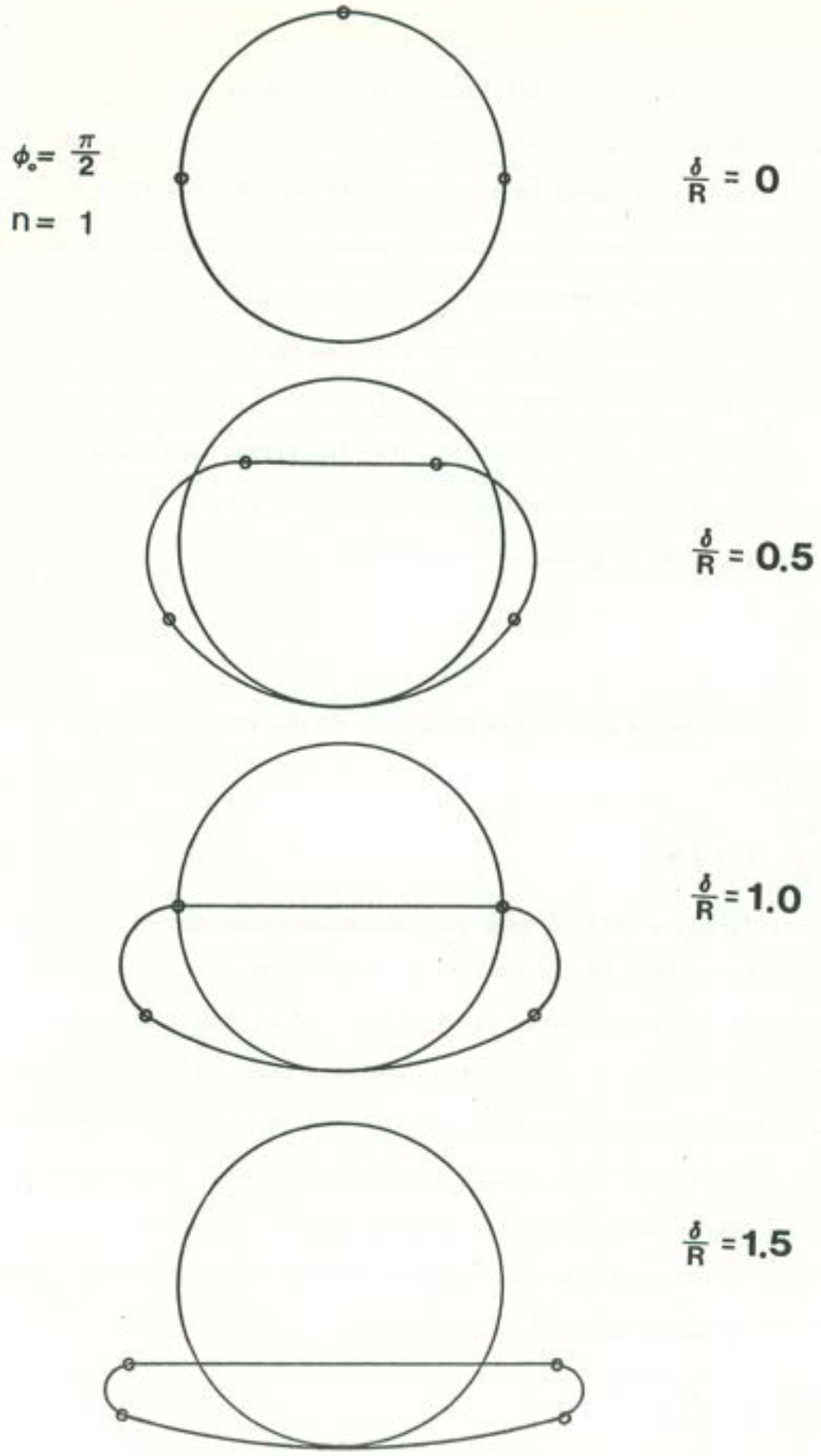

Fig. 9 Initial and intermediate shapes of deformed rings with $\phi_o = \pi/2$ and n=1.

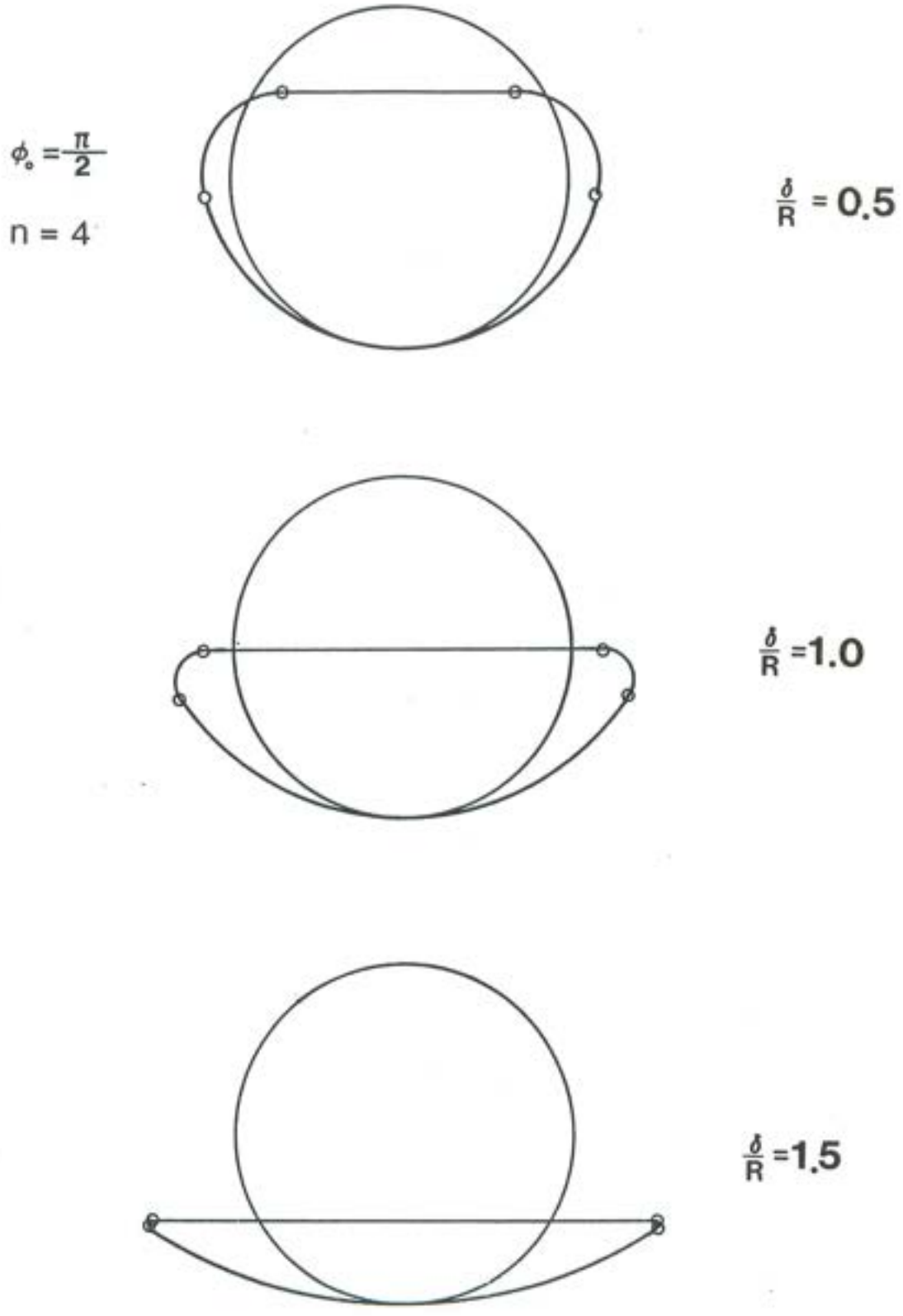

Fig. 10 Initial and intermediate shapes of deformed rings with $\phi_o = \pi/2$ and n=4.

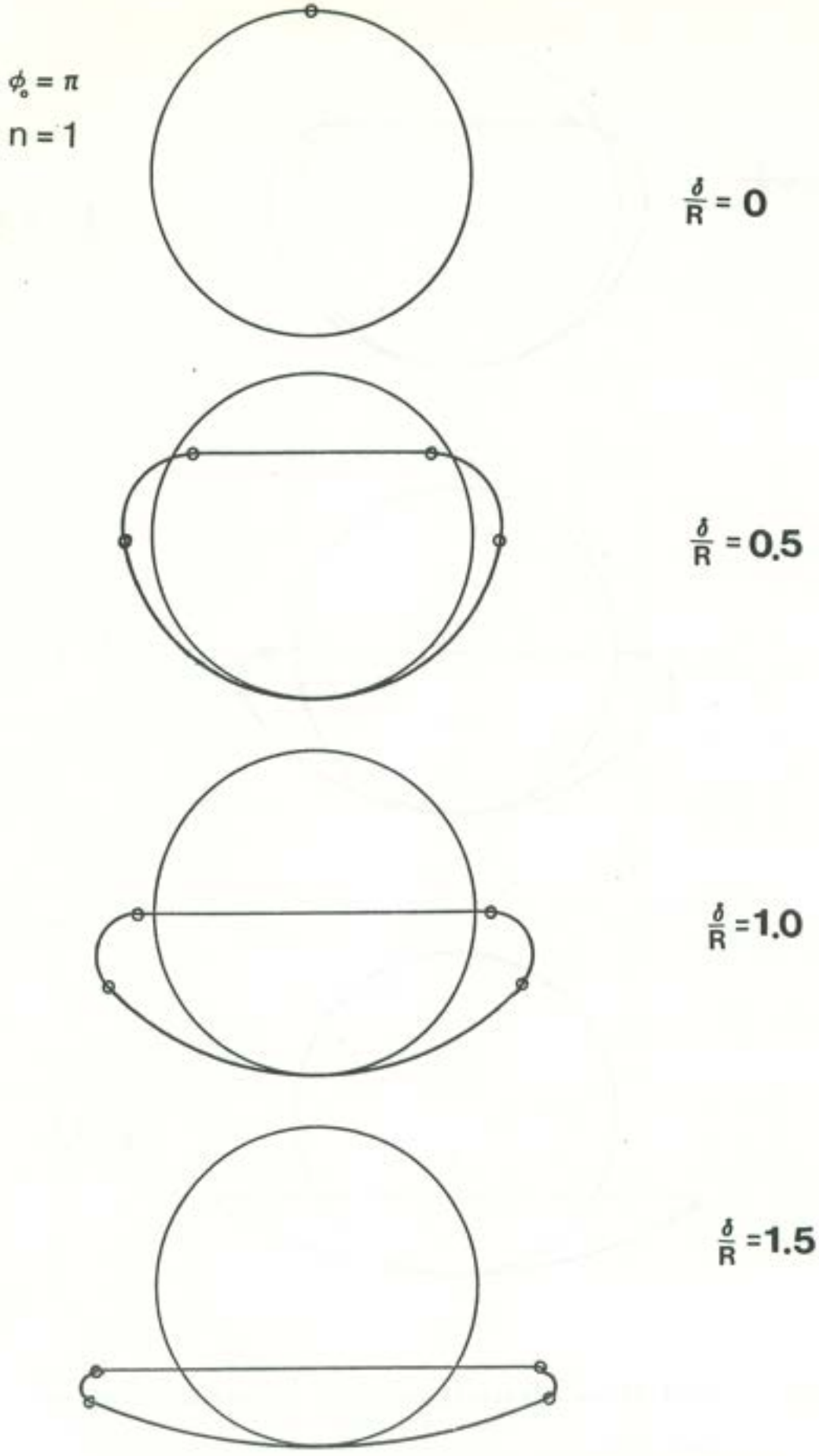

Fig. 11 Initial and intermediate shapes of deformed rings with $\phi_o = \pi$ and n=1.

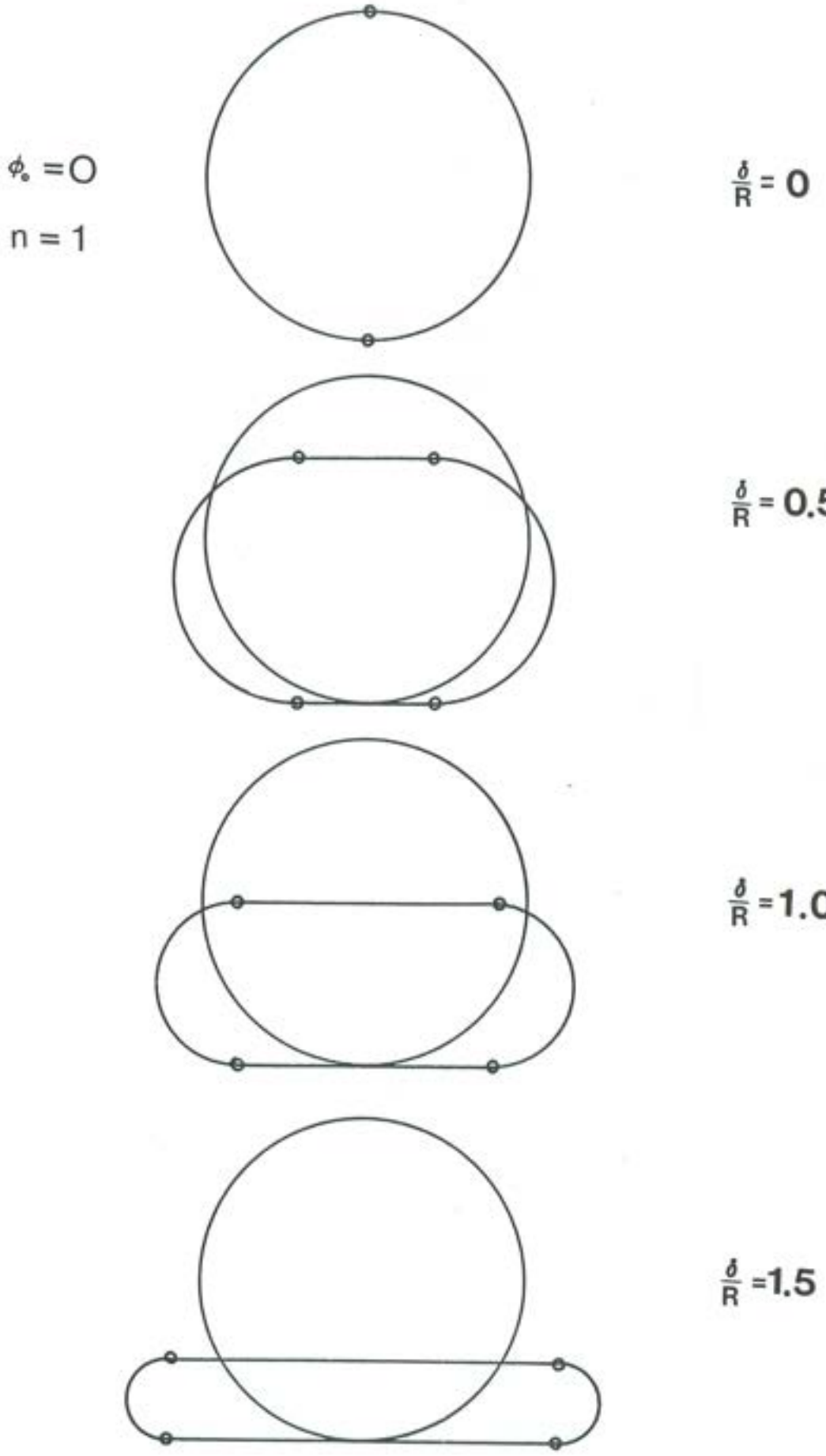

Fig. 12 Initial and intermediate shapes of deformed rings with $\phi_o=0$ and n=1.

This is less than half of either Eq. (21) or Eq. (22).

In this context it is in place to mention the experimental theoretical findings by Reid [39], who showed that initial collapse load and the entire load-deflection characteristics of rings increases when the deformation changes from a symmetric to an unsymmetric mode.

The total crushing energy in the dented zone is obtained by substituting Eqs. (20 to 22) into Eq. (5). This results in

$$\dot{E}_{crush} = 2\int_0^{\xi} \frac{8M_o}{R}(\dot{w}_c)(x)\, dx \tag{23a}$$

$$\dot{E}_{crush} = 2\int_0^{\xi} \frac{8M_o}{R}\left[1 + \frac{\bar{w}_c}{2}(x)\right] \dot{w}_c(x)dx \tag{23b}$$

for the constant and parabolic crushing force respectively. In order to perform the integration, the velocity profile of the generators should be known. In addition, the integrand of Eq. (23b) involves the displacement profile of the generators $\bar{w}_c(x)$ which is unknown and is sought as a part of the solution. An iterative procedure would then be necessary to solve the title problem using Eq. (23b).

Following the analysis of large dynamic deformations of rigid-plastic beam [9], [16] the velocity field of the leading generator can be assumed to vary linearly with x, according to

$$\dot{w}_c = \dot{\delta}\left(1 - \frac{x}{\xi}\right) \tag{24}$$

where $x=\xi$ is the point of an instantaneous rotation. With the above expression, the integration of Eq. (23a) can be performed to give

$$\dot{E}_{crush} = \frac{8M_o \xi \dot{\delta}}{R} \tag{25}$$

It will be shown in Section 6 that the solution of the indentation problem of a tube with full end fixity, based on Eq. (25) leads to the simple parabolic displacement profile of the leading generator in the dented zone.

$$w_c(x) = \delta\left(1 - \frac{x}{\xi}\right)^2 \tag{26}$$

Introducing Eq. (24) and Eq. (26) into Eq. (23b), we obtain an improved expression for the rate of energy in the crushing mode

$$\dot{E}_{crush} = \frac{8M_o\xi\dot{\delta}}{R}\left[1 + \frac{1}{6}\left(\frac{\delta}{R}\right)^2\right] \tag{27}$$

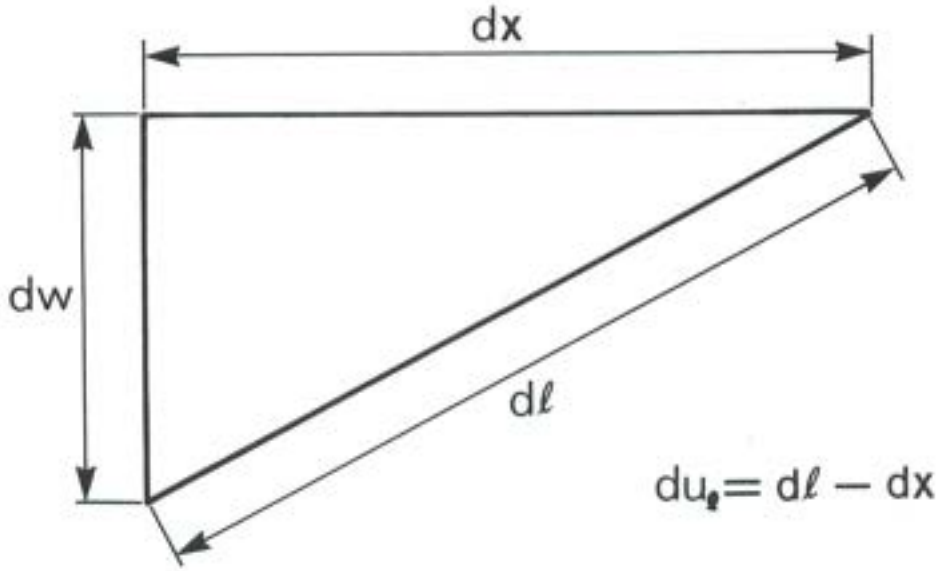

Fig. 13 Geometry of a deformed generator in the total Lagrangian description.

5. DEFORMATIONS OF GENERATORS

The axial strain are $\dot{\varepsilon}_{xx}$ appearing in Eq. (6) should be evaluated in the current deformed configuration. The fact that $\dot{\varepsilon}_{xx}$ is a linear differential operator of velocities makes it possible to decompose $\dot{\varepsilon}_{xx}$ into three parts:

(i) The strain rate $\dot{\varepsilon}_1$ due to local denting. This component is different for every generator.

(ii) The strain rate $\dot{\varepsilon}_2$ due to the uniform compression or extension of the tube.

(iii) The strain rate $\dot{\varepsilon}_3$ due to the overall bending and rotation of the cross-section. The component $\dot{\varepsilon}_3$ changes from a generator to generator.

The expression for the rate of energy dissipation by a generator, given by Eq. (6) takes then the form

$$\dot{\bar{E}}_{gen} = 2N_o \left| \int_{\mathcal{L}} (\dot{\varepsilon}_1 + \dot{\varepsilon}_2 + \dot{\varepsilon}_3) d\ell \right| \tag{28}$$

Because no change of sign of total strain rate $\dot{\varepsilon}_{xx} = \dot{\varepsilon}_1 + \dot{\varepsilon}_2 + \dot{\varepsilon}_3$ takes place within a given generator, the absolute value sign can be taken outside the integration sign.

The last two components appearing in the integrand are normally present in the classical theory of plastic thin-walled columns without sectional collapse. The first one introduces the effect of the local dent.

Since the integration Eq. (28) can be carried out term by term, consider first the contribution of $\dot{\varepsilon}_1$. From the definition of the strain rate in the updated Lagrangian description

$$\dot{\varepsilon}_1 = \frac{d\dot{u}_\ell}{d\ell} \tag{29}$$

where $\dot{u}_\ell$ is the component of the velocity vector in the tangential direction to the deformed generator.

Integrating Eq. (21) accorting to Eq. (28) we obtain

$$\int \dot{\varepsilon}_1 d\ell = \int d\dot{u}_\ell = \dot{u}_\ell\Big|_{\ell=\mathcal{L}} - \dot{u}_\ell\Big|_{\ell=0} \tag{30}$$

At the end of the plastically deforming zone $\ell=\mathcal{L}$, the tangential velocity vanishes $\dot{u}_e(\ell=\mathcal{L}) = 0$.

The assumption that planes remain planes in the denting process of tubes provides a relation between the tangential and normal component of the velocity field shown in Fig. 13.

$$\frac{d\dot{u}_\ell}{dx} = \frac{\frac{dw}{dx}\frac{d\dot{w}}{dx}}{[1 + (\frac{dw}{dx})^2]^{1/2}} \tag{31}$$

Integrating Eq. (31) in the limits $(0,\xi)$ we obtain

$$-\dot{u}_\ell\Big|_{x=0} = \int_0^\xi \frac{\frac{dw}{dx}\frac{d\dot{w}}{dx}}{[1 + (\frac{dw}{dx})^2]^{1/2}} dx \tag{31a}$$

Taking $(dw/dx)^2$ to be small compared to unity and assuming a linear velocity field described by Eq. (24), the integration can be performed to give $u_\ell(x=0) = \dot{w}_o w_o/\xi$. But the points $x=0$ and $\ell=0$ are identical so that the contribution of the rate of energy dissipation by a generator is equal to

$$2N_o \int \dot{\varepsilon}_1 d\ell = \frac{w_o \dot{w}_o}{\xi} \; 2N_o \tag{32}$$

The bending and extension strain rates result from the beam-like theory

$$\dot{\varepsilon}_2 + \dot{\varepsilon}_3 = \frac{d\dot{u}}{dx} + z\dot{K} \tag{33}$$

where $\dot{K} = d\dot{\theta}/dx$. To be consistent with the above definitions, the integration is performed with respect to the undeformed axis of the tube

$$\int_0^{\xi} (\dot{\varepsilon}_2+\dot{\varepsilon}_3)dx = \dot{u}\Big|_{x=\xi} - \dot{u}\Big|_{x=0} + z\dot{\theta}\Big|_{x=\xi} - z\dot{\theta}\Big|_{x=0} \tag{34}$$

Observing that $\dot{u}\Big|_{x=o} = \dot{\theta}\Big|_{x=o} = 0$ and denoting $\dot{u}\Big|_{x=\xi} = \dot{u}_o$ and $\dot{\theta}\Big|_{x=\xi} = \dot{\theta}_o$, the total dissipated by the deforming generator is equal to

$$\dot{E}_{gen} = 2N_o \left| \frac{w_o \dot{w}_o}{\xi} + \dot{u}_o + z\dot{\theta}_o \right| \tag{35}$$

The magnitude of the displacement and velocity of the generators is a function of the arc length s or the central angle $\alpha = s/R$ measured from the leading generator. Those functions were calculated in the Appendix B for the optimum ring model with $\phi_o = \pi/2$ and n=1. Plots of the displacement $w_o(\alpha)/R$ and the product $w_o(\alpha)\,\dot{w}_o(\alpha)/R^2$ are shown in Figs. 14 and 15 for several values of the depth of the dent δ/R.

The area under the respective curves is always positive and, according to Eq. (7) represents the total rate of energy absorbed in the dented zone by the generators in the absence of any overall rotation $\dot{\theta}_o$ and translation $\dot{u}_o$.

This energy was calculated in Ref. [12] in an approximate way using a triangular distribution of the function shown in Fig.15 by the dashed line

$$\frac{\dot{w}_o w_o}{R^2} = \frac{\dot{\delta}\delta}{R^2}\left(1 - \frac{\alpha}{\pi}\right) \tag{37}$$

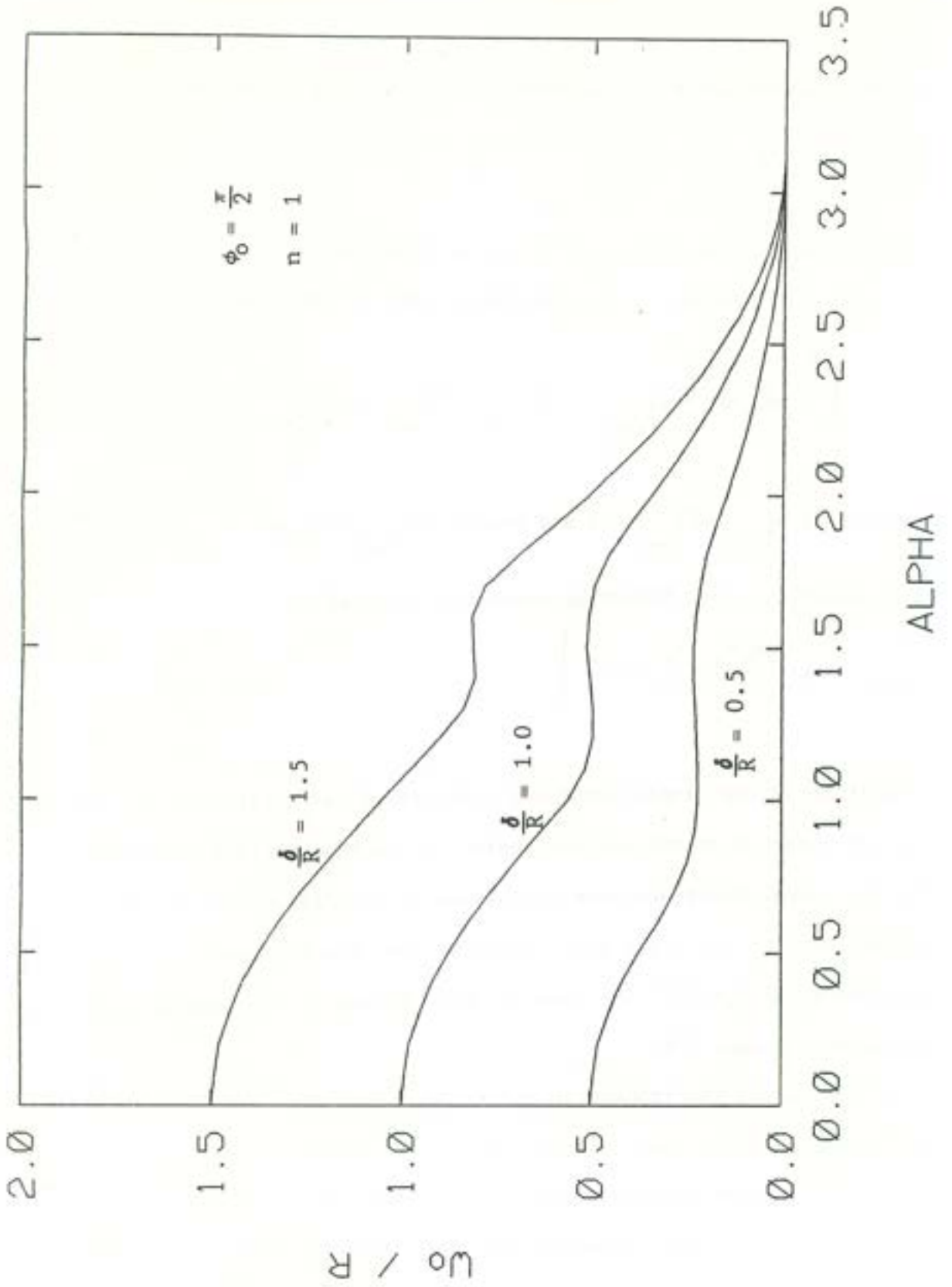

Fig. 14 Displacement of generators at the symmetry plane x=0 as a function of the circumferential coordinate α at two values of the dent depth.

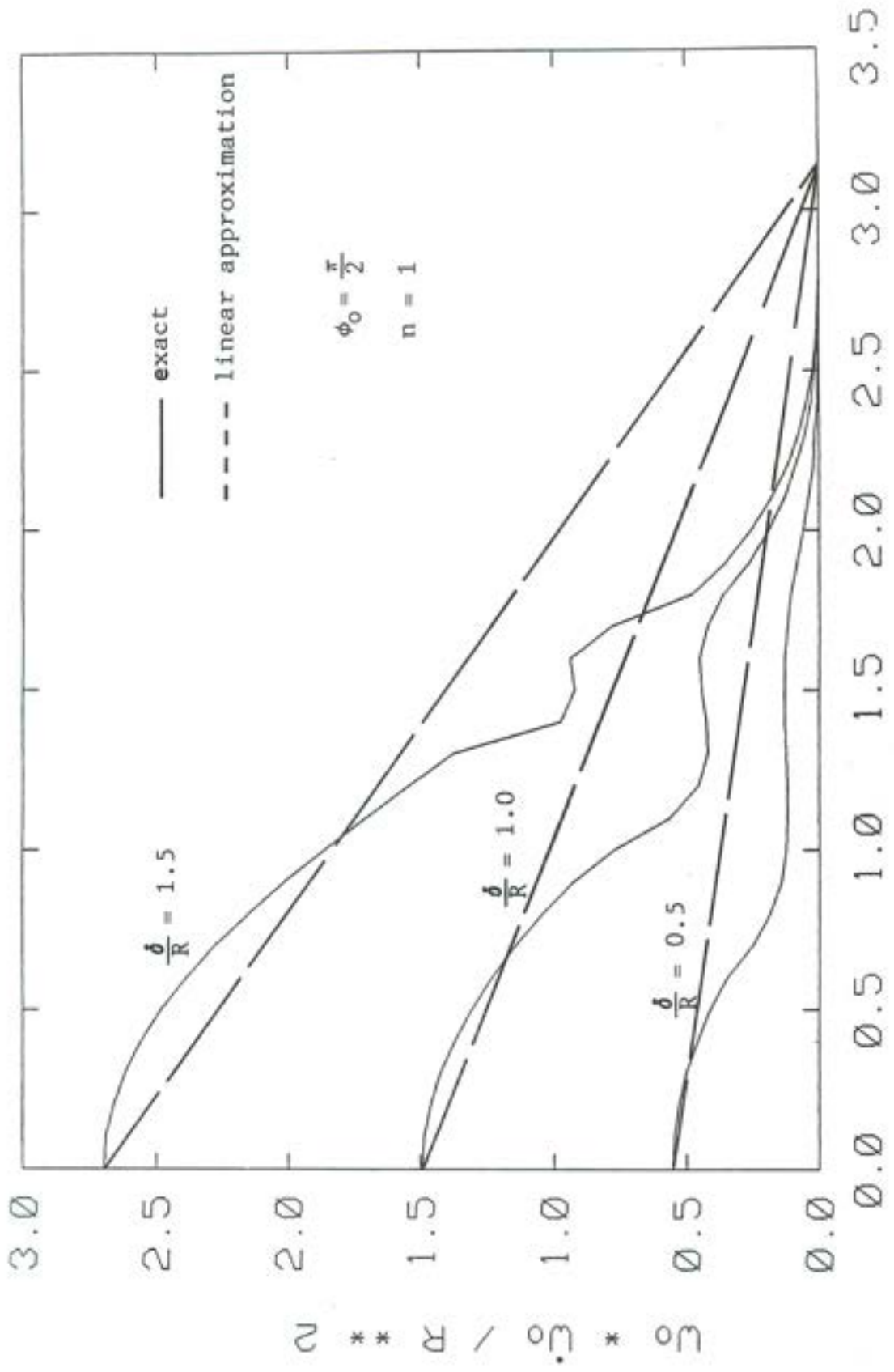

Fig. 15 Distribution of dimensionless energy dissipation of generators along the circumference of the tube for three values of dent depth

The resulting dissipation rate is given by the equation

$$\dot{E}_{gen} = 2\pi N_o R \frac{\delta}{\xi} \dot{\delta} \tag{38}$$

which overestimates the actual energy by a considerable amount.

A more accurate result is obtained by taking a parabolic approximation, Fig. 16

$$\frac{\dot{w}_o w_o}{R^2} = \frac{\delta\dot{\delta}}{R^2} \left(1 - \frac{\alpha}{\pi}\right)^2 \tag{39}$$

Substituting Eq. (39) along with $\dot{\theta}_o = \dot{u}_o = 0$ into Eqs. (35) and (7) a lower value of the dissipation is obtained.

$$\dot{E}_{gen} = \frac{4}{3} \pi N_o R \frac{\delta}{\xi} \dot{\delta} \tag{40}$$

As can be seen from Fig. 16, Eq. (39) provides a reasonably good approximation of the function $w_o(\alpha)\dot{w}_o(\alpha)$ in the range $\pi/2<\alpha<\pi$ but poor approximation for $0<\alpha<\pi/2$. A more accurate representation of the same function for small α is obtained by a different parabolic formula, expressed by

$$\frac{w_o \dot{w}_o}{R^2} = \frac{\delta\dot{\delta}}{R^2} \left[1 - \left(\frac{2\alpha}{\pi}\right)^2\right] \tag{41}$$

The integration of Eqs. (7) and (35) is again straightforward leading to the expression identical to Eq. (40). In most of the calculations to follow the function of Eq. (39) will be used. The only exception is the case of a free-free tube where zero moment condition requires a more precise representation of the energy dissipated by the generators in the dented zone, i.e., for small α. Accordingly, the formula of Eq. (41) was found to yield better results.

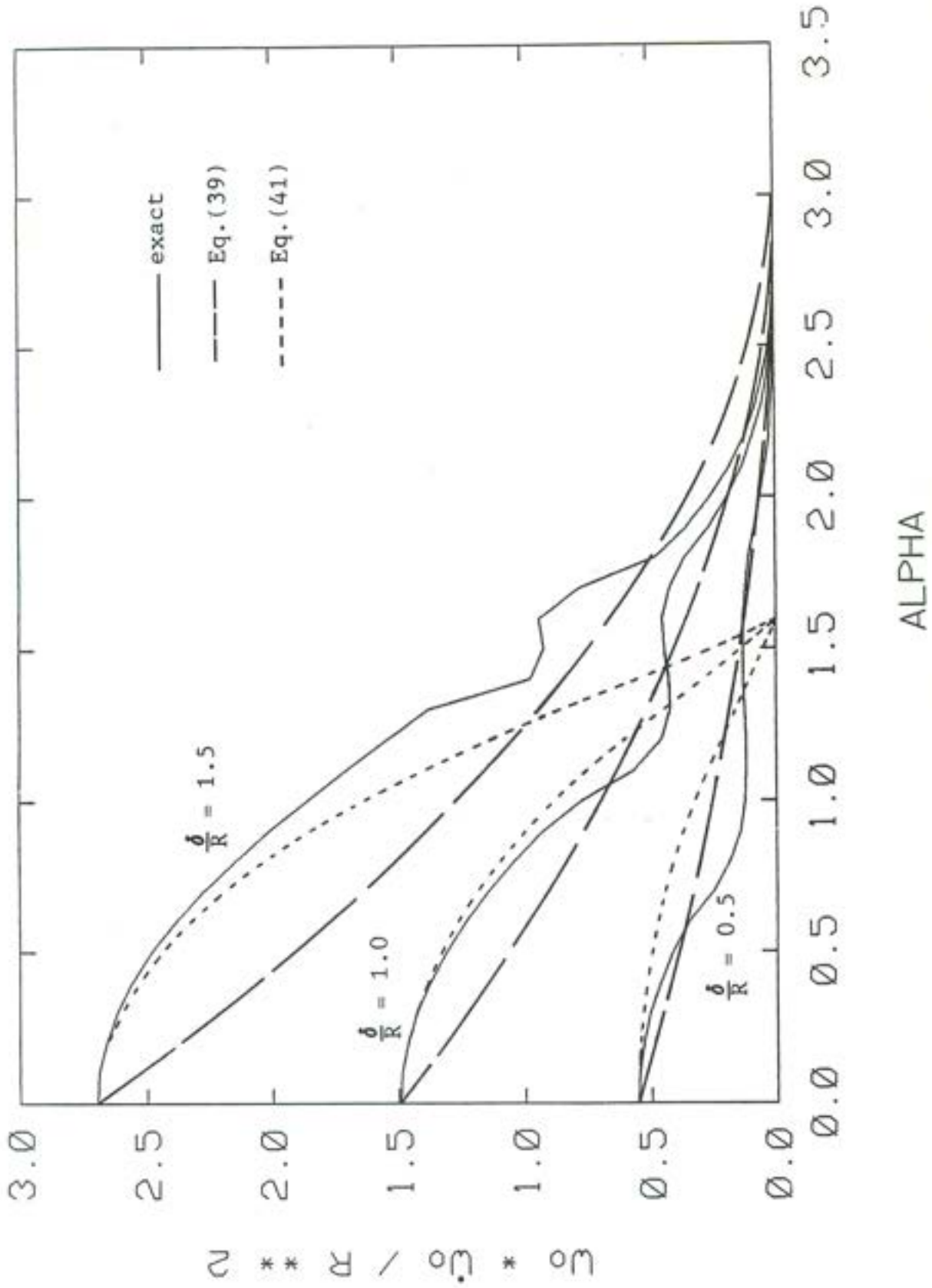

Fig. 16 Exact plot of rate of energy of generators $\dot{E}_{gen}$ and two parabolic approximations, Eq. (39) is denoted by dashed lines and Eq. (41) by dotted lines.

Returning to the general case of Eq. (35) the function $\dot{u}_o$ describes a uniform elongation or shortening of the tube and thus is independent of the coordinate s or α. The z-coordinate appearing in Eq. (35) can be uniquely related to the angle α by identifying each generator on the undeformed section of the tube

$$z = R \cos\alpha \tag{42}$$

For a fixed depth of the dent δ, the extensional energy becomes a function of four parameters ξ, $\dot{\delta}$, $\dot{u}_o$ and $\dot{\theta}_o$. Those parameters will be determined from the boundary conditions and the energy minimization procedure, as described in the next section.

6. INDENTATION OF A CONTINUOUSLY SUPPORTED TUBE

The boundary condition for the present problem can be specified with the help of the expression of Eq. (2) for the rate of external work. In this section we shall consider loading of finite length tube resting on a rigid foundation. In all cases the deformations are induced by pressing into the tube a rigid indentor at a constant rate $\dot{\delta}$. The indentation depth δ is then an increasing function of time. The reaction force under the punch $P(\delta)$ is unknown and will be found as a part of the solution. Out of four remaining parameters in the Eq. (2), two should be prescribed to uniquely define $\dot{E}_{ext}$. There are four possible combinations depending on which static or kinematic quantities are prescribed. This gives rise to four general types of boundary conditions. In addition, a few subcases will be considered when one or two quantities of interest vanish. This brings the total number of possible boundary condition to eight. All of them are described and illustrated in Table 1.

In order to illustrate the present methodology, the solution for the cases 1, 2a and 4c will be worked out in details.

Tube with full end fixity. The ends of the tube are constrained against rotation and axial displacement. Since the sections of the tube outside the dented zone $x > \xi$ are rigid, the boundary conditions imply that $\dot{u}_o=0$ and $\dot{\theta}_o=0$. The rate of external work is reduced to $\dot{E}_{ext} = P\dot{\delta}$. The rate of internal work is a sum of the dissipation of rings and generators $\dot{E}_{int} = \dot{E}_{crush} + \dot{E}_{gen}$. As a first approximation consider expressions of Eqs. (25) and (40) for the crushing and external energy respectively. The energy balance postulate of Eq. (1) yields

$$P\dot{\delta} = \frac{8M_o\xi\dot{\delta}}{R} + \frac{4}{3}\pi N_o R\frac{\delta}{\xi}\dot{\delta} \qquad (43)$$

Table 1

No	Prescribed			
1	$\dot{\delta}$	$\dot{u}_o = 0$	$\dot{\theta}_o = 0$	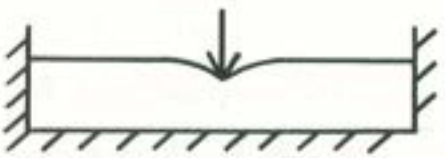
2	$\dot{\delta}$	N	$\dot{\theta}_o = 0$	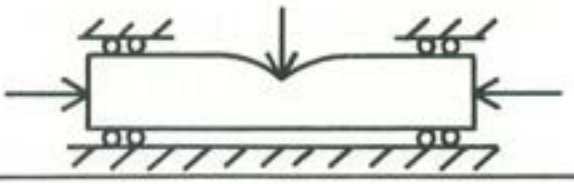
2a	$\dot{\delta}$	$N = 0$	$\dot{\theta}_o = 0$	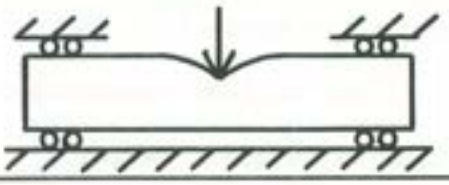
3	$\dot{\delta}$	$\dot{u}_o = 0$	M	
4	$\dot{\delta}$	N	M	
4a	$\dot{\delta}$	$N = 0$	M	
4b	$\dot{\delta}$	N	$M = 0$	
4c	$\dot{\delta}$	$N = 0$	$M = 0$	

Eight Possible Cases of Boundary Conditions

The term $\dot{\delta}$ can be dropped out from both sides of the above equation. The Eq. (41) provides the solution to the indentation problem in terms of a single unknown parameter ξ. It is plausible that the length of the locally dented zone adjusts itself in such a way as to minimize the crushing force at any stage of the indentation process. Indeed the minimum force exists for each value of the indentation depth and the relation between ξ and δ, found from $\partial P/\partial \xi = 0$ is given by

$$\frac{\xi}{R} = \sqrt{\frac{2\pi\delta}{3t}} \tag{44}$$

Substituting Eq. (44) back into Eq. (43), we obtain the desired force-deflection characteristics of the indentation process

$$\frac{P}{M_o} = 16\sqrt{\frac{\pi}{3}}\sqrt{\left(\frac{D}{t}\right)\left(\frac{\delta}{R}\right)} \quad \text{- Present} \tag{45}$$

The present solution can be compared with a still more crude approximation derived in Ref. [12], using a triangular rather than parabolic variation of the rate of energy dissipation by generators of Eqs. (37) and (38). The difference is only in the coefficient

$$\frac{P}{M_o} = 16\sqrt{\frac{\pi}{2}}\sqrt{\left(\frac{D}{t}\right)\left(\frac{\delta}{R}\right)} \quad \text{- Ref. [12]} \tag{46}$$

Despite their simplicity, the solutions of Eqs. (44) and (45) describe all important features of the plastic behavior of tubes under lateral concentrated loads. The crushing force is seen to depend linearly on the flow stress of the material and there is a square root dependence on both the diameter-to-thickness ratio and the normalized dent depth.

Having found the dependence of ξ on δ it is possible to derive an expression for the deflection profile of the dented region. The instantaneous velocity in the dented region is linear $\dot{w}(x,t) = \dot{\delta}[1 - x/\xi(t)]$. However, because the extent of the damaged zone ξ also changes in time, the resulting permanent deflection shape is nonlinear. The deflection is a time-integral of velocities

$$w(x,t) = \int_{T(x)}^{t} \dot{w}(x,t)dt = \int_{T(x)}^{t} \dot{\delta}(t)\ (1 - \frac{x}{\xi(t)})\ dt \qquad (47a)$$

where $T(x)$ is the time at which $x=\xi$. Changing the integration variable from t to δ,Eq. (47a) can be written in an alternative form

$$w(x,\delta) = \int_{[T(x)]}^{\delta} (1 - \frac{x}{\sqrt{\frac{2\pi R}{3t}}\ \sqrt{\delta}})\ d\delta \qquad (47b)$$

Integrating the above expression and noting that at $x=\xi$, $\dot{\delta} = 3tx^2/2\pi R^2$, the deflection profiles becomes

$$w(x,\delta) = \delta(1 - \frac{x}{\xi})^2 \qquad (48)$$

It is worth noting that an identical expression for the deflection profile was derived in Ref. [12] using a crude model of the shell. This rather surprizing result follows from the fact that derivation of the normalized shape of the dented zone is insensitive to the detailed calculation of the bending and extensional deformation mode. What matters here is the functional dependence of $\dot{E}_{crush}$ on ξ and $\dot{E}_{gen}$ on $1/\xi$, which is the same in our present and 1982 model.

Improvements in the present solution can be introduced by considering more exact expression for the total extensional energy. A small computer program was written for that purpose and the corresponding results are shown in Fig. 19 along with the approximate solution of Eq. (45).

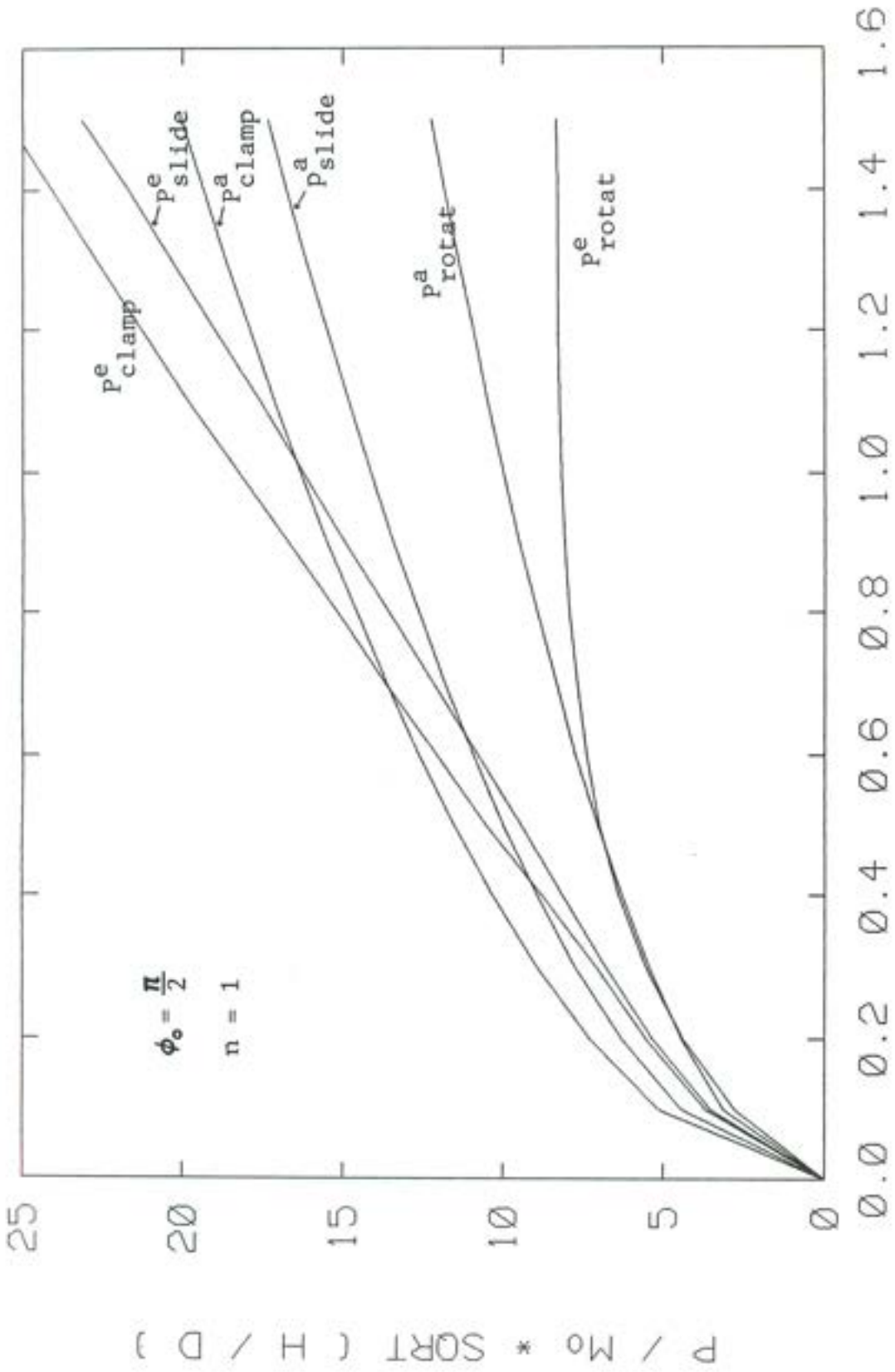

Fig. 19 Comparison of "exact" and approximate force-deflection characteristics of the plastic indentation process for all three types of boundary conditions.

Tube free to move axially but restricted from rotation (Case 2a). This is the next step in complexity in the series of nine different boundary conditions. With N=0 and $\dot{\theta}_o=0$, the rate of external energy is the same as in the case of a fully clamped tube, i.e., $\dot{E}_{ext} = P\dot{\delta}$. The rate of internal work, and more specifically the rate of energy dissipation by the generators will differ because, according to Eq. (35), there are two independent components of the velocity $\dot{\delta}$ and $\dot{u}_o$. The missing relation between $\dot{\delta}$ and $\dot{u}_o$ is obtained from the condition of zero axial force N=0. The total axial force in the cross-section is defined by

$$N = 2\,\sigma_o t R \int_0^{\pi} \text{sign}(\dot{\varepsilon}_{xx})\,d\alpha \tag{49}$$

It is worth noting that the axial force calculated from the above definition is the same for any cross-section $0<x<\xi$. The condition N=0 is met if the change of the sign of the extensional strain rate $\dot{\varepsilon}_{xx}$ occurs at the point $\alpha = \pi/2$. The strain rate due to the denting alone is purely extensional (positive). Therefore, in order to change the sign of $\dot{\varepsilon}_{xx}$, a uniform compressive velocity $\dot{u}_o$ must be superimposed so that the point along the circumference of the tube with zero strain rate corresponds to $\alpha = \pi/2$, Fig.17. The magnitude of $\dot{u}_o$ relative to $\dot{\delta}$ would depend on the particular shape of the function $w_o\dot{w}_o/\xi$. We shall illustrate the procedure taking a parabolic approximation of this function $w_o\dot{w}/\xi$ as discussed earlier. It follows from simple calculation that the condition is N=0 is satisfied if

$$\dot{u}_o = -\frac{1}{4}\frac{\delta\dot{\delta}}{\xi} \tag{50}$$

Introducing the above result into Eqs. (6) and (38) and taking proper care of the integration with an absolute value sign we obtain an expression

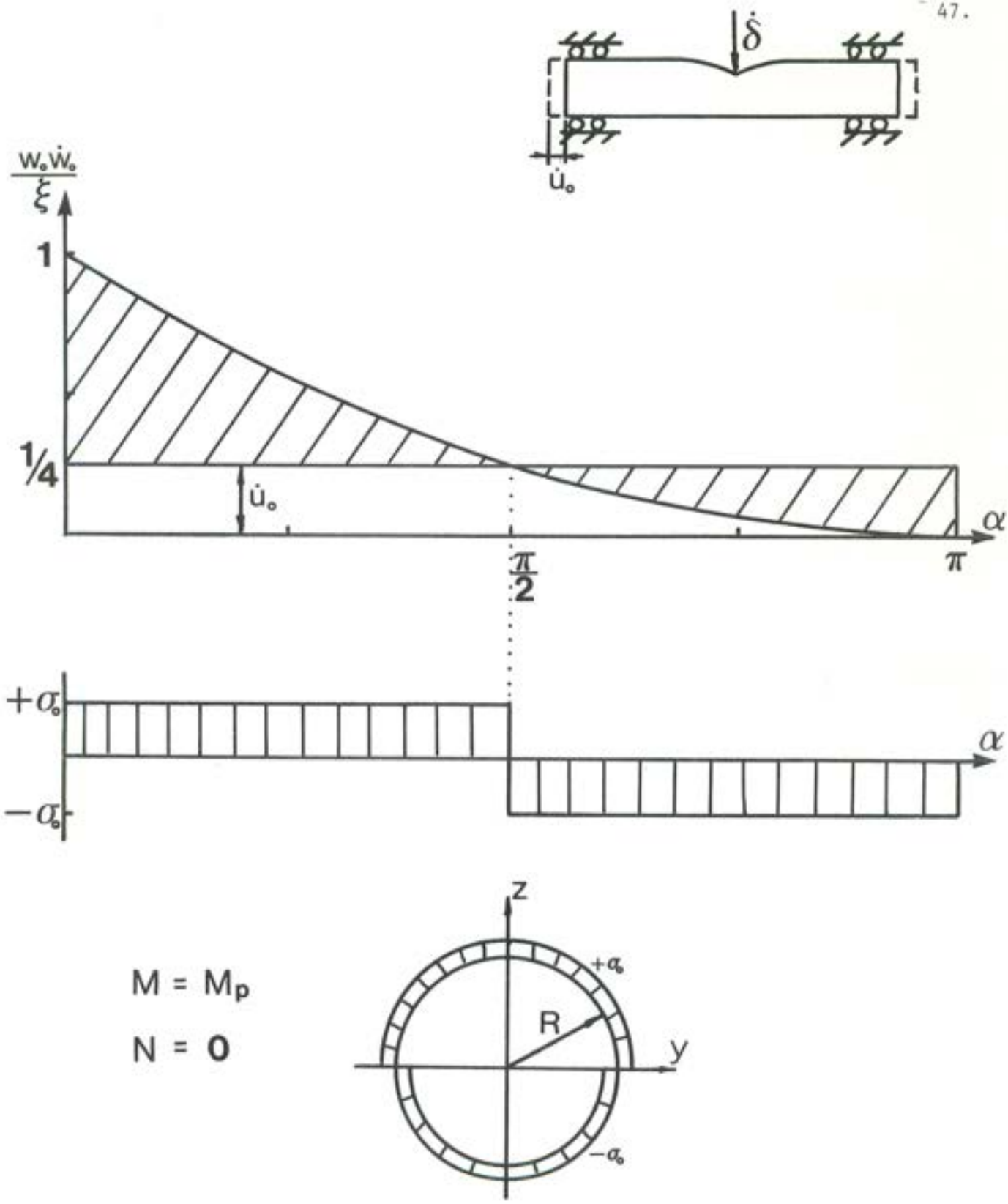

Fig. 17 Reduction of the rate of energy dissipated by generators for the tube with freely sliding boundaries, N=0.

for the total work of internal work in the generators

$$\dot{E}_{gen} = \frac{\pi N_o R \delta \dot{\delta}}{\xi} \tag{51}$$

The sliding freedom of the tube has thus reduced the rate of dissipation in the generators by the factor 3/4 compared to the tube with the axial freedom restricted. In the present illustrative example the ring solution with the constant crushing strength will be used.

The energy balance equation becomes

$$P\dot{\delta} = \frac{8M_o \xi}{R} \dot{\delta} + \frac{\pi N_o R \delta}{\xi} \dot{\delta} \tag{52}$$

After minimization with respect to ξ we obtain

$$\frac{\xi}{R} = \sqrt{\frac{\pi \delta}{2t}} \tag{53}$$

and the force deflection relationship takes the same form as before with an amplitude reduced by the factor

$$\sqrt{\frac{3}{4}} = 0.85 \tag{54}$$

$$\frac{P}{M_o} = 16 \sqrt{\frac{D}{t}} \sqrt{\frac{\pi}{4} \frac{\delta}{R}} \tag{55}$$

This factor becomes even smaller if more exact expressions for the extensional and crushing energies are considered, as discussed in the previous section. The difference between the "exact" solution based on true function $\overline{\dot{E}}_{gen}(\alpha)$ and the approximate solution is shown in Fig. 15.

We can conclude that by relaxing the boundary conditions in the axial direction from full fixity $\dot{u}_o=0$ $(N=N_p)$ to freely sliding N=0, the crushing strength reduces by approximately 10%. In the previous analysis of the same problem the reduction was found to be unrealistically high, equal to $1/\sqrt{2}$ which is about 30% [12].

Those two types of boundary conditions provides bounds on the general case 2, defined in Table1, where an arbitrary tensile axial force $0 \leq N \leq N_p$ was applied to the axis of the tube during the indentation process. If the axial force were compressive rather tensile, the situation would have changed dramatically. The analysis of this problem will be presented in Section 9.

We are now in a position to find the relation between the axial shortening of the tube u_o and the depth of the dent δ. Introducing (53) into (50) and integrating with respect to time, the following formula is obtained for the shortening of one side of the tube

$$u_o = 0.133 \frac{\delta}{R} \sqrt{\delta t} \tag{56}$$

For example a tube with $R/t=50$ undergoing indentation equal to the tube radius $\delta=R$ should suffer a total shortening equal to twice wall thicknesses Such a shortening could be easily to detect experimentally although no such measurements are known to the authors. It remains now to calculate the bending moment in the dent-affected zone. This moment decreases continuously from the maximum value M_p at the undeformed section $x=\xi$ to the minimum value at the mostly deformed section x=0. Furthermore, the centroidal axis also changes with x but because there is no net axial force, this variation has no effect on the bending moment.

The bending moment at an arbitrary section x is defined by

$$M = 2\sigma_o t \int_o^{\pi R} \text{sign}(\dot{\varepsilon}_{xx}) z ds \tag{57}$$

where the dependence of z on s is different for every cross-section. The bending moment at the end of the plastically deforming zone $x=\xi$ can be calculated taking $z=R\cos\alpha$, $ds = Rd\alpha$. Simple integration shows that the moment is equal to the fully plastic bending moment of the cross-section.

$$M(x=\xi) = M_p = \pi\sigma_o R^2 t \tag{58}$$

The variation of the bending moment over the dented zone $0<x<\xi$ is possible in view of the presence of the distributed reaction force p(x) between the tube and the rigid foundation.

Tube with rotational and translational freedom (case 4c)

As a last type of boundary conditions we shall consider a tube totally unrestrained from rotational and axial motion. Because both the bending moment and axial force vanish at the tube ends, M=N=0, the only contribution to the rate of work of external forces comes from the lateral force P. Like in the previous cases, two solutions will be presented. First, the approximate closed-form solution will be derived to illustrate the method. Then, an exact force-indentation curve will be determined numerically and the two will be compared.

In order to satisfy both N=0 and M=0, the axial strain rate and stress should change the sign twice between the end points $\alpha=0$ and $\alpha=\pi$. From the

definitions of Eqs. (49) and (51) the coordinates of points at which the total extensional strain rate $\dot{\varepsilon}_{xx}$ vanishes are found to be $\alpha_1 = \pi/4$, $\alpha_2 = 3\pi/4$. It was found that the best approximation can be obtained by taking a parabolic function $w_o\dot{w}_o/R^2$, described by Eq. (41). Introducing this function into Eq. (35) the total extensional strain rate in any generator can be expressed as the function of α

$$\dot{\varepsilon}_{xx} = \frac{\delta\dot{\delta}}{\xi}\left[1 - \left(\frac{2\alpha}{\pi}\right)^2\right] + \dot{u}_o + R\cos\alpha\ \dot{\theta}_o \tag{59}$$

The conditions $\dot{\varepsilon}_{xx}=0$ at $\alpha = \alpha_1$ and α_2 provide two linear algebraic equations for $\dot{u}_o$ and $\dot{\theta}_o$,

$$\frac{3}{4}\frac{\delta\dot{\delta}}{\xi} + \dot{u}_o + \frac{\sqrt{2}}{2}\ R\dot{\theta} = 0$$

$$\dot{u}_o - \frac{\sqrt{2}}{2}\ R\dot{\theta} = 0 \tag{60}$$

whose solution is

$$\dot{u}_o = -\ 0.375\ \frac{\delta\dot{\delta}}{\xi} \tag{61}$$

$$\dot{\theta}_o = -\ 0.53\ \frac{\delta\dot{\delta}}{\xi R} \tag{62}$$

Because the integrand of Eq. (6) involves an absolute sign and the function $\dot{\varepsilon}_{xx}(\alpha)$ changes sign twice, the integration in Eq. (6) should be split into three parts according to

$$\dot{E}_{gen} = \int_0^{\alpha_1} \dot{\bar{E}}_{gen} R d\alpha - \int_{\alpha_1}^{\alpha_2} \dot{\bar{E}}_{gen} R d\alpha + \int_{\alpha_2}^{\pi} \dot{\bar{E}}_{gen} R d\alpha \tag{63}$$

where $\dot{E}_{gen}$ is defined by Eq. (35) with the substitution of Eq. (61) and Eq. (62). After straightforward calculations we obtain

$$\dot{E}_{gen} = \frac{\pi}{2} N_o R \frac{\delta\dot{\delta}}{\xi} \tag{64}$$

It is seen that the relative rotation and translation of tube end cross-sections release the tensile stresses in the dented zone and reduce more than twice the energy dissipated by the generators. This is illustrated in Fig.18 where the shaded area represents the actual dissipation.

The rest of calculations are straightforward. The reaction force $P(\delta,\xi)$ is defined by the rate of energy balance equation

$$P\dot{\delta} = \frac{8M_o\xi\delta}{R} + \frac{\pi}{2} N_o R \frac{\delta\dot{\delta}}{\xi} \tag{65}$$

The optimality condition $\partial P/\partial\xi=0$ leads to

$$\frac{\xi}{R} = \sqrt{\frac{\pi}{4}\frac{\delta}{t}} \tag{66}$$

Combining Eqs. (65) and (66) the strength characteristics of the tube under lateral concentrated force is given by the formula

$$\frac{P}{M_o} = 16\sqrt{\frac{\pi}{8}\frac{\delta}{R}\frac{D}{t}} \tag{67}$$

The "exact" solution was also worked out by calculating the quantity $\dot{E}_{gen}$ using the actual rather than parabolic distribution of the function $E_{gen}(\alpha)$. The resulting P-δ curve is compared with the formula of Eq. (67) in Fig. 19 showing a good agreement of both solutions. Fig. 20 illustrates how the free translation and rotation of the tube ends reduce the energy dissipation of generators.

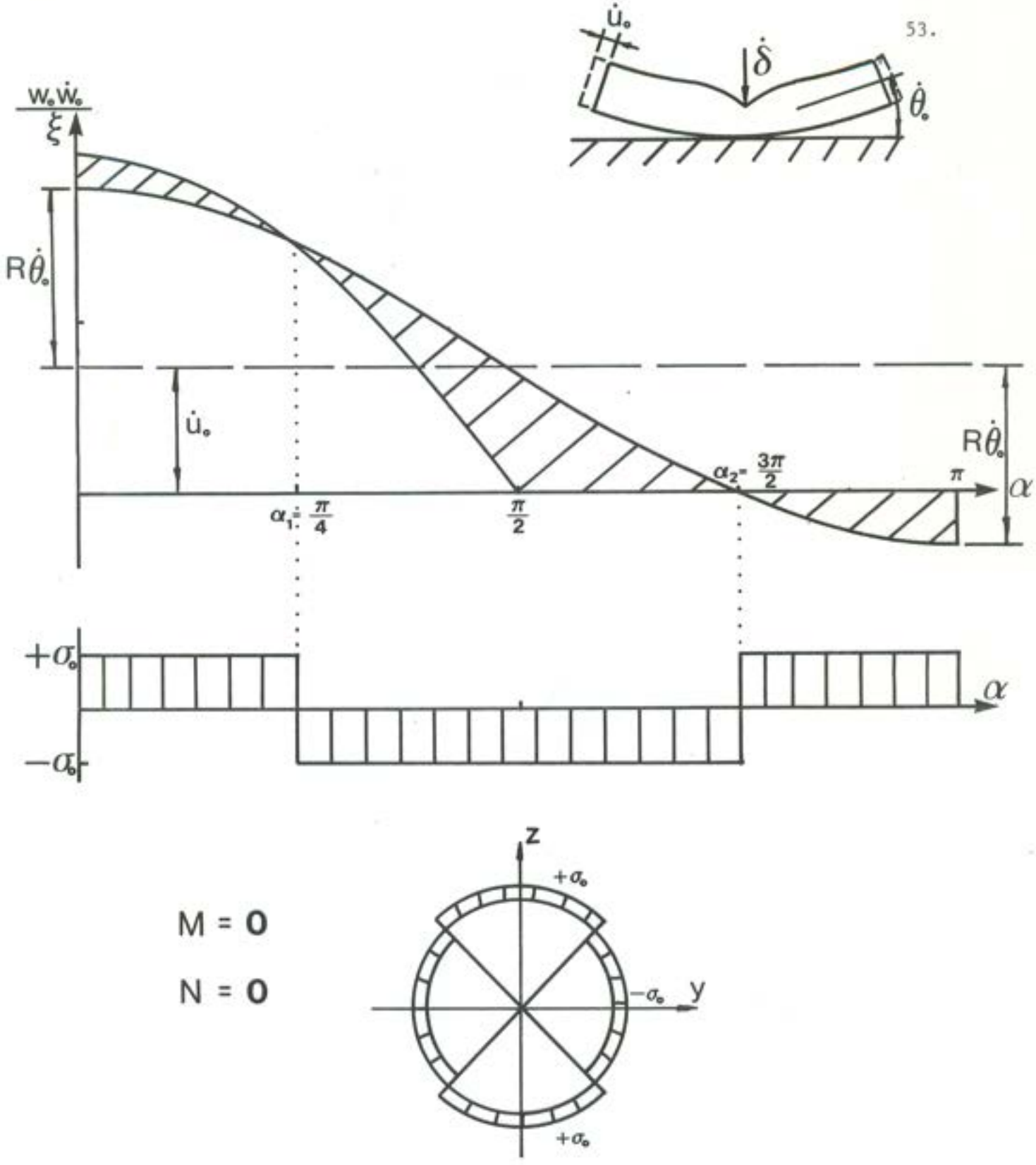

Fig. 18 Further reduction of the rate of energy dissipated by generators for the free-free tube.

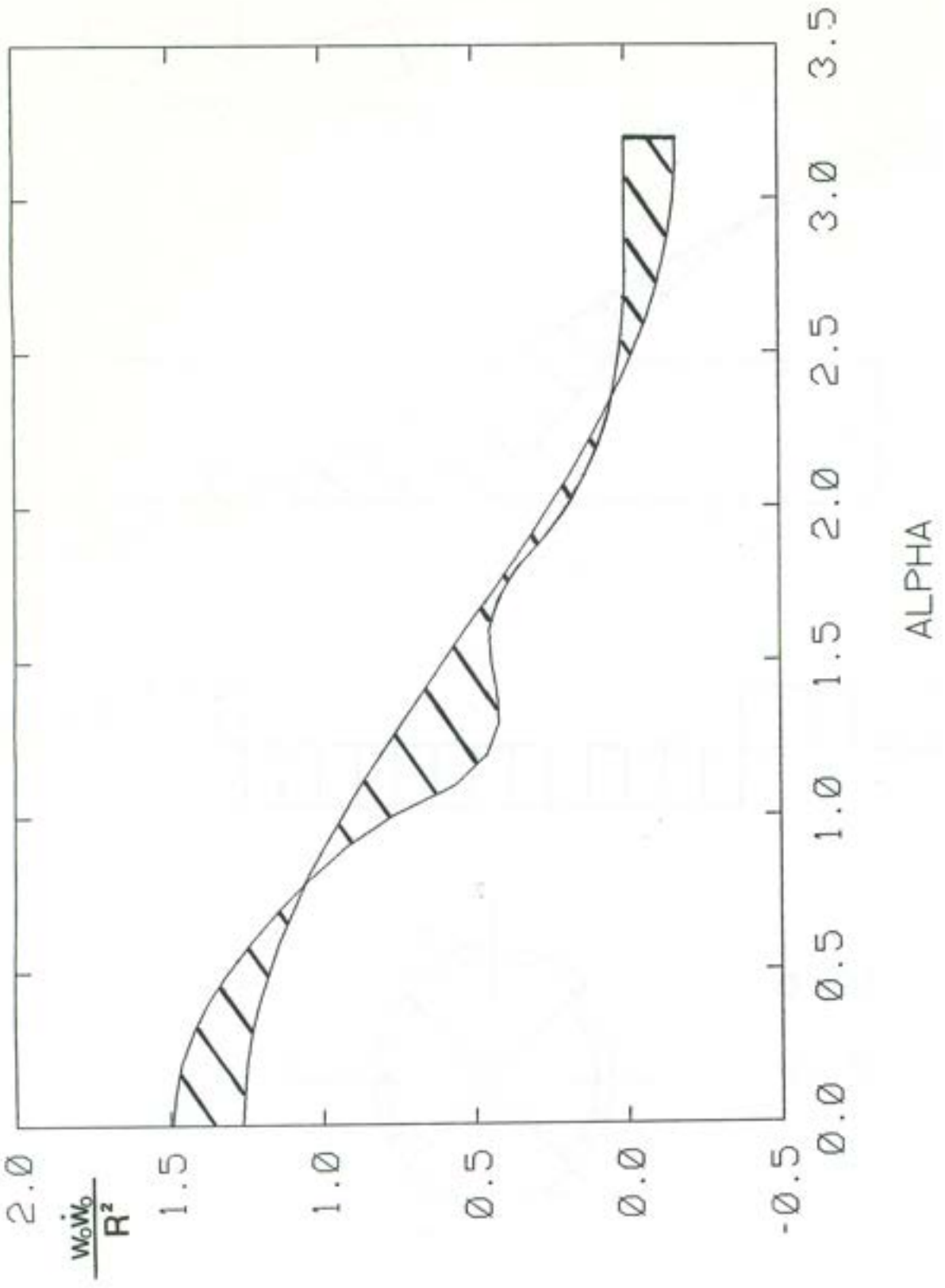

Fig. 20 A plot illustrating a superposition of extensional strain due to local denting (exact curve) and overall translation and rotation.

The last step in the present analysis is the calculation of the rotation angle θ_o as a function of the indentation depth δ. The relation of Eq. (62) between the rates or increments of those quantities is linear. Integrating this relation with the help of the expression of Eq. (66) gives the sought formula

$$\theta_o = 0.3987\frac{\delta}{R}\sqrt{\frac{\delta t}{R^2}} \quad \text{in radian} \tag{68}$$

or

$$\theta_o = 22.84\,\frac{\delta}{R}\sqrt{\frac{\delta t}{R^2}} \quad \text{in degrees} \tag{69}$$

For example, the rotation angle of one side of the tube having the aspect ratio D/t = 50 is predicted by Eq. (69) to be equal to 4.568 degrees when the indentation reaches the tube diameter δ=R. Rotations of free-free tubes were observed by Smith et al. [21] in their model and full scale experiments with much smaller indentation depths. To the best of our knowledge no attempts were made in the open literature to quantify theoretically this effect. The formulas derived by us appear to be the first solution of this important and practical problem.

7. DISCUSSION AND COMPARISON WITH EXPERIMENTS

The present analysis draws attention to the fact largely overlooked in the literature which is the influence of boundary conditions on the strength characteristics of the tube subjected to transverse concentrated loads. In order to focus on the local process of plastic indentation and to eliminate the interaction between the local and global modes of tube failure, the analysis was restricted to those types of boundary conditions in which the external work is done only by the transverse force P on the corresponding velocity $\dot{\delta}$. With this limitation four conditions need to be considered out of which the one with $\dot{u}_o=0$ and $M=0$ is insignificant in practical application. The remaining three conditions were studied in great detail and the corresponding solutions were derived in the previous section.

In all cases predictions were made on the strength resistance of the tube as well as on the magnitude of kinematic quantities $\xi(\delta)$, $w_c(x,\delta), u_o(\delta)$ and $\theta_o(\delta)$ describing the geometry of the locally damaged zone.

In comparing Eq. (67) for the freely rotating case with similar solutions corresponding to the freely sliding in Eq. (54) and the fully fixed tube of Eq. (45) we observe that the functional form of the solutions is the same and only the amplitude changes from case to case. The reduction of the tube strength compared to the fully fixed solution is 0.87 and 0.60 for the freely sliding and freely rotating case respectively. This is illustrated in Fig.19 where "exact" and approximate solution are defined by the full and broken lines, respectively. The extent of the plastically

deforming zone as a function of the indentation depth is given by Eqs. (44), (53) and (66) for the fully fixed, freely sliding and freely rotating case, respectively. From those equations and Fig. 21 we can see that there is a tendency for the locally dented zone to shrink by relaxing the kinematical constraints at the tube ends.

It is important to note that all the derived relations between the geometrical quantities involved are independent of the parameters characterizing the material of the tube. This property of the solution can be explained by the fact that local geometry of the damage zone depends on relative values of stresses and deformations in the shell rather than on the absolute magnitudes of those quantities. A limited amount of reliable experimental data exist in the literature to verify the present theory. In some cases incomplete data were published for confidential reasons (see Ref. [4]) or precise description of the test procedure and the end conditions were missing (for example [28]). Smith et al. [21] reported on a carefully executed indentation tests on full scale and model tubes with almost identical length to diameter and diameter to thickness ratios. One full scale test (F2) and one small scale test (F2S) were fully documented as far as the measurements of the force-deflection characteristics $P-\delta$ and total rotation angle θ_o were concerned. In addition, the profile of the dented zone $w_c(x)$ in the F2 test was measured.

The circles in Fig.22 represent the measured shape of the leading generator, normalized with respect to the central deflection $w_c(x)/\delta$. The actual profile results from the local denting and overall bending. In order to compare the shape of the generator produced by a pure indentation, with the prediction of Eq. (48), the experimental profile should be corrected for the global rotation. The rotation angle $(\theta_o)_{exp}$

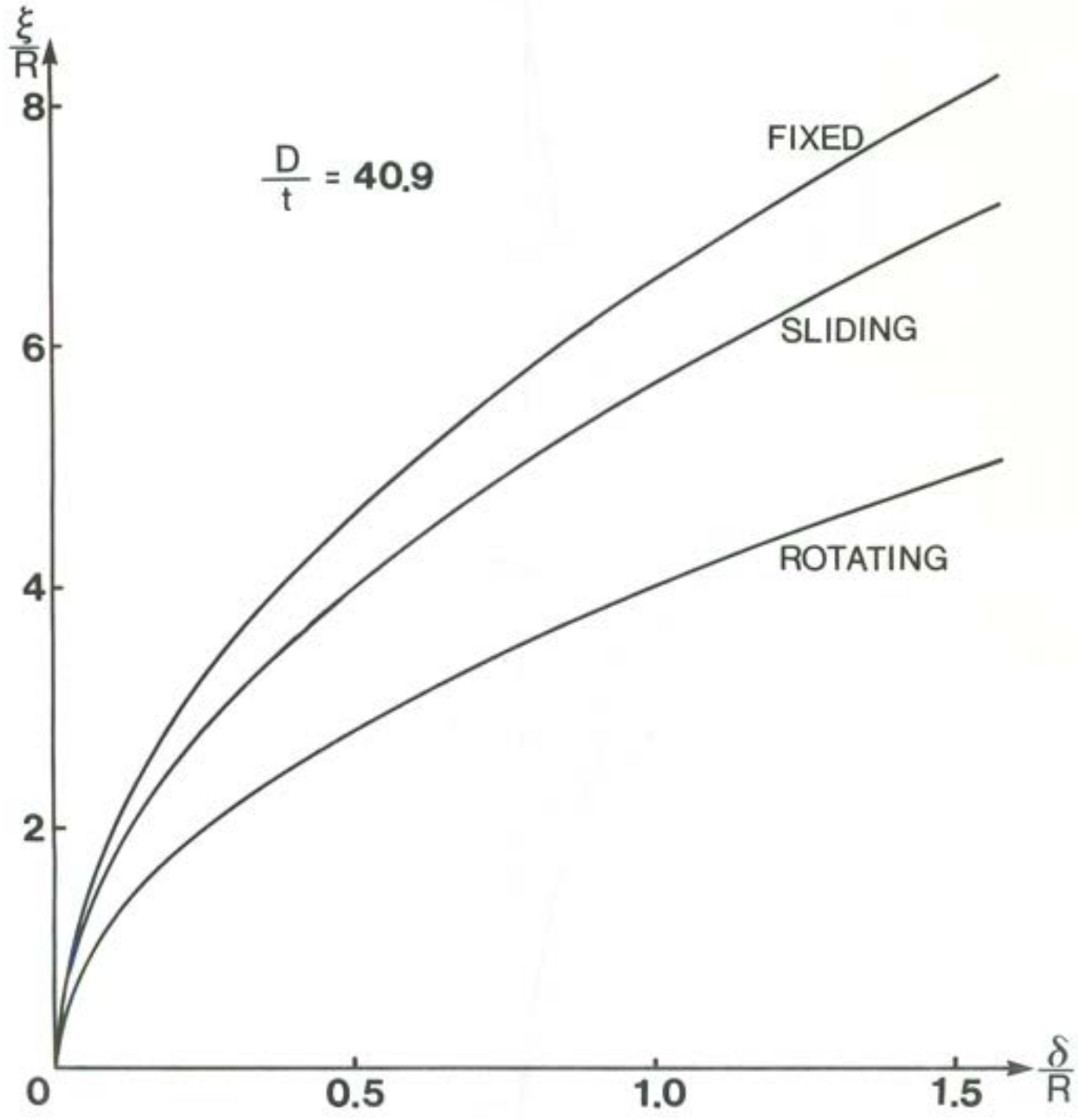

Fig. 21 Spread of the locally damaged zone in the tube as a function of the dent depth. Comparison of solutions for three boundary conditions.

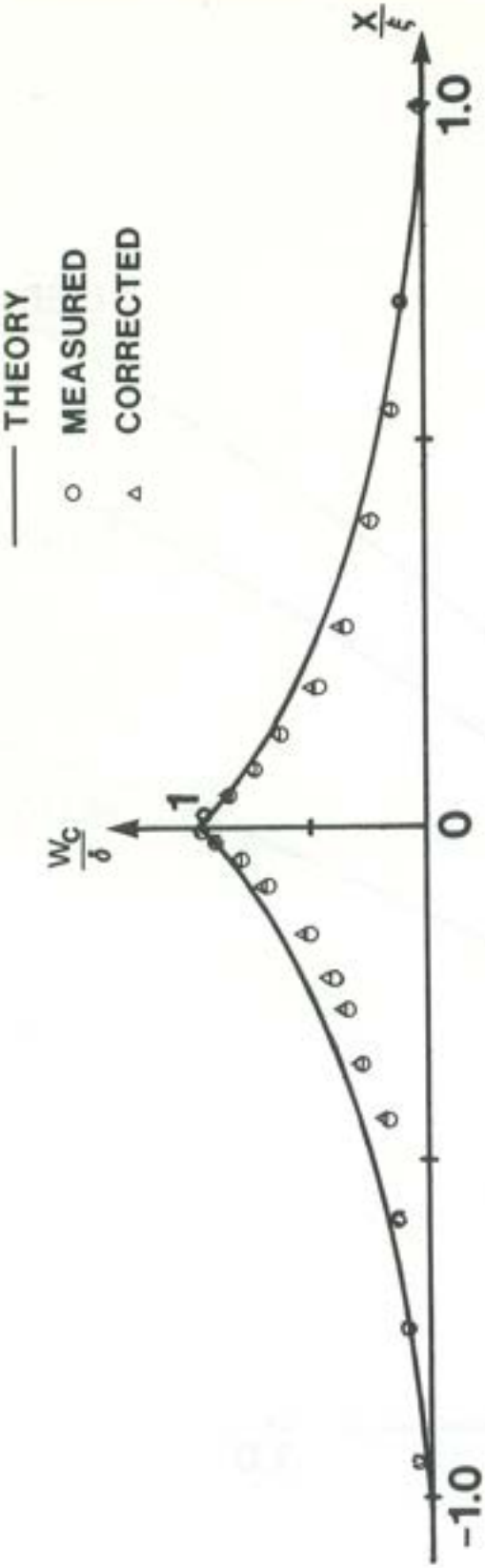

Fig. 22 Theoretical and experimental profile of the leading generator in the damaged zone. Triangles represent test results corrected for global rotation.

measured in the test was equal to $\theta_o = 2\delta_p/\ell = 0.01$ [rad]. The points corresponding to the corrected normalized profile of the dent are denoted in Fig. 22 by triangles while the solid line represents the present theoretical solution. The agreement is good which supports the presently assumed computational model of the tube.

A three-dimensional sketch of the dented zone, showing theoretically predicted shapes of rings and generators is shown in Fig. 23 . Again, the picture closely resembles a photograph of the dent-affected zone of the tube, shown in Fig. 1. The shaded area in Fig. 23 represents a portion of the tube with zero Gaussian curvature. This portion is composed of flat segments of rings, as explained in Section 4.

The overall lateral deflection δ_p measured in Ref. [21] in a test with the small scale tube F2S was equal to $\delta_p = 0.005L$, where L is the length of the tube. This is equivalent to the experimental rotation

$$(\theta_o)_{2xp} = \frac{2\delta_p}{L} = 0.010 \tag{70}$$

attained when the depth of the dent was equal to δ=5.2t. The diameter to thickness ratio of the tube in question was D/t=40.9. Substituting those values into the formula of Eq. (68), the rotation predicted by our model becomes

$$(\theta_o)_{th} = 0.0113 \tag{71}$$

The agreement with experiments is excellent considering the complexity of the problem.

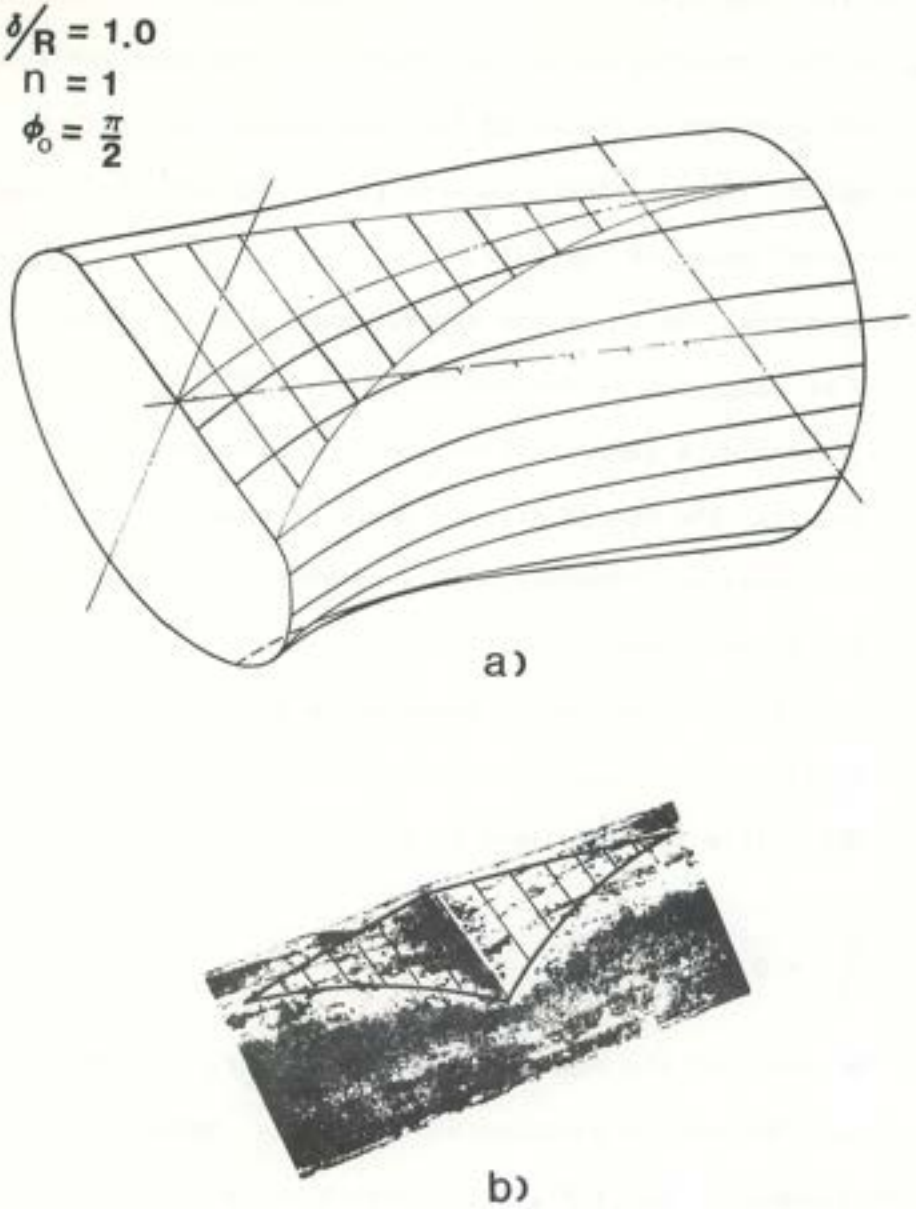

Fig. 23 A calculated and experimentally observed shape of the locally damaged zone in the tube indentation problem.

The present analysis also indicates that tubes with the same D/t and δ/R ratios should suffer the same rotations. However, the rotation in the full scale tube was reported in Ref. [21] to be more than two times smaller than that for the small scale tube with almost identical D/t. We feel that the dead weight of the tube could provide for a sufficient restraint bending moment, which prevents from developing large rotations. The bending moment acts as soon as the end of the tube is lifted. Its magnitude equals to

$$M = \frac{1}{4} RtL^2 \rho g \tag{72}$$

where ρ and g denote respectively mass density of the tube material and the gravitational acceleration. The ratio of this moment to the fully plastic bending moment of the cross-section given by Eq. (58) is

$$\frac{M}{M_p} = \frac{\pi}{8} \left(\frac{\rho g L}{\sigma_o}\right) \frac{L}{D} \tag{73}$$

The scale effect is clearly visible since in tubes with the same L/D but different L the restoring bending moment will not be the same. The indentation problem in tubes with the prescribed bending moment and axial force is more difficult to treat analytically and its solution will be reported in the future publication.

The present theoretical solution for the strength characteristics of the freely-rotating tube, Eq. (67), will be correlated with two sets of data reported by Smith et al. [21]. Figure 24 shows the force-deflection characteristics measured in the indentation test of the model tube with

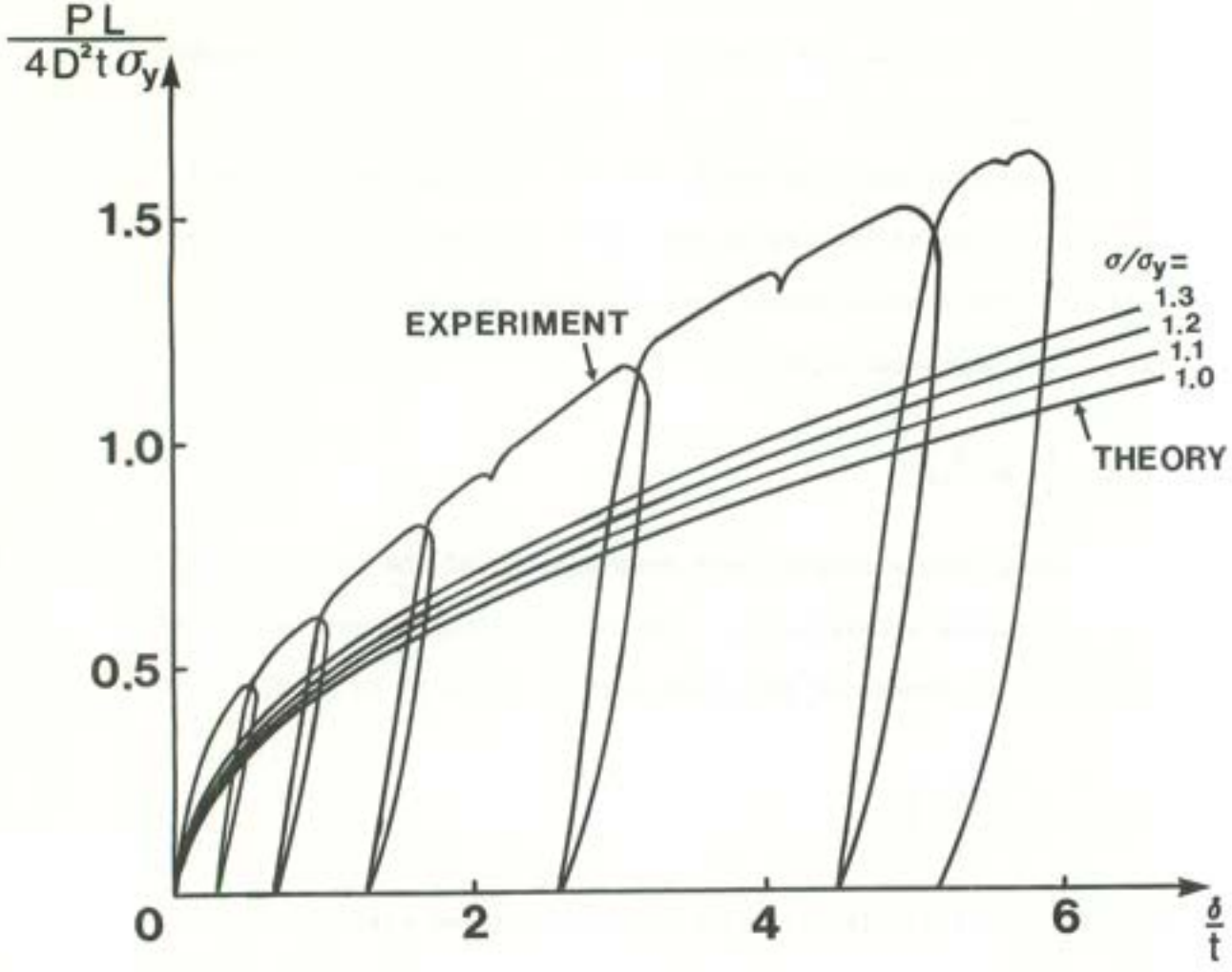

Fig. 24 The force-deflection characteristics for a free-free tube. The experimental curve due to Smith [21] shows unloading and reloading. The present theoretical curves are drawn for several values of the ratio of the flow stress to the initial yield stress σ_o/σ_y.

the dimensions D=65.1 mm, t=1.59 mm and L=1325 mm and the yield stress σ_y=280 N/mm^2. Transforming Eq. (67) to the coordinates used in Fig. 24 we obtain

$$\overline{P} = \frac{PL}{4\sigma_y t D^2} = 0.886 \frac{\sigma_o}{\sigma_y} \frac{Lt}{D^2}\sqrt{\frac{\delta}{t}} = 0.44\sqrt{\frac{\sigma_o}{\sigma_y}}\sqrt{\frac{\delta}{t}} \qquad (74)$$

The formula of Eq. (74) has been dimensionalized with respect to the initial yield stress of the material σ_y whereas in the present analysis the so-called "flow stress" σ_o is used. The flow stress is understood as the best fit of the actual stress-strain curve in the expected range of strains with the present rigid-plastic material idealization. As pointed out in Section 2, the bending and axial strains reach 3% for the depth of the dent equal to the tube radius δ=R. The average strain is ε_{av} = 1.5% and the flow stress can be defined as $\sigma_o = \sigma(\varepsilon_{av})$, Fig. 25 According to the above definition, σ_o is a function of the work-hardening property of the material as well as the magnitude of the average strain attained in the deformation process. While the latter quantity can always be calculated by the present shell model, the information on the work-hardening parameter of the steel tubes used by Smith et al. is not available. Therefore theoretical curves were drawn in Fig. 24 for a few constant values of the ratio σ_o/σ_y = 1.0; 1.1; 1.2; 1.3. The present theory is seen to predict correctly the functional dependence of the solution on all geometrical parameters of the problem. However, in the absence of the data on the strain-hardening parameters, no definite conclusion can be drawn regarding the quantitative agreement between the theory and experiment. We feel that the present solution underestimates the actual strength of the tube by 10 ÷ 20%.

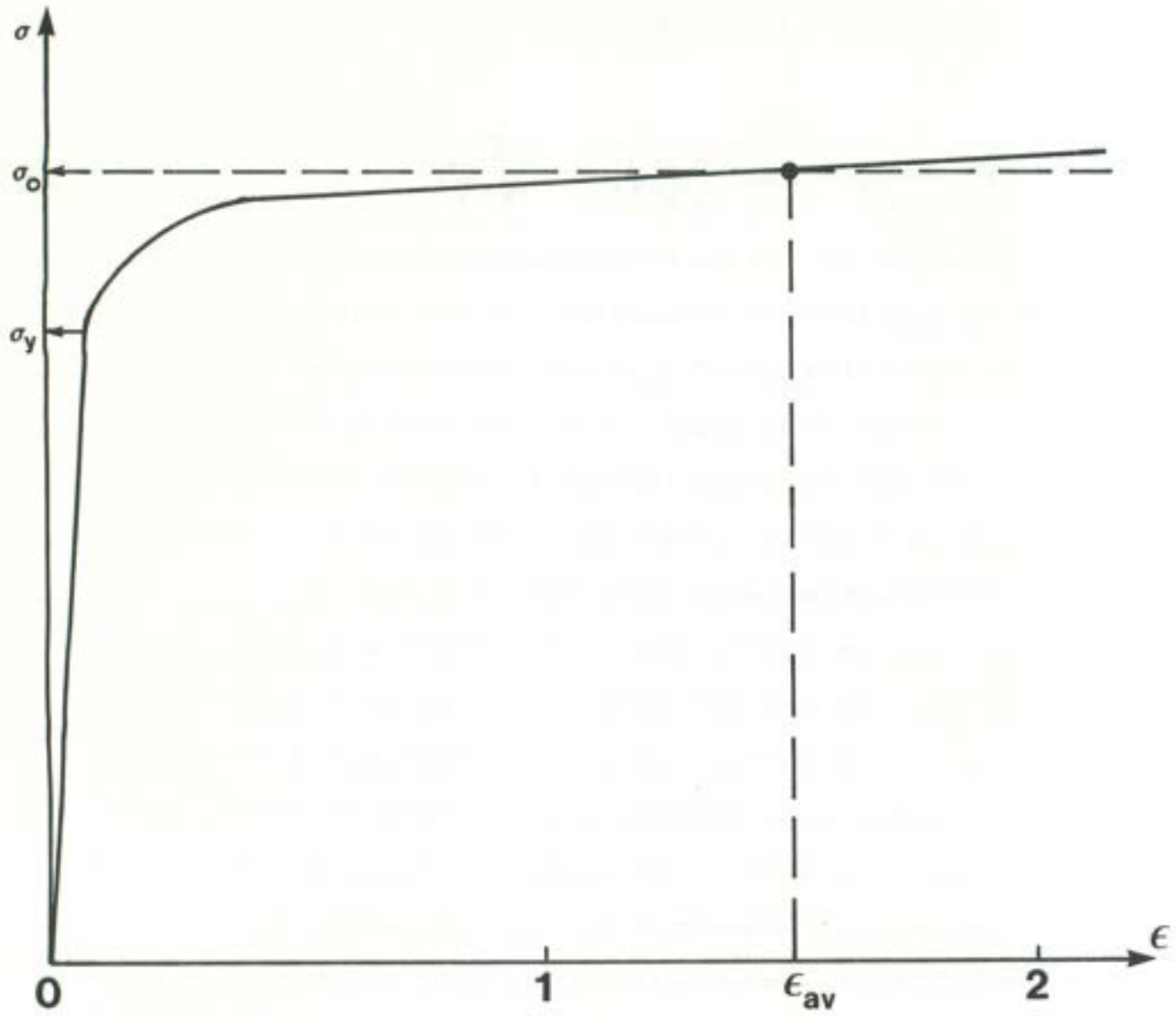

Fig. 25 Actual stress-strain curve of the material and a rigid-perfectly plastic idealization at the level of an average flow stress.

The experimental results for the full scale tubes were presented in Ref. [21] in physical quantities. Introducing the definition of M_o into Eq. (67) one gets

$$P[KN] = 4 \times 10^{-3} \sigma_o t^2 \sqrt{\frac{\pi}{4} \frac{\delta}{t}} \tag{75}$$

Taking the tube D=396 mm, t=9.9 mm, L=7754 mm and the same yield stress as before, the formula of Eq. (67) reduces to

$$P[KN] = 31 \frac{\sigma_o}{\sigma_y} \sqrt{\delta[mm]} \tag{76}$$

Again, plots of the above function were made for several different values of the ratio σ_o/σ_y and those are shown by dotted lines in Fig. 26 . The full line is the experimental curve. The correlation is seen to be good considering the fact that, no "forge factor" was introduced in the present analysis.

In our opinion consideration of the shear effects in the dented zone would bring the present prediction right on the experimental curve. This problem will be addressed in the approximate way in the next section.

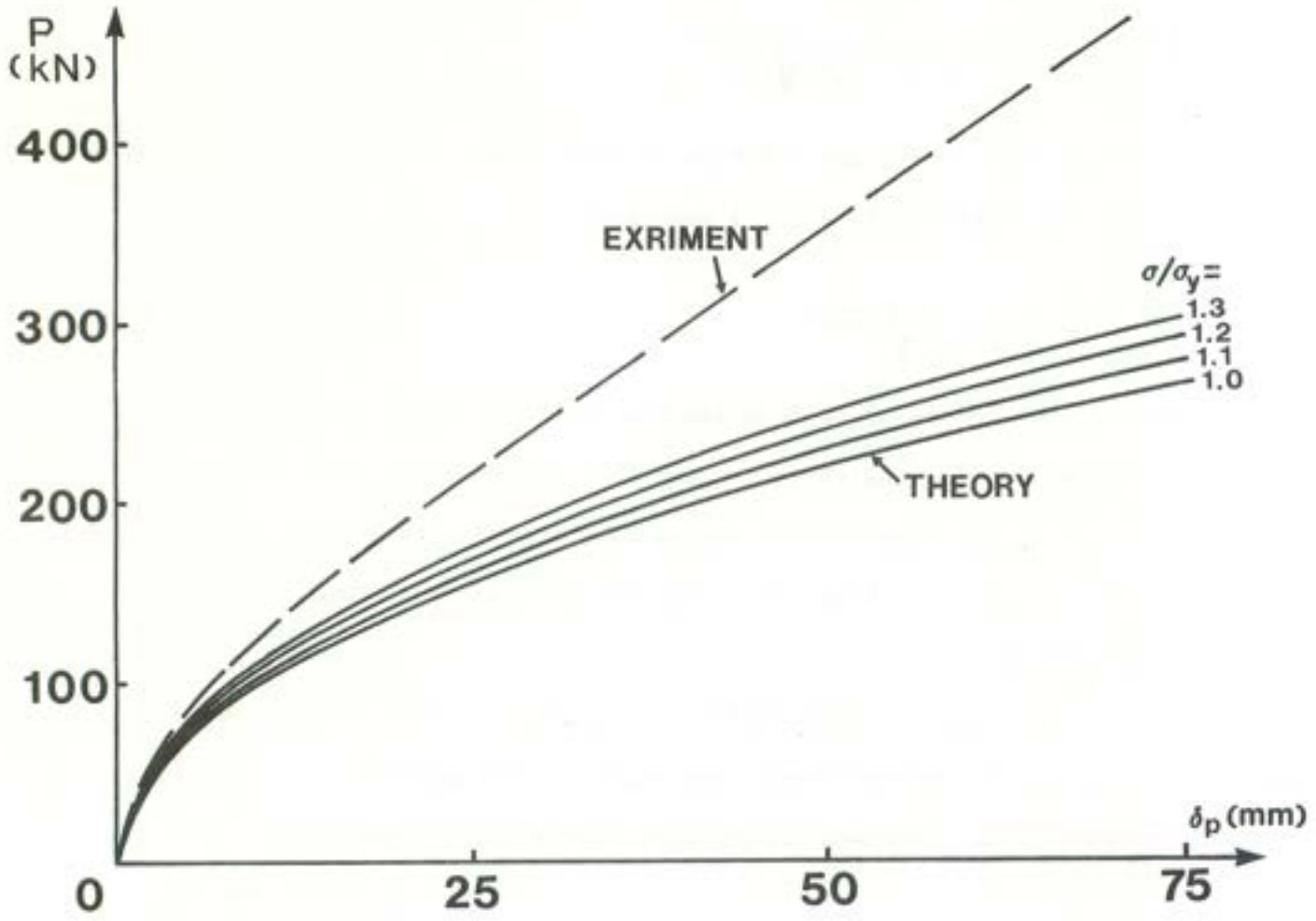

Fig. 26 Correlation of the present theoretical solution with the result of full scale test reported by Smith [21]. The theoretical curves were drawn for several values of σ_o/σ_y.

8. ESTIMATION OF SHEAR EFFECT

An approximate of expression for the rate of energy due to shear deformation will be derived using a simple model of an equivalent tube with rectangular cross-section. This model has previously been used in Ref. [12] to estimate the rate of extensional energy in the tube indentation problem. A similar model has been proved useful in explaining the importance of shear deformation in the problem of confined and unconfined buckle propagation [37].

Consider a thin-walled square tube whose circumference is the same as that of the original circular tube $4a = 2\pi R$. The equivalent length of each side is thus equal to

$$a = \frac{\pi R}{2} \tag{75}$$

Suppose the tube is subjected to a symmetric denting of the depth $\delta/2$ on each side, Fig.27a. It is possible to construct a paper model of such a deformed tube without cutting the paper along the fold lines to release possible extensions or shear. This construction provides the simplest proof that symmetric collapse of the square or rectangular section tube does not produce any shear strains.

By contrast, the unsymmetric sectional collapse, which resembles the tube indentation mode, cannot be reproduced by simply folding the tube walls along hinge lines. The unsymmetric mode is shown in Fig. 27b. It can be obtained from the symmetric mode by shearing the side walls, through the angle γ as explained in Fig. 28. The angle γ is related to the geometry of the dented zone by

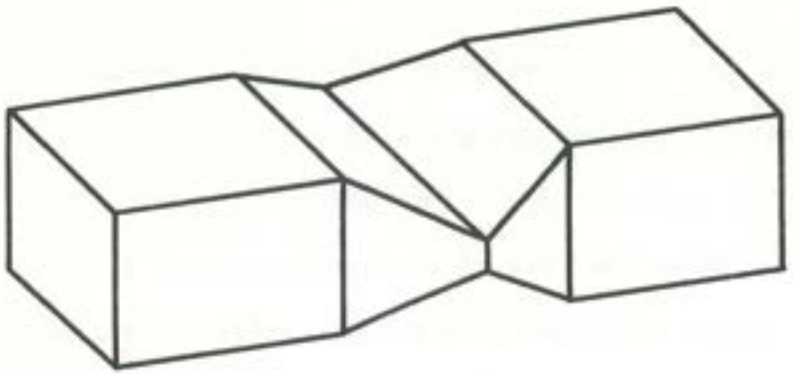

a)

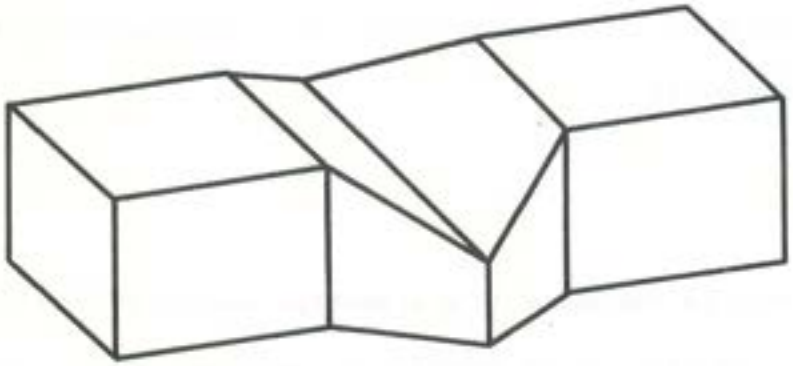

b)

c)

Fig. 27 Conceptual model of a tube showing symmetric sectional collapse (no shear) and unsymmetric collapse (significant shear).

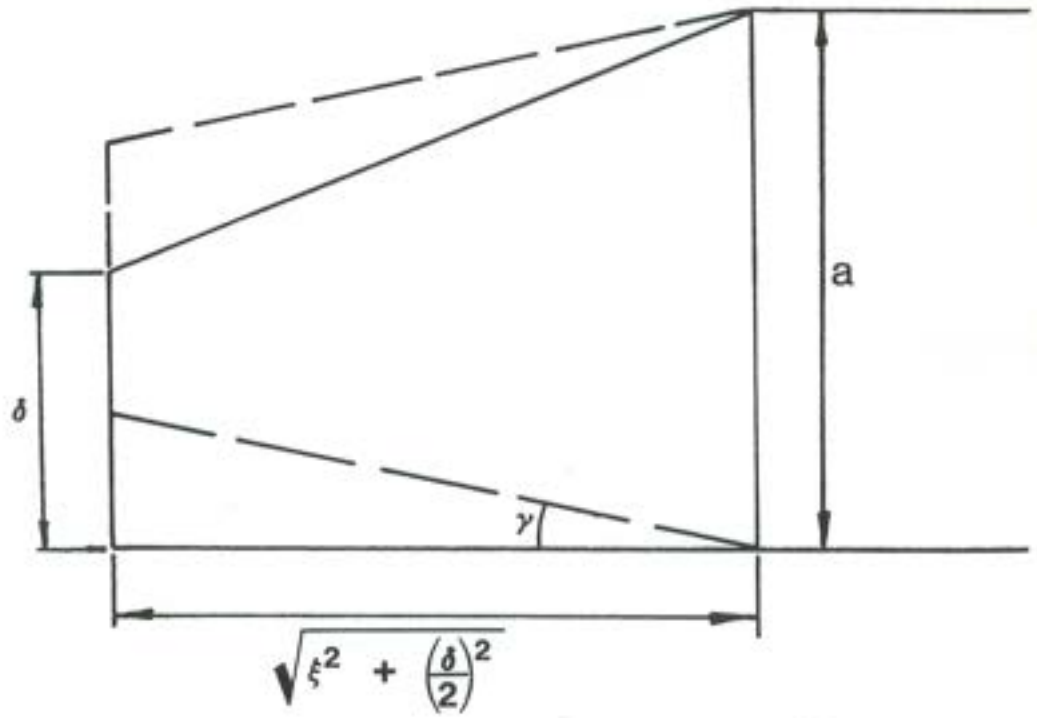

Fig. 28 Transition from symmetric to unsymmetric sectional collapse through simple shear.

$$\gamma = \frac{\delta}{2\xi} \tag{76}$$

The rate of shear strain is defined as

$$\dot{\gamma} = \frac{d\gamma}{dt} = \frac{1}{2}\frac{d}{dt}\left(\frac{\delta}{\xi}\right) \tag{77}$$

The rate of energy dissipation due to shear is

$$\dot{E}_{shear} = t\int_A |k\dot{\gamma}|dA \tag{78}$$

where k is the yield stress in simple shear and the integration is performed over the shear affected zone of the equivalent tube. For the Tresca yield condition $k = \sigma_o/2$. The integral of Eq. (78) can easily be calculated assuming the strain rate $\dot{\gamma}$ to be uniform over the two lateral trapezoidal surfaces of the area $\frac{1}{2}(2a-\delta)\xi$ each

$$\dot{E}_{shear} = \frac{\sigma_o t}{2}\, 2(2a-\delta)\xi\ \dot{\gamma} \tag{79}$$

The above expression involves a time rate of the unknown quantity ξ. In order to proceed with the solution further, an iterative procedure will be used.

The function ξ appearing in the definition of $\dot{\gamma}$ will first be estimated using a closed form solution derived for the same problem without shear. This will provide a unique expression for $\dot{E}_{shear}$ which is linear in $\dot{\delta}$. The calculated shear dissipation will be substituted back into the global rate of energy balance and the entire solution process can be repeated. We shall apply this procedure to the case of a fully clamped tube. Using Eq. (44), the strain rate is found to be

$$\dot{\gamma} = \frac{1}{4R}\ \frac{3t}{2\pi}\frac{\dot{\delta}}{\sqrt{\delta}} \tag{80}$$

Substituting Eqs. (75) and (80) into Eq. (79), the rate of shear energy becomes

$$\dot{E}_{shear} = \frac{1}{2} N_o \left(\frac{\pi R}{2} - \frac{\delta}{2}\right) \frac{\xi}{R} \frac{3t}{2\pi} \frac{\dot{\delta}}{\sqrt{\delta}} \tag{81}$$

Now, adding the above term into the right hand side of the energy balance postulate Eq. (43) the corrected or first iterative solution is obtained in the form

$$(P)_{with\ shear} = \beta (P)_{without\ shear} \tag{82}$$

where $(P)_{without\ shear}$ is given by Eq. (45) and the correction factor is defined by

$$\beta = \left[1 + \frac{R}{8t} (\pi - \frac{\delta}{R}) \sqrt{\frac{3}{2\pi} (\frac{t}{R}) \frac{R}{\delta}}^{1/2}\right] \tag{83}$$

Consider a tube with the ratio D/t=40.9, as used in Smith's experiments. The function $\beta(\delta/R)$ for few values of the indentation depth δ/R is shown below

δ/R	0.5	1.0	1.5	2.0
β	1.568	1.355	1.234	1.147

With increasing indentation depth, the correction factor is decreasing to an asymptotic value $\beta_{as} = 1.0$. At very small central deflections δ/R, the formula of Eq. (83) predicts an unrealistically high resistance of the tube. Clearly, there must be an alternative mode of tube deformation which suppresses large shear strain rates developed at the onset of the plastic indentation process. It is plausible that the tube undergoes initially

a symmetric mode even though the force is applied on the top only, Fig.27c. The resulting initial symmetric ovalization of the tube section, provides for a mechanism which eliminates the shear strains and minimizes initially the denting resistance of the tube. The ovalization of the tube under bending, known as the Brazier effect has been observed and reported by many authors.

The infinite value of the shear energy is a consequence of the singularity in the slope of the ξ-δ function at $\delta = 0$. In reality, however, the length of the dented zone is initially finite and so must be the contribution of shear. The finite width of the plastic zone could be predicted by the present theory if the terms $M_{xx}\,\dot{K}_{xx}$ were retained in the energy balance equation.

In conclusion of the present discussion of the shear effects we can state the following:

(i) Shear strain may contribute significantly to the overall rate of energy dissipation and thus may rise the resistance of the tube to denting.

(ii) The effect of shear is most pronounced for small dent depths. For deep dents of the order of tube radius shear increases the tube resistance by not more than 10%.

(iii) The model of the equivalent square tube is too crude to make a realistic estimate on the shear effects for small δ. Thus, no attempt was made to quantify this effect in order to compare it with experimental data recorded for $\delta/R < 0.1$.

9. PLASTIC INSTABILITY OF AXIALLY COMPRESSED TUBE UNDER LATERAL INDENTATION

So far we have considered a class of boundary conditions in which the axial force N applied at the tube ends was either tensile or zero. The simplicity and relative accuracy of the present solution method encouraged us to look at the more general case of tube loading in which the axial force (tensile or compressive) of a specified magnitude is applied to the tube prior to the local indentation. Such a pre-stressed tube is then subjected to local lateral indentation. Our task is to determine the force-deflection characteristics of the tube as a function of the load N as a parameter. The calculations to be shown reveals the existence of a critical magnitude of the compressive force N_c below which a violent sectional collapse of the tube takes place under an arbitrarily small lateral disturbance. The tensile force is taken to be positive while the compressive force is negative. We start the derivation by writing down the rate of energy equation for the tube subjected to combined denting and compression

$$P\dot{\delta} + 2N\dot{u}_o = \frac{8M_o\xi}{R}\dot{\delta} + 4N_oR\int_0^{\pi}\left|\frac{\delta\dot{\delta}}{\xi}\left(1-\frac{\alpha}{\pi}\right)^2 + \dot{u}_o\right|d\alpha \qquad (84)$$

Since two components of the external loading $\dot{\delta}$ and N are prescribed independently, there are two terms in the rate of external energy dissipation. The second term on the left hand side of Eq. (84) vanishes when N=0 or $\dot{u}_o$=0. Those two special cases were already considered earlier in Section 6 . In the absence of denting deformations $\dot{\delta}$=0, Eq. (84) reduces to

$$2N\dot{u}_o = 4N_o R \int_0^{\pi} \left|\dot{u}_o\right| \, d\alpha \tag{85}$$

which yields after integration

$$N\dot{u}_o = N_p|\dot{u}_o| \tag{86}$$

The above equations have two solutions

$$\begin{aligned} N &= N_p \\ N &= -N_p \end{aligned} \tag{87}$$

which mean that the tube develops its full axial strength by reaching yield stress respectively in tension or compression. The tube remains rigid if the axial force stays inside those limiting values $-N_p < N < N_p$. The axial force acting alone may not lead to the tube failure but may dramatically change the denting strength of the pre-stressed tube, as we will see in the sequel.

In the absence of rotational deformation, the axial force is now given by, according to the definition of Eq. (49)

$$N = 2\sigma_o tR \int_0^{\pi} \{\text{sign } [\frac{\delta\dot{\delta}}{\xi} (1 - \frac{\alpha}{\pi})^2 + \dot{u}_o]\} \, d\alpha \tag{88}$$

The argument of the sign function in the integrand of Eq. (88) changes sign at $\alpha=\alpha_1$ defined by

$$\frac{\delta\dot{\delta}}{\xi} (1 - \frac{\alpha_1}{\pi})^2 = - \dot{u}_o \tag{89}$$

so that after integrating, Eq. (88) becomes

$$N = -2\pi Rt\sigma_o (1 - \frac{2\alpha_1}{\pi}) = - N_p(1 - \frac{2\alpha_1}{\pi}) \tag{90}$$

The above condition says that for any choice of N from the interval $-N_p<N<N_p$, there is a unique point on the tube circumference $\alpha=\alpha_1$ at which axial strain rate vanishes and stresses change from tension to compression Fig. 29. Having determined this switching point, the integration of Eq. (84) with the absolute sign can be performed to give

$$P\dot{\delta} + 2N\dot{u}_o = \frac{8M_o\xi}{R}\dot{\delta} + 2N\dot{u}_o + \frac{4\pi N_o R\dot{\delta}}{3\xi}\left[1 - \frac{1}{4}\left(1 - \frac{N}{N_p}\right)^3\right] \tag{91}$$

where $\dot{u}_o$ is related to $\dot{\delta}$ and N by Eqs. (89) and (90). The two identical terms on both side of Eq. (91) can be dropped out and the expression for P takes the form

$$P = \frac{8M_o\xi}{R} + \frac{4\pi N_o R}{3\xi}\left[1 - \frac{1}{4}\left(1 - \frac{N}{N_p}\right)^3\right] \tag{92}$$

On comparing Eq. (43) with Eq. (92) we observe that both equations are the same except of the presence in the latter equation the correction factor for N. After minimizing with respect to ξ, the force-deflection relationship takes the final form

$$\frac{P}{M_o} = 16\sqrt{\frac{\pi}{3}\frac{D}{t}\frac{\delta}{R}}\sqrt{1 - \frac{1}{4}\left(1 - \frac{N}{N_p}\right)^3} \tag{93}$$

where N is a parameter. Several special cases, previously considered in the paper can be recovered from the above expression.

Tube with full end fixity - Substituting $N=N_p$ into Eq. (93), the correction factor becomes unity and Eq. (93) reduces to Eq. (45).

Tube free to move axially. On substituting N=0 the reduction factor is $\sqrt{3/4}$, as predicted by Eq. (54).

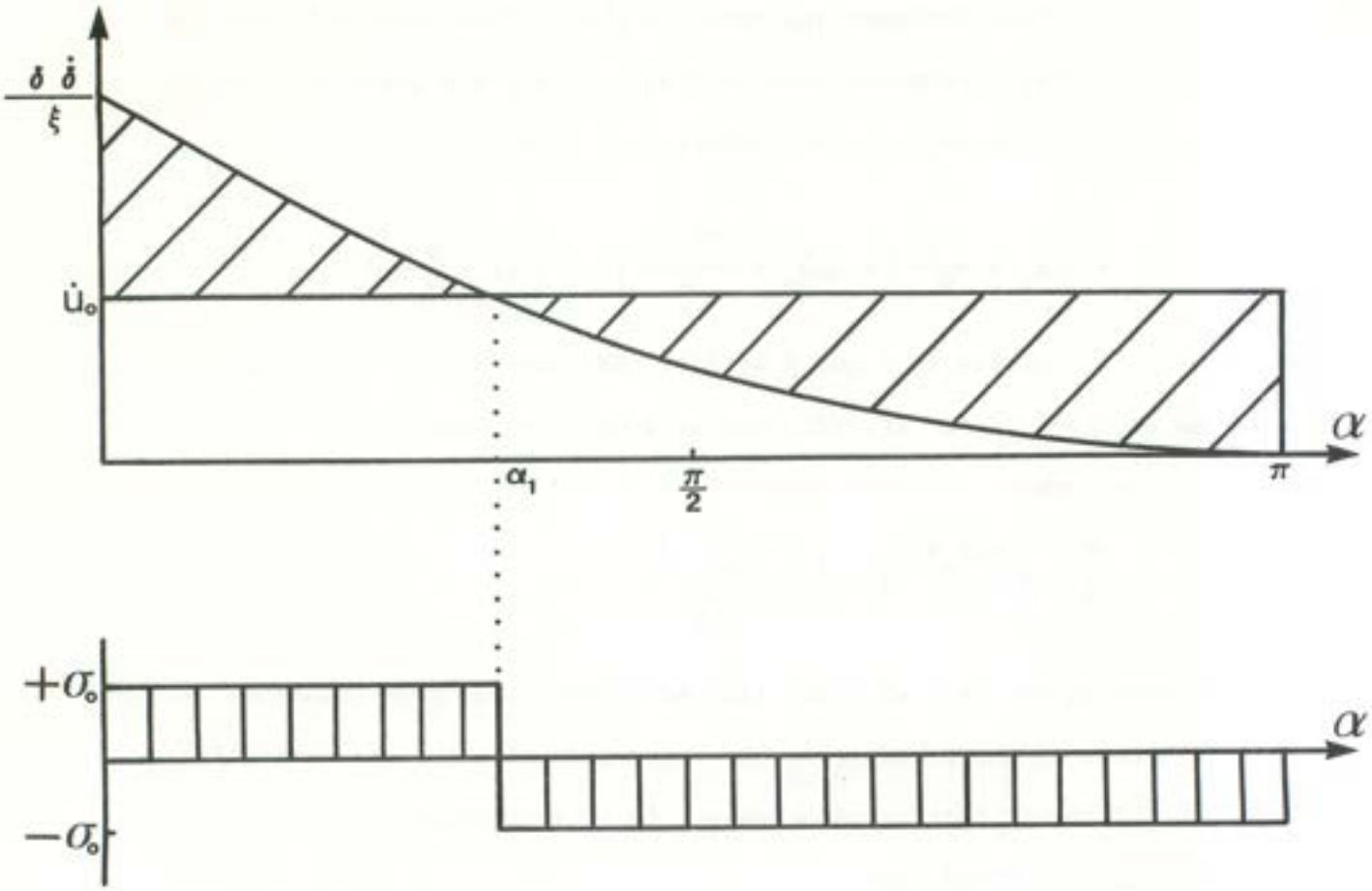

Fig. 29 A construction illustrating changing sign of strain rates and stresses to ensure development of a prescribed axial force in the tube.

Tube subjected to the ultimate compressive load (Squash load) $N=-N_p$. The term under the square root becomes negative and a real solution for P does not exist. In order to investigate this interesting case further, plot was made of the normalized crushing force, i.e., the correction factor versus the magnitude of the dimensionless axial force N/N_p, Fig. 30. It is seen that the resistance of the tube against lateral denting diminishes as N/N_p decreases from full tension through zero towards compression. When the compressive force attains the value

$$\frac{N}{N_p} = 1 - \sqrt[3]{4} = -0.5874 \tag{94}$$

the tube resistance drops to zero and no lateral force can be equilibrated by the system if the compressive force is further increased towards full squash load $-N_p$.

The existence of a critical value of the compressive force under which local spontaneous sectional collapse of the tube takes place has not been reported previously in the literature and thus requires a careful examination. First we shall interpret the above results within the realm of the present approximate theory. Consider the equilibrium statement of Eq. (91). In the general case the rate of external work goes on both plastic dissipation of rings [first term on the right hand side of Eq. (91)] and generators (two last terms). Each of those two contributions are non-negative. However, the term $2N\dot{u}_o$ on the right hand side of Eq. (91) is seen to equilibrate the rate of external work due to axial compression. In the resulting expression for P [Eq. (92)] the first term on the right hand side is always positive while the second term can be positive or negative depending on whether N is greater or smaller than N_c. If

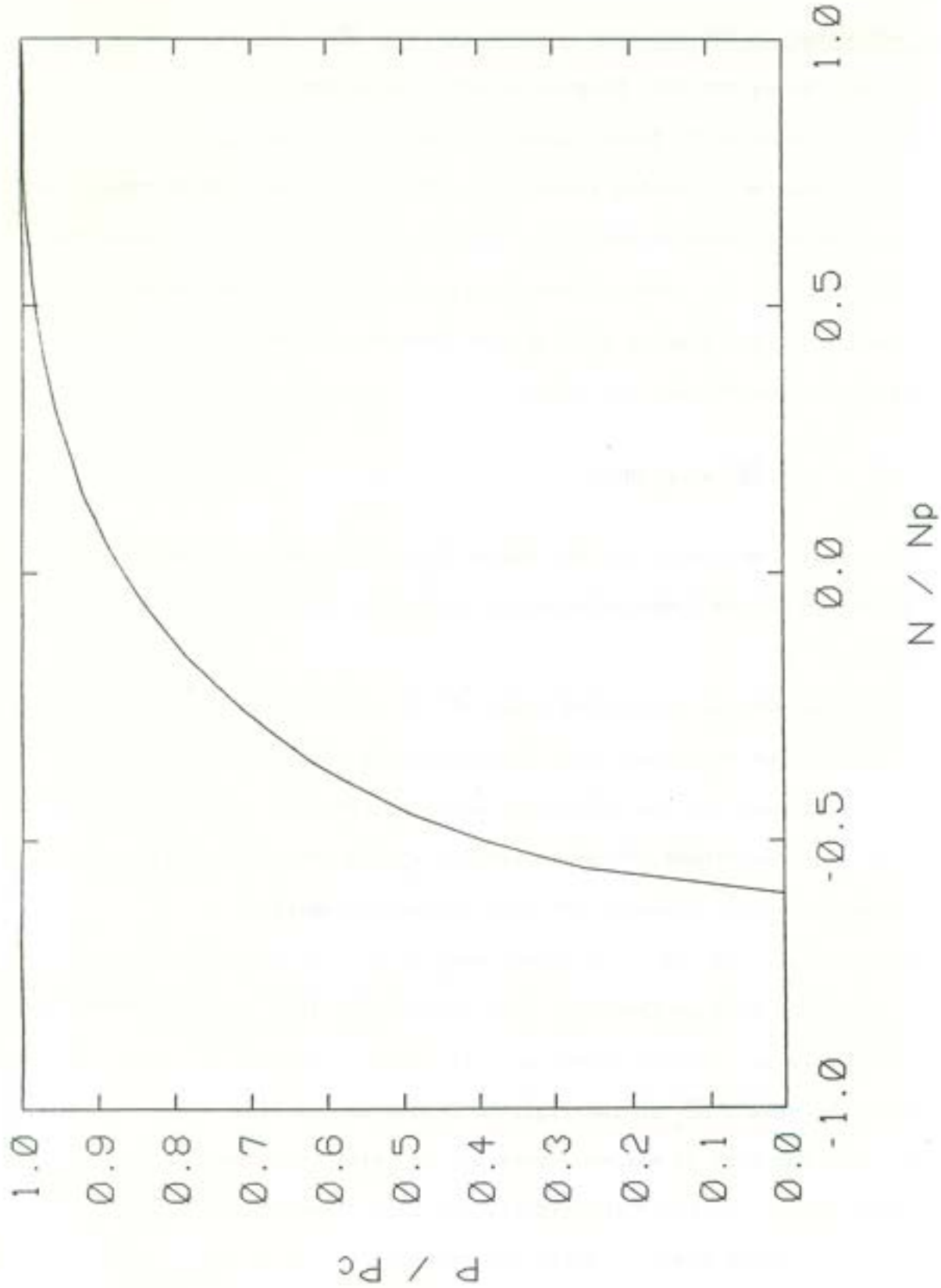

Fig. 30 Reduction of the normalized lateral force with the magnitude of compressive load. Result for the approximate solution.

$N>N_c$, the analytical minimum for P with respect to ξ exists and this occurs at

$$\frac{\xi}{R} = \left\{ \frac{2\pi\delta}{3t} \left[1 - \frac{1}{4} \left(1 - \frac{N}{N_p} \right)^3 \right] \right\}^{1/2} \tag{95}$$

Substituting Eq. (95) back into Eq. (92), the present solution is obtained. If on the other hand $N<N_c$, the second term in Eq. (92) changes sign into negative. Remembering that negative values of P do not have physical sense we see that a non-analytical minimum exists at the same magnitude of ξ as before, but the corresponding force P is zero.

From the above mathematical proof follows a physical interpretation of this interesting phenomenon. First observe that according to our model any infinitesimal increment of δ i.e., any positive $\dot{\delta}$ will bring all the generators to the yield point. Furthermore $\dot{\delta}$ uniquely determines the axial velocity $\dot{u}_o$, for a given set of δ and ξ, as specified by Eq. (89). Now the increment of external work should be equilibrated by the increment of the internal work. At $N=N_c$ the only available component of the internal rate of work is equal to $2N_c\dot{u}_o$ which just suffices to equilibrate the work increment in axial direction. Thus no surplus of internal energy or the tube strength exists to equilibrate the lateral force which therefore must vanish. For any magnitude of the lateral force greater than zero the increment of external energy exceeds that of internal energy meaning unstable behavior of the system.

Another way of interpreting the phenomenon of plastic instability is to observe that the magnitude of α_1 which corresponds to the critical force N_c is chosen in such a way that a net rate of energy of generators (shaded area in Fig. 29) be equal to the rectangular area $\pi\dot{u}_o$. Therefore the tube can bifurcate from pure symmetric compression into localized unsymmetric denting at no energy added to the system. All what is needed is to disturb the tube from one equilibrium state into the other by imposing an arbitrary transverse velocity $\dot{\delta}$ at the lateral surface of the tube. From the above discussion it transpires that indeed we have here a classical example of unstable structural behavior, this time for a rigid-perfectly plastic cylinder.

All the above conclusions are valid within the assumptions of parabolic distribution of the rate of energy, given by Eq. (39) and the rotational restraints at the tube ends. As shown in Fig. 16 the shape of actual functions $\dot{w}w/\xi$ differs from parabola. We have followed the procedure described above taking actual functions for several chosen values of δ/R. The resulting P-N curves are plotted in Fig. 31 as dotted lines. It is seen that the "exact" numerical solution differs from the analytical solution of Eq. (93) but the general conclusion remains the same.

The P-N curves are now moved slightly to the left so that the "exact" critical value of the compressive force is $N_c=0.763\ N_p$. The coefficient in the approximate closed form solution was 0.5874.

The question arises how our findings relate to experimental results performed on cylindrical shells in hundreds of laboratories around the world. The fact that compressed tubes may loose stability at axial load equal to 0.763 of the squash load of the tube suggests that a catastrophic sectional collapse should be a common phenomenon easily observable in simple tests.

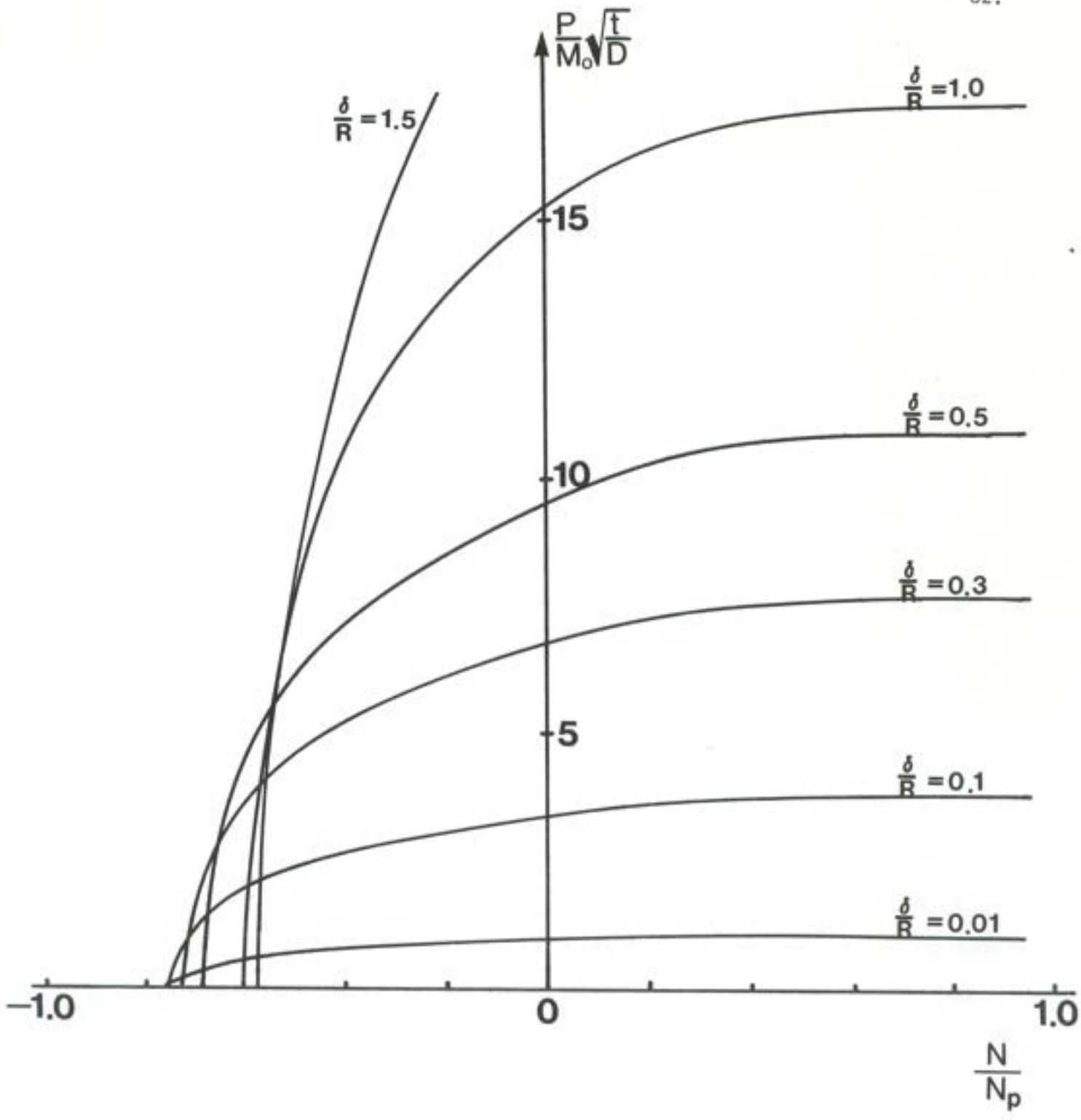

Fig. 31 Reduction of the resistance of the tube to indentation with the magnitude of the axial compression.

Actually, general experience with axially compressed cylinders confirm our conclusion. Figure 32 shows the so-called "knock-down" factor, i.e., the ratio of experimental to theoretical ultimate strength of cylindrical shells as a function of D/t. Our analysis is applicable for moderate-to thick tubes $20<D/t<60$ and predicts 25-30% reduction of the tube strength with single dimple-like imperfections. This finding is generally in accord with the trend of experimental points. However, there is lack of a sufficient data on the diagram with experimental points to fully confirm the present results. Thicker tubes with or without local dents were tested in Britain [24] and Norway [27] under different end conditions to the present one. If the simple-supported rather than clamped boundary conditions are imposed additional bending moment M=Ne resulting from the load eccentricity has a decremental effect on the measured knock-down factor, especially for larger dent depth.

Another interesting result of the present solution is the existence of a threshold value of the lateral disturbance which bring the system into an unstable pattern. This property of the solution is best illustrated in Fig. 33 where the results of Fig. 31 are replotted in the coordinate system with the dent depth as an independent variable and axial force as a parameter. It is seen that for $N>N_a$, all curves are monotonically increasing functions of δ/R . For $N<N_a$, the situation changes. Consider for example the curve corresponding to $N/N_p=-0.6$. The lateral resistance of the tube increases initially, and reach a peak value at $\delta/R \approx 0.5$. The magnitude of δ corresponding to the maximum lateral load is called the threshold value. If the axial load is further increased towards the

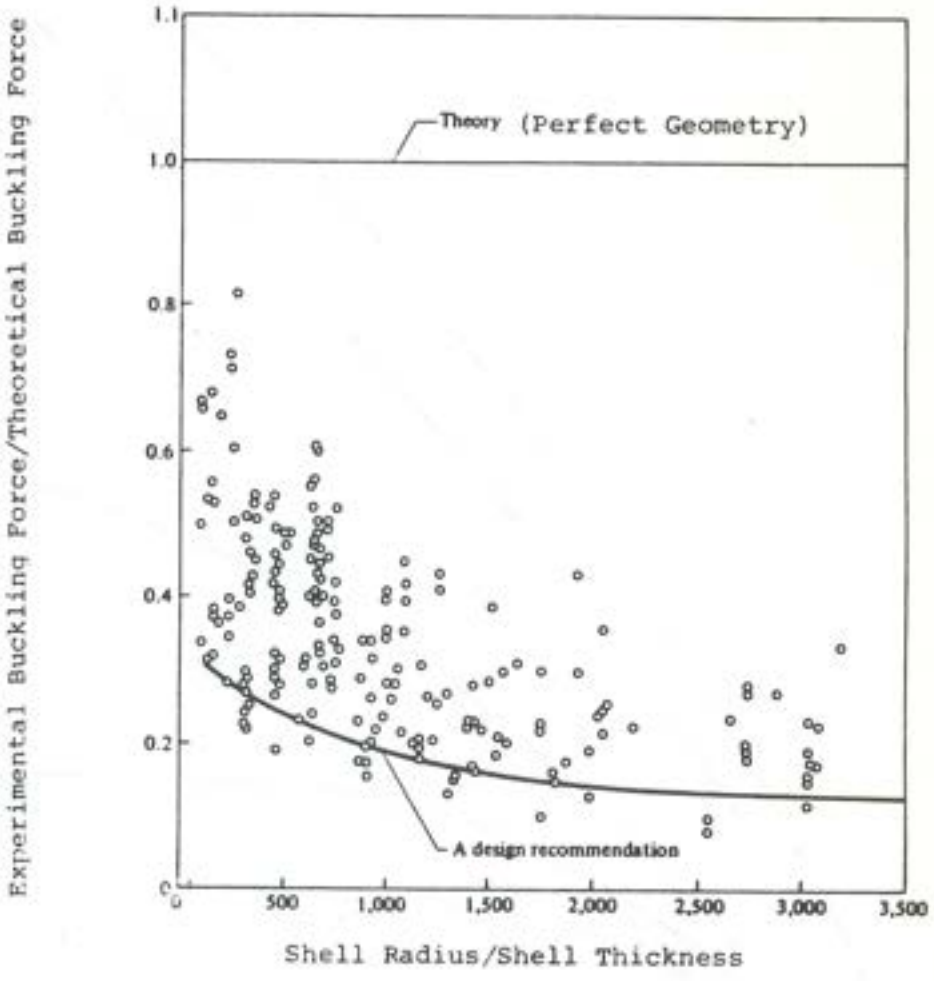

Fig. 32 Effect of radius to thickness ratio and imperfections on the buckling strength of cylindrical shell (after Almroth and Bush).

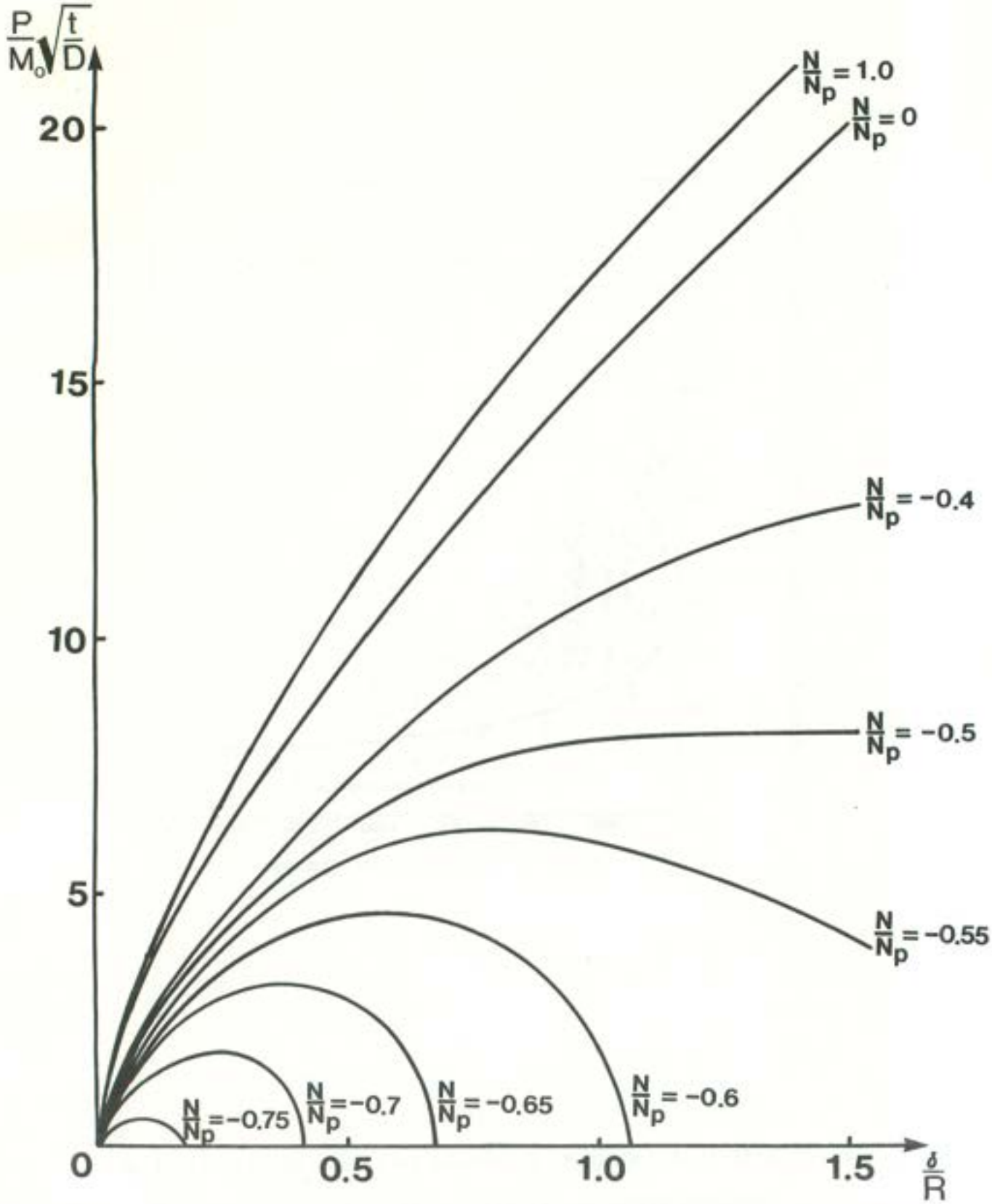

Fig. 33 Force-deflection characteristics of the dented tube for various values of the compressive force. The graph shows the existence of two critical values of the force $N_a = -0.5\ N_p$ and $N_c = -0.763\ N_p$.

squash load N/N_p=-0.7, the threshold displacement δ/R becomes less than 0.1. This means that the tube brought in compression up to 70% of its load-carrying capacity can tolerate in the stable way only small local indentation equal to 10% of its radius. If the depth of the dent exceeds this threshold value a spontaneous collapse of the section takes place.

The present findings may have a profound implication in the offshore industry when designing tubular members against accidental and impact loads. If a short tubular transmitting axial compression is designed with a factor of safety less than 1.5, a small lateral force caused by a collision may trigger a complete collapse of the member. The amount of the impact energy dissipated by such a tube is only a small fraction of the energy which otherwise could be absorbed by a similar tube without compressive load. Our theory can also explain the mechanism of progressive collapse of complex frameworks made of tubulars. It is plausible that the load redistribution after one member has failed can bring some other members closer to the squash load and make them vulnerable to the local collapse described above should additional transverse loading occur, for example in the form of an extreme hydrodynamic wave impact.

Finally a word can be added on the energy absorption capabilities of tubulars subjected to lateral concentrated load. The maximum energy that the tube can absorb is obtained by integrating the P-δ function from δ=0 to δ=2R

$$E(N) = \int_0^{2R} P(\delta)d\delta = \frac{4}{3}\sqrt{\frac{\pi}{6}}\sigma_o\, t^{1.5}\, D^2\, \eta(N) \qquad (96)$$

where the approximate expression for $\eta(N)$ is given by Eq. (93b) and is plotted in Fig. 30 by a solid line. The dotted line represents the present "exact solution". In both cases the energy is seen to rapidly diminish with increasing compression and reach zero at $N=N_c$. In view of the above results a word of caution should be given as to the applicability of similar analysis performed in the past [4] in which the influence of the axial compression on energy absorption capabilities of tubulars was not taken into account. It is worth mentioning that the symmetrically deforming tube, such as that shown in Fig. 27a, does not experience plastic instability of the type described above.

10. RESIDUAL STRENGTH OF DENTED TUBES

The results presented in the preceding section offers an attractive possibility of estimating the remaining axial strength of the tube weakened by a local dent of the depth δ. A distinctive feature of our method is that prediction is made on a purely theoretical basis. In the previous analyses of this problem semi-empirical or empirical methods were used to assess the strength of the tube in the damaged zone [23], [28]. Gellin studied the effect of imperfections on plastic buckling of short cylinders subjected to axial compression [8]. He calculated the decrease of axial strength as a function of the amplitude of imperfection. These results are valid however for small amplitudes comparable to the wall thickness t. Also an assumption was made in his analysis that the variation of amplitudes of imperfections in both axial and circumferential directions could be described by harmonic functions. By contrast we are concerned with a single dent-like imperfection.

The present prediction of the residual strength of dented tubes follows from the following argument. For each fixed N, the P-δ curves calculated by us represent equilibrium paths. A family of P-δ curves is shown in Fig.33. Consider one curve out of this family exhibiting an unstable behavior. There are two equilibrium points at which the lateral force P is zero. One such point corresponds to $\delta=0$ i.e., to the equilibrium state in the undamaged tube. The resulting uniform compressive stresses are below yield and the tube remains rigid. Another equilibrium point occurs at $\delta=\delta^*$. For any $0<\delta<\delta^*$ a finite lateral force is needed to deform the

tube further. As the dent depth increases at constant N, a point $\delta=\delta^*$ is reached when the tube collapses at no lateral load. Conversely with a constant prescribed dent depth one can increase the compressive load until the so-called residual strength of the tube is reached. Plotting the coordinates of the intersection points of the curve P-δ with the horizontal axis for each constant N, subsequent points of the so-called residual strength curve are obtained. This solution is shown in Fig.34 by the full line. The present theory also predicts the existence of an asymptotic value of the axial force meaning that no matter how deep the dent may be, the tube will always support the axial load smaller than N_c. The accuracy of the present analysis depends to a large extent on the choice of the ring deformation mode. Our choice is believed not to be good for very small dent depths. For comparison also shown in Fig.34 is the prediction of the approximate theory, based on Eqs. (93) and (94). The tube strength suddenly drops to the critical value N_c and then stays constant independent of δ. The actual residual strength of tubes is clearly underestimated by this approximate theory. However, the asymptotic values of the critical axial strength are almost the same in the exact and approximate solutions.

A practical lesson learned from the above discussion is that short tubular compressive members should be designed for axial load smaller than $0.587\ N_p$ or the safety factor should be greater than $1/0.587 = 1.7$. Such a design will be indifferent to the presence of small or even large dents and therefore will be unconditionally safe against accidental dents.

For more slender members the rotational deformations comes into play and the above conclusion is no longer valid. As mentioned earlier in the

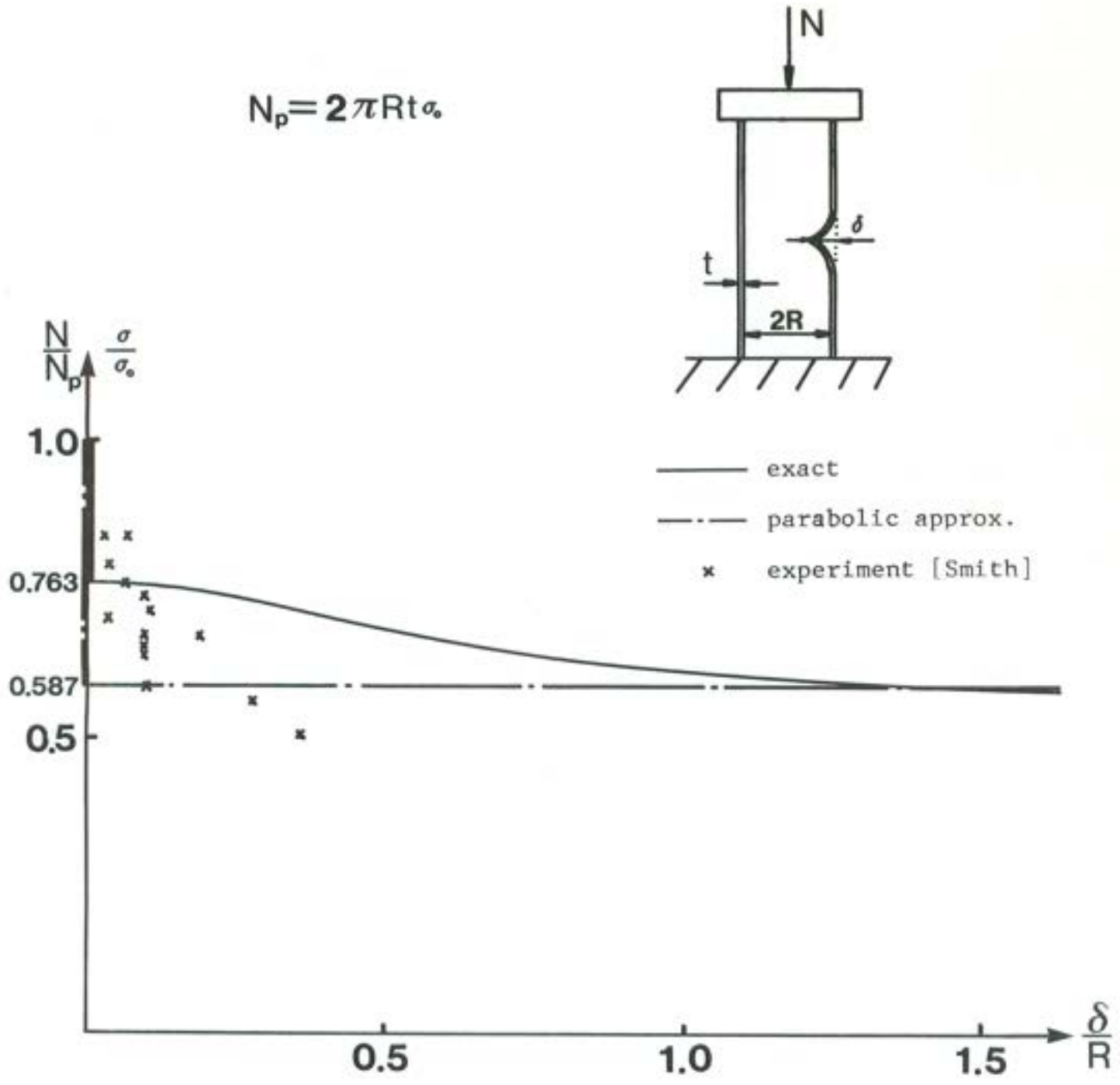

Fig. 34 Plot of residual strength of dented tube versus the dent depth. Exact solution denoted by full line and approximate solution by dotted line.

experiments on the residual strength of dented tubes performed by Smith [21] pin-pin end condition were used. It is therefore not appropriate to correlate the present theory with his data. In the absence of any other experimental data we have reproduced the test points due to Smith, recognizing the limitation of such a comparison. We took only the data corresponding to short tubes (small slenderness parameter λ) and no or very little initial overall bending amplitude $d \approx 0$. It is seen that for shallow dent depth $\delta < 0.1R$, the experimental points lie above the present "exact" solution. Our prediction is too conservative in this range because the details of the local dented zone is not adequately descrived by the ring model with four moving hinges. On the other hand, the tested tubes were much weaker for $\delta > 0.1R$ than the theoretical curve mainly because of the large imposed bending moment due to load eccentricity. The problem of residual strength of tubes with the end rotations allowed will be the subject of future publication.

11. SUMMARY AND CONCLUSIONS

1. The most important and new conclusion of the present paper is that the resistance of the tube to the local indentation by a rigid object strongly depends on the type of boundary conditions. Several typical boundary conditions were examined including axially and rotationally unrestrained and restrained tubes. The variation in the axial force covered the whole possible range from fully plastic tension N_p to fully compressive squash load $-N_p$. As far as the bending moment were concerned, we have considered two limiting cases $M=M_p$ (fully fixed ends) and $M=0$ (ends with rotational freedom). It was found that for tubes restrained from rotations $\dot{\theta}_o=0$, the force-deflection relationship can be written as a single equation

$$P = 16\, M_o \sqrt{\frac{\pi}{3}\frac{D}{t}\frac{\delta}{R}}\;\; \eta\left(\frac{N}{N_p}\right) \tag{97}$$

where the numerical factor $\eta(\frac{N}{N_p})$ depends on the magnitude of the axial force. The approximate expression for the factor η is

$$\eta = \left\{1 - \frac{1}{4}\left(1 - \frac{N}{N_p}\right)^3\right\}^{1/2} \tag{98}$$

The solution for other boundary conditions considered in the paper has also the same functional form of Eq. (97) but the numerical factor takes on a different value. Table 2 summarizes most of the results obtained in the present paper.

2. Present calculation revealed the existence of a critical magnitude of the compressive load $N_c = -0.763\, N_p$, where N_p is the squash load $N_p=2\pi Rt\sigma_o$.

Table 2

Case	Type	N	M	u_o	θ_o	η
1	fully clamped	$N=N_o$	$M=0$	$u_o=0$	$\theta_o=0$	1
2a	freely sliding	$N=0$	$M=M_o$	$u_o=0.133\,\frac{\delta}{R}\sqrt{\delta t}$	$\theta_o=0$	$\sqrt{\frac{3}{4}}$
4c	freely sliding and rotating	$N=0$	$M=0$	not calculated	$\theta_o=0.4\,\frac{\delta}{R}\sqrt{\frac{\delta t}{R^2}}$	$\sqrt{\frac{3}{8}}$
2	prescribed force with no rotation	N-prescribed	not calculated	not calculated	$\theta_o=0$	$\left[1-\frac{1}{4}\left(1-\frac{N}{N_p}\right)^3\right]^{1/2}$

$$\frac{P}{M_o} = 16\sqrt{\frac{\pi D}{3t}\,\frac{\delta}{R}}\;\eta$$

SUMMARY OF RESULTS FOR PLASTIC DENTING OF TUBES UNDER FOUR DIFFERENT BOUNDARY CONDITIONS

The load which is at or above critical load $-N_p<N<N_c$ causes a sectional collapse of an initially undeformed (perfect) tube in the unsymmetric mode. By imposing initial "dimple-like" imperfections or local dent the strength of the tube is further decreased up to an asymptotic value $N_a = -0.5\ N_p$. A practical implication of our findings that short rotationally restraint tubulars should be designed to transmit not more than 1/2 of the fully plastic load carrying capacity N_p. Such a design would appear to be insensitive to the local dents, even of quite large amplitudes. The members can take larger axial load up to 3/4 N_p but the safety factor will gradually diminish with increasing the dent depth. Tubes loaded beyond this range will unconditionally collapse.

3. The present solution for the load-deflection characteristics of dented tubes were shown to be within 10-20% of the experimentally measured values. This relatively high degree of correlation together with the fact that the shape of the dented zone is accurately predicted by the theory justify the practical value of our analysis.

12. ACKNOWLEDGEMENT

The work reported herewith was supported by the joint Industry/MIT Sea Grant project entitled "Residual Strength of Dented Tubes". We would like to extend our thanks to Professor C. Chryssostomidis, the Director of the Sea Grant College Program at M.I.T., for his continuous encouragement, advice and guidance throughout our work.

Interest in the project shown by Dr. Constantine Caracostis of the Shell Development Company and Mr. Ted Blum of the Marathon Oil Company, who monitored the work on behalf of industry is highly appreciated. Thanks are due also to Dr. Sverre Valsgard of Veritex (formerly Det norske Veritas Research Department) for permission to publish our original 1982 DnV Report, on which some of the present developments are based. Also useful discussions with Dr. S. Bhat of AMOCO Oil Co. on the formulation of the ring model are gratefully acknowledged.

Finally, special gratitude is extended to Ms. Linda Sayegh for her patience and skill in typing this manuscript.

REFERENCES

1. Birkemoe, P.C., Prion, H.G.L., Sato, J.A., Compression Behavior of Unstiffened Fabricated Steel Tubes, ASCE Annual Convention and Structures Congress, Houston, Texas, Oct. 18, 1983.
2. De Runtz, J.A., and Hodge, P.G., Crushing of Tubes Between Rigid Plates, J. Appl. Mech., vol. 30, 1963, pp. 391-395.
3. Ellinas, C.P., Ultimate Strength of Damaged Tubular Bracing Members, J. Structural Division, Proc. ASCE 1984.
4. Ellinas, C.P. and Walker, A.C., Damage on Offshore Tubular Bracing Members, Proc. IABSE Colloquium on Ship Collision with Bridges and Offshore Structures, Copenhagen 1983, pp. 253-261.
5. Ellinas, C.P. and Valsgard, S. Collisions and Damage of Offshore Structures: A State-of-the-Art, J. Energy Resources Technology, Vol. 197, Sept. 1985, pp. 297-314.
6. Foss, G., Gjerde, P., Xirouchakis, P.C. and Olaisen, K., Ultimate Compression Capacity of Tubular Columns in Braced Frames, DnV Report, August 1982.
7. Frieze, P.A. and Sachinis, A., Compressive Strength of Stress-Relieved Ring-Stiffened Cylinders Including Local Damage, Proc. Int. Symposium on Marine Safety, University of Glasgow, Sept. 7-9, 1983, Marine and Offshore Safety, ed., Frieze, P.A., et al., Elsevier, 1984.
8. Gellin, S., Effect of an Axisymmetric Imperfections on the Plastic Buckling of an Axially Compressed Cylindrical Shells, J. Appl. Mech., Vol. 46, March 1979, pp. 125-131.

9. Hopkins, H.G., On the Behavior of Infinitely Long Rigid-Plastic Beans under Transverse Concentrated Load, J. Mech. Phys. Solids, Vol. 4, 1955, pp. 38-52.

10. Hutchinson, J.W., On the Postbuckling Behavior of Imperfect-Sensitive Structures in the Plastic Range, J. Appl. Mech., Vol. 39, March 1972, pp. 155-162.

11. Morris, A.J. and Calladine, C.R., Simple Upper Bound Calculations for the Indentation of Cylindrical Shells, Int. J. Mechanical Sciences, Vol. 13, 1971, pp. 331-343.

12. Oliveira, J., Wierzbicki, T. and Abramowicz, W., Plastic Behavior of Tubular Members under Lateral Concentrated Loading, DnV Technical Report 82-0708, June 1982.

13. Onoufriou, A. and Harding, J.E., Effect of Impact Damage on the Residual Strength of Ring-Stiffened Cylinders, Proc. OMAE Symposium, Tokyo, April 1986.

14. Ostapenko, A. and Gunzelman, S.X., Local Buckling Tests on Three Steel Lange Diameter Tubular Columns, Proc. 4th Int. Conference on Cold-Formed Steel Structures, St. Louis, Missouri, June 1978.

15. Ostapenko, A. and Grimm, D.F., Local Buckling of Cylindrical Tubular Columns Made of A-36 Steel, Technical Report No. 450.7, Lehigh University, February 1980.

16. Parkes, E.W., The Permanent Deformation of a Cantilever Struck Transversaly at its Tip, Proc. Roy. Soc. London, A, Vol. 228, 1955, pp. 462-476.

17. Reid, S.R. and Reddy, T.Y., Effect of Strain Hardening on the Lateral Compression of Tubes Between Rigid Plates, Int. of Solids Structures, Vol. 14, 1978, pp. 213-225.

18. Sato, J.A., The Compression Behavior of Unstiffened Fabricated Tubes, M.S. Thesis 1985, Dept. Civil Engineering, University of Toronto.

19. Sherman, D.R., Report on Bending Capacity of Fabricated Pipes, University of Wisconsin-Milwaukee, Technical Report, February 1983.

20. Smith, C.S., Kirkwood, W., Swan, J.W., Buckling Strength and Post-Collapse Behaviour of Tubular Bracing Members Including Damage Effects, Proc. 2nd International Conf. on Behaviour of Offshore Structures (BOSS 79), London, August 1979.

21. Smith, C.S., Somerville, W.L., Swan, J.W., Residual Strength and Stiffness of Damaged Steel Bracing Members, Proc. OTC, Houston, May 1981.

22. Smith, C.S., Strength and Stiffness of Damaged Tubular Beam Columns, in Buckling of Shells in Offshore Structures (ed., J.E. Harding, et al.) Granada, London, 1982.

23. Smith, C.S., Assessment of Damage in Offshore Steel Platforms, Proc. International Conf. on Marine Safety, Glasgow, Sept. 1983.

24. Smith, C.S., Residual Strength of Tubulars Containing Combined Bending and Dent Damage, Proc. Energy Resources Technology Conf., February 1986.

25. Søreide, T.H. and Amdahl, J., Deformation Characteristics of Tubular Members with Reference to Impact Loads from Collision and Dropped Objects, Norwedian Maritime Research, Vol. 10, 1982, No. 2.

26. Symonds, P.S., Parkes Revisited, On Rigid-Plastic and Elastic-Plastic Dynamic Structural Analyses, Int. J. Impact Eng., Vol. 2, No. 1, 1984, pp. 1-36.

27. Taby, J., Moan, T., Rashed, S.M.H., Theoretical and Experimental Study of the Behaviour of Damaged Tubular Members in Offshore Structures, Norwegian Maritime Research, Vol. 9, No. 2, 1981.

28. Taby, J., Moan, T., Collapse and Residual Strength of Damaged Tubular Members, Proc. 4th International Conf. on Behaviour of Offshore Structures (BOSS 85), Delft, July 1985.

29. Thomas, S.G., Reid, S.R., and Johnson, W., Large Deformations of Thin-Walled Circular Tubes Under Transverse Loading-I, Int. J. Mechanical Science, Vol. 18, 1976, pp. 325-333.

30. Ueda, Y., Rashed, S.M.H., Behaviour of Damaged Tubular Structural Members, Proc. 4th International Symposium on Offshore Mechanics and Arctic Engineering (OMAE), Dallas, Feb. 1985.

31. Walker, A.C. and David, P., Effect of Impact Loading on Denting of Tubulars Unpublished Report, J.P. Kenny and Partners Ltd., London, England.

32. Walker, A.C., and Kwok, M., Process of Damage in Thin-Walled Cylindrical Shells, Proc. 5th OMAE Symposium, April 1980, Tokyo, Japan.

33. Watson, A.R., Reid, S.R., and Johnson, W., Large Deformations of Thin-Walled Circular Tubes Under Transverse Loading-III, Int. J. Mech. Sci., Vol. 18, 1976, pp. 501-509.

34. Watson, A.R., Reid, S.R., Johnson, W., and Thomas, S.G., Large Deformations of Thin-Walled Circular Tubes Under Transverse Loading-II, Int. J. Mech. Sci., Vol. 18, 1976, pp. 387-397.

35. Wierzbicki, T. and Bhat, S., "A Moving Hinge Solution for Axisymmetric Crushing of Tubes," in print, Int. J. Mechanical Sciences.

36. Wierzbicki, T. and Bhat, S., "On the Initiation and Propagation of Buckles in Pipelines," in print, Int. J. Solids Structures.

37. Wierzbicki, T. and Bhat, S., "On the Transition Zone in Unconfined Buckle Propagation," Proceedings Symposium on Current Practice and New Technology in Ocean Engineering, Energy-Sources Technology Conference and Exhibition, February 23-28, 1986, New Orleans. Also submitted to J. Energy Resources Technology.

38. Montgomery, G.C., Deformation of Pinch Loaded Tubes, M.Sc. Thesis, University of Aberdeen (Scotland), 1985.

39. Reid, S.R., Metal Tubes as Impact Energy Absorbers, in Metal Forming and Impact Mechanics, William Johnson Commemorative Volume, Ed. S.R. Reed, Pergamon Press, 1985.

APPENDIX A

A complete set of dimensionless equations describing the crushing behavior of a unit width ring is

$$\dot{r}_1 = \frac{[-\dot{r}_2(\pi-\phi-\sin\phi) + r_2(1+\cos\phi)](\phi+\sin\phi) - [\pi-r_2(\pi-\phi-\sin\phi)](1+\cos\phi)}{(\phi+\sin\phi)^2}$$

$$\bar{\dot{w}}_c = -\dot{r}_1(1-\cos\phi) - r_1\sin\phi - \dot{r}_2(1+\cos\phi) + r_2\sin\phi$$

$$V_1 = -\dot{r}_1\phi - r_1$$

$$V_2 = (\dot{r}_1-\dot{r}_2)\sin\phi + (r_1-r_2)\cos\phi$$

$$\frac{\frac{P_c}{4M_o}}{R} = \frac{1}{\bar{\dot{w}}_c}\left[\left|\frac{V_2}{r_2}\right| + \left|V_1\left(\frac{1}{r_2}-\frac{1}{r_1}\right)\right| + \left|(\pi-\phi)\frac{\dot{r}_2}{r_2}\right| + \left|\phi\frac{\dot{r}_1}{r_1}\right|\right]$$

$$\dot{r}_2 = n\left(\frac{\phi}{\phi_o}\right)^{n-1}\frac{\dot{\phi}}{\phi_o}$$

APPENDIX B

1. Calculation of w_o/R and $w_o\dot{w}_o/R^2$

As shown in Fig. 3 any point on the original cross section suffers a translation $w_o(\alpha)$ as the section deforms. Each point on the original cross section is defined by the angle α. Thus, for a given value of the local coordinates s, giving the distance along the circular arc to the vertical axis, is equal to $R\alpha$, where R is the radius of a circle. Assuming that the section is inextensional in the circumferential direction, then on the deformed section the new location of this point is such that it lies also at a distance along the deformed arc from the vertical axis.

(i) AB section $(0 \leq \alpha \leq (r_1-r_2)\sin\phi)$

The original coordinates of any point are

$$X_o = R \sin\alpha$$

$$Y_o = R \cos\alpha$$

The new coordinates of any point are

$$Xn = R\alpha$$

$$Yn = R - \delta$$

The translation becomes

$$\left(\frac{w_o}{R}\right)^2 = (\alpha-\sin\alpha)^2 + (1-\overline{\delta}-\cos\alpha)^2$$

Differentiation with respect to ϕ gives

$$\frac{w_o\dot{w}_o}{R^2} = (1 -\overline{\delta} - \cos\alpha)(- \dot{\overline{\delta}})$$

(ii) BC section $[(r_1-r_2)\sin\phi \leq \pi \leq \pi-r_1\phi]$

The new coordinates of any point are

$$Xn = (R_1-R_2)\sin\phi + R_2\sin\beta$$

$$Yn = R - \delta - R_2(1-\cos\beta)$$

where

$$\beta = \frac{R}{R_2}\alpha - \left(\frac{R_1}{R_2} - 1\right)\sin\phi$$

Similarly,

$$\left(\frac{w_o}{R}\right)^2 = [(r_1-r_2)\sin\phi + r_2\sin\beta - \sin\alpha]^2 + [1-\bar{\delta}-r_2(1-\cos\beta) - \cos\alpha]^2$$

$$\frac{w_o\dot{w}_o}{R^2} = [(r_1-r_2)\sin\phi + r_2\sin\beta - \sin\alpha][(\dot{r}_1-\dot{r}_2)\sin\phi + (r_1-r_2)\cos\phi +$$

$$\dot{r}_2\sin\beta + r_2\cos\beta\dot{\beta}] + [1-\bar{\delta}-r_2(1-\cos\beta)-\cos\alpha][-\dot{\bar{\delta}}-r_2(1-\cos\beta) - r_2\sin\beta\dot{\beta}]$$

where

$$\dot{\beta} = -\frac{\alpha\dot{r}_2}{r_2^2} - \frac{\dot{r}_1r_2-r_1\dot{r}_2}{r_2^2}\sin\phi - \left(\frac{r_1}{r_2} - 1\right)\cos\phi$$

(iii) CD section $(\pi-r_1\phi \leq \alpha \leq \pi)$

The new coordinates of any point are

$$Xn = R\sin(\phi-\psi)$$

$$Yn = R_1[1-\cos(\phi-\psi)] - R$$

where

$$\psi = (\alpha-\pi)\frac{R}{R_1} + \phi$$

Similarly,

$$\left(\frac{w_o}{R}\right)^2 = [r_1\sin(\phi-\psi) - \sin\alpha]^2 + \{r_1[1-\cos(\phi-\psi)] - 1 - \cos\alpha\}^2$$

$$\frac{w_o\dot{w}_o}{R^2} = [r_1\sin(\phi-\psi) - \sin\alpha][\dot{r}_1\sin(\phi-\psi) + r_1\cos(\phi-\psi)(1-\dot{\psi})]$$

$$+ \{r_1[1-\cos(\phi-\psi)] - 1 - \cos\alpha\}\{\dot{r}_1[1-\cos(\phi-\psi)] + r_1\sin(\phi-\psi)(1-\dot{\psi})$$

where

$$\dot{\psi} = (\pi-\alpha)\frac{\dot{r}_1}{r_2^2} + 1$$

2. Calculation of rate of extensional energy

The rate of extensional energy is obtained by the calculation of the area under the curve of $w_o\dot{w}_o/R^2$

(i) AB section $(0 \leq \alpha \leq (r_1-r_2)\sin\phi)$

$$A_1 = \int_o^{\alpha_f} (1-\bar{\delta}-\cos\alpha)(-\dot{\bar{\delta}})\, d\alpha$$

where

$$\alpha_f = (x-y)\sin\phi$$

(ii) BC section $((r_1-r_2)\sin\phi \leq \alpha \leq \pi - r_1\phi)$

$$A_2 = \int_{\alpha_f}^{\beta_f} \{[(r_1-r_2)\sin\phi + [r_2\sin\beta - \sin\alpha][(\dot{r}_1-\dot{r}_2)\sin\phi + (r_1-r_2)\cos\phi +$$

$$\dot{r}_2\sin\beta + r_2\cos\beta\dot{\beta}] + 1-\bar{\delta}-r_2(1-\cos\beta) - \cos\alpha][-\dot{\bar{\delta}} - \dot{r}_2(1-\cos\beta) - r_2\sin\beta\dot{\beta}]\}\, d\alpha$$

where

$$\beta_f = \pi - r_1\phi$$

(iii) CD section ($\pi - r_1 \phi \leq \alpha \leq \pi$)

$$A_3 = \int_{\beta_f}^{\pi} \{[r_1 \sin(\phi-\psi) - \sin\alpha][\dot{r}_1 \sin(\phi-\psi) + r_1 \cos(\phi-\psi)(1-\dot{\phi})]$$

$$+ [r_1[1-\cos(\phi-\psi)] - 1-\cos\alpha][\dot{r}_1[1-\cos(\phi-\dot{\psi})] + r_1 \sin(\phi-\psi)(1-\dot{\psi})]\}d\alpha$$

$$Z = A_1 + A_2 + A_3$$

The rate of extensional energy becomes

$$\dot{E}_{ext} = \frac{4NR^3 Z}{\xi}$$